

Stellingen behorende bij het proefschrift van Gabrie Meesters:
Mechanisms of droplet formation

Taylors theory describing liquid cones has often been scrutinised. It was never the intention of G.I. Taylor to describe the phenomenon of all the possible liquid cones in one single equation. It was merely an exercise to prove that, for a certain special case, a simple equation describes that specific cone.

A liquid cone, a pendant droplet exposed to a high electric field, constitutes in fact a corona discharge around a sharp liquid needle, where the curvature of the liquid needle adjusts to diverge the local electric field. In contrast to corona discharges around solid needles, where the curvature remains constant, the amount of space charge is changed to diverge the local field.

When trying to produce droplets of uniform size by using mechanically oscillated jet breakup, many people have tried to determine the point where the satellites and the main droplets are of equal volume. They forget that this point can occur only at low wavenumbers. Here the total volume of the satellites may be equal to that of the main droplet, but the whole satellite volume consists of at least two droplets.

Truly uniformly sized liquid droplets, of low viscosity, can only be produced, by jet breakup, at wavenumbers higher than $k \cdot a = 0.6$.

Reizen is een goede belegging; Weliswaar levert het geen tastbare rente op, maar het is een bezit voor het leven.

Simon Carmiggelt

With the expenditure of a few minutes at the end of a lecture, an experimental demonstration can turn an academic discussion into a highly motivating experience.

James R. Melcher
IEEE Trans. Education, E-17(2), (1974), 100

'If we don't do it, who else will'

Prof S.K. Friedlander speaking about loss prevention and pollution control as a chemical engineer.

The lack of interest in patent literature reflects the ignorance of students and researchers towards the patent philosophy. More practical commercial process information is assembled in patents than is available from other sources.

Het is schrikbaar om te zien hoe naïef vele eerste jaars studenten scheikundige technologie zijn t.a.v. de maatschappelijke effekten die mede veroorzaakt worden door ons, Scheikundig Ingenieurs. Het is echter bemoedigend dat door het eerste jaars vak Chemie en Samenleving, er in ieder geval bij enkelen enige bewustwording plaatsvindt.

Iedere wetenschapper zou tenminste, bijvoorbeeld na zijn studie, enkele maanden in een ontwikkelingsland moeten vertoeven. Dit om enigzins de relevantie van ons bestaan in de moderne maatschappij vast te kunnen stellen.

(Geschreven Oktober 1990, Jungle van Noord-Thailand; ten tijde van de golfcrisis, in een kamp van een lokale bergstam, waar het woord "golfcrisis" van geen enkele betekenis was).

It sometimes seems that biotechnology did not have the enormous impact on our society which we expected in the early 1980's. In fact, in the last decades enormous progress has been made in the field of biotechnology. Although not noticed by many, it has slowly entered into the society of today and we have become dependent on it.

Environmental contamination is an inevitable consequence of the activities of man. Pollution is excessive contamination, which interferes with the health and happiness of a population, and must be considered amoral.

After: N.I. Sax, (1974), *Industrial Pollution*

552146

20172747

TR diss 2065

**TR diss
2065**

Mechanisms of droplet formation

Mechanisms of droplet formation

Proefschrift

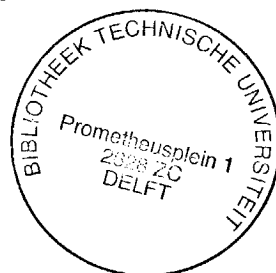
Ter verkrijging van de graad van doctor aan de Technische Universiteit Delft, op gezag van de Rector Magnificus, prof. drs. P.A. Schenck, in het openbaar te verdedigen ten overstaan van een commissie, aangewezen door het College van Dekanen, op 9 juni, 1992 te 10.00 uur.

door

Gabriël Marinus Henricus Meesters

geboren te Den Haag

Scheikundig ingenieur



Delft University Press / 1992

Dit proefschrift is goedgekeurd door de promotoren:
prof. B. Scarlett M.Sc.
dr. ir. J.C.M. Marijnissen

CIP-DATA KONINKLIJKE BIBLIOTHEEK, DEN HAAG

Meesters, Gabriël Marinus Henricus

Mechanisms of droplet formation / Gabriël Marinus
Henricus Meesters. - Delft : Delft University Press. - I11.
Thesis Technische Universiteit Delft. - With ref. -
With summary in Dutch
ISBN 90-6275-765-0
Subject heading: droplet formation

Contents

1	Introduction	1
1.1	General Introduction to this thesis	1
1.2	Introduction to the experiments and people contributing	4
1.2	References	5
Dispersion of liquids by exposure to high electric fields	7	
2	Electrostatic spraying of liquids	8
2.1	Introduction	8
2.2	Electrostatic spraying of liquids	9
2.3	References	11
3	History	12
3.1	History	12
3.2	References	20
4	Experiments based on visually seen phenomena	21
4.1	Visual observations of cone processes	21
4.2	Measurement of the current pulses of the cone	25
4.3	Measuring corona discharge	27
4.3.1	Corona discharge	27
4.3.2	Measurements of light emission from the corona glow	32
4.4	Current voltage characteristics	35
4.4.1	Current voltage characteristic of solid needles	35
4.4.2	Current voltage characteristic of the cones	35
4.5	Mobility of charged particles	40
4.6	Cone angle	42
4.7	Potential drop over cone surface	44
4.8	Multiple cone regime	45
4.9	Hysteresis in the current voltage curve	46
4.10	Visualisation of the cone apex through a microscope	49
4.11	Electric wind	53
4.11.1	Theory of electric wind	53
4.11.2	Electric wind measurements	53
4.12	Ansoft Computer Simulations	57
4.12.1	Solving Routines	57
4.12.2	Results of simulations	61
4.12.3	Conclusions	64
4.13	References	65
5	Practical applications of liquid cones	67
5.1	Generation of micron sized droplets from the Taylor cone	67
5.1.1	Introduction	67
5.1.2	Delft Aerosol Generator design	68
5.1.3	Delft Aerosol Generator operation	70
5.1.4	Droplet production	71
5.1.5	Conclusions	75
5.2	Electrostatic Emulsification	76
5.2.1	Introduction	76
5.2.2	Emulsification setup	78
5.2.3	Measurements of size distribution using forward light scattering	79
5.2.4	Influence of the applied potential on the droplet sizes	81
5.2.5	Stability of the emulsions produced	83
5.2.6	Influence of the flow rate on the droplet sizes	84
5.2.7	Influence of the conductivity on the droplet sizes	85

5.2.8	Onset potentials of the emulsification	85
5.2.9	Emulsification by applying high fields to a premixed liquid phase	87
5.2.10	Conclusions	90
5.3	References	91
6	General Conclusions	93
Jet break-up by mechanical vibrations		97
7	Introduction	98
7.1	References	99
8	Stability analysis of cylindrical jets	101
8.1	Rayleigh Break-up: Inviscid cylindrical jet break-up	102
8.2	Weber break-up: Viscous cylindrical jet break-up	104
8.3	Non-linear capillary instability	106
8.4	Detachment from the jet	108
8.5	Satellites	108
8.6	Ligament detachment	109
8.7	Contraction of extended droplets	109
8.7.1	Swell formation	110
8.7.2	Global contraction	110
8.7.3	Capillary instability	110
8.7.4	Competition of the mechanisms	111
8.8	Coalescence of satellite with main droplet through harmonics	111
8.9	Calculations based on Yuen's theory	112
8.10	References	112
9	Uniform droplets	114
9.1	Jet break-up, giving uniformly sized droplets	115
9.2	Experimental setup	118
9.3	Initial displacements	120
9.4	Growth rate of disturbance	125
9.5	Regions of uniform jet break-up	128
9.6	Size distributions of produced droplets	132
9.7	Tailor made particle size distributions	135
9.7.1	Particle size distributions produced, using the software	136
9.8	References	139
10	General conclusions	140
Summary		142
Samenvatting		145
Dankwoord		149
Curriculum Vitae		151

Aan mijn familie....

*I break inside my aloneness to knowledge
the end of knowing;
a billowing of an air current;
a movement towards necessity*

William Wharton (1978), Birdy

1 Introduction

1.1 General Introduction to this thesis

Defined particle size distributions are of importance to the pharmaceutical and chemical industry. Many products of the process industries have the form of powders, pastes, emulsions or suspensions, and the specifications of these products are achieved through control of the particle size distribution.

Well-defined particle size distributions are useful in the production of numerous industrial products. Sustained release pharmaceuticals of a defined particle size distribution have a controlled release to the body over a longer period of time than conventional pharmaceuticals. One can also think of the production of catalyst particles and the immobilization of micro-organisms, both processes deriving their benefit from a better defined particle size distribution.

A wide range of applications can also be found in the field of process equipment. Test materials of well-defined particle size distributions are very important, for example the testing of filters. Particles of well-defined size distribution in the range from 0.1 to 100 μm , are much in demand, especially if they can be produced in a simple and cheap way.

At this moment latices of narrow size distribution are readily available. They are produced using polymerisation techniques. A disadvantage is the relatively high price of these materials and that they are white, solid particles suspended into a liquid. Liquid droplets of narrow size distribution are not jet easily available. Most nebulisers produce droplets in the range of a few hundred microns down to a few microns. Narrow size distributions can only be obtained by impaction of the larger droplets, or

by deflection of the smaller ones. This causes the nebuliser efficiency to be poor. Larger particle, above 50 μm , are usually produced from glass, by well-controlled dripping procedures. When broad size distributions are needed a wide range of nozzles and atomisers is available (Lefebvre, 1989).

Presently the most common way to produce solids of a defined particle size distribution is by grinding, classification and mixing of different sizes of particles. Particles which are too small are recycled, particles which are too large are re-ground. Sometimes, however, chemistry simply prevents particles from being recycled and waste is produced. To achieve a specific distribution, considerable additional and difficult processing is needed. It is obviously more elegant if the required distribution can be produced directly.

The first part of this thesis concerns the production of droplets in the micrometer range. The liquids are dispersed with the help of a strong electric field. A phenomenon referred to as the Taylor cone is used for the dispersion of the liquid. A Taylor cone is a conically shaped liquid droplet from whose apex small droplets are emitted (Taylor, 1964). The phenomena of these liquid cones were further investigated.

The liquid cones have been known for a long time, but much has still to be investigated. This first part of the thesis describes the electrical behaviour of the liquid cones and an analogy to the well-known corona discharge phenomenon is found. With this analogy the electric behaviour of the liquid cones can be better understood and much of the electric behaviour can be explained. The space charge formed below the cones was found to be crucial to their existence and regulation of the local field. The cone shapes itself to the imposed field thus also regulating the field.

Two applications of these cones, their development and experimental results are also discussed. The first application is the development of an aerosol generator, referred to as the Delft Aerosol Generator, the DAG. The liquids dispersed in the air from these cones form a cloud of highly charged droplets of about one micron. The DAG was developed in order to discharge these droplets so they can easily be used. The droplets were discharged by placing a shielding electrode strategically within the electric field required for formation of the cones. The shielding electrode induces a corona discharge of opposite charge. The ions released from this corona recombine with the oppositely charge droplets, thus neutralising them. The droplets can then be transported to any required place without loss through migration to earthed objects.

The second application concerns the production of emulsions. The process is essentially the same as the first but the system is now immersed in another non-miscible liquid. By again applying a high electric field a liquid cone is formed although it is much smaller in size. From the tip of this cone small droplets are also ejected. The dispersed droplets remain in the continuous phase thus producing an emulsion. The

average droplet size lie between 1 and 5 μm , depending on the liquid properties. The emulsions were found to be stable. The power consumption of this process was found to be very low compared to the conventional ways of producing emulsions.

The second part of the thesis concerns the production of droplets a few decades larger in diameter, between 70 μm and 2 mm. Here a liquid jet is forced to break up by applying a vibration onto the jet causing it to breakup with the imposed frequency. It has already been described by others that liquid jets can breakup when a mechanical vibration is induced on the jet surface. Rayleigh (1878) and Weber (1931) laid the foundations for the theory of the break up of a liquid jet caused by axis-symmetrical disturbances having a wavelength greater than the circumference of the jet. Later, others performed experiments to verify their theoretical analysis. For practical purposes it is necessary to know at what frequencies a jet will break up dependent on the liquid properties and the apparatus configuration. Only Sakai *et al.* (1980, 1982, 1985), in the early eighties, made an attempt at describing regions of uniform jet breakup, when a needle is vibrated longitudinally. They were the first to take into account the liquid properties in addition to the jet diameter, liquid velocity and applied frequency.

In this investigation a modified version of the setup used by Sakai *et al.*, was used. Instead of the vibrating needle a stationary pinhole plate was used. This causes less clogging and is much more easily scaled up to a multi-nozzle system. Defined uniformly sized droplets in the range from 100 μm to 3 mm in diameter were produced. Two pieces of equipment producing uniform droplets from a jet originating from a stationary orifice were built. The first one was constructed of glass and was used to investigate the break up behaviour of liquids of low viscosity such as water, ethylene glycol, ethylene glycol/water mixtures and 1 (w/w)% of sodium alginate solution in water.

A second apparatus was constructed from steel to withstand pressures up to 15 bar. It was used to study the production of uniform droplets using liquids of higher viscosity and to study the possibilities for scaling up the process. To enable computer control, this apparatus was linked to a personal computer by means of a Labmaster interface card.

Both apparatus had a stationary orifice. The disturbance necessary for the jet break up, was introduced by using an oscillating bellows. This bellows was connected to a loudspeaker on one side and was immersed in the liquid on the other side.

Using the mechanical vibration process and knowing the uniform region, it is possible with only a few different nozzle sizes to define a particle size distribution over a wide range of diameters and to tailor it. Manipulating velocity, frequency and nozzle diameter and knowing the limits of the 'uniform region', control of the droplet size and provides us a tool to tailor the particle size distribution. Since the production rate is small compared to the grinding and classification method, this process is mainly of

interest for products produced in small quantities and for products having a high added value.

1.2 Introduction to the experiments and people contributing

The work described in this thesis was made possible through the cooperation of many people. Professor Scarlett and Jan Marijnissen gave the necessary scientific feedback during often refreshing discussions.

Most of the experimental work was performed by students who graduated on the topics described. First Aart van der Dool, with whom I visited prof. Sakai and Dr. M. Sato, of the Gunma University, in Japan. They introduced us to the electrical and mechanical breakup of liquid jets. Due to our enthusiasm when we came back from Japan a new PhD-research project was made possible by Prof. Scarlett, started in September 1987. Aart built and tested the electrostatic equipment. Due to Aart's curiosity we discovered the liquid cones, not seen or heard of by us before.

It was Anne-Mieke Reedijk who followed Aarts preliminary tests and performed experiments dealing with the shape of the liquid cones at different applied potentials. She also performed the first electric field calculations. To understand the droplet sizes Anne-Mieke built and tested the configuration needed for producing the emulsions through electrical dispersion.

Alexander Krekel followed and carried out all the experiments concerning the electrostatic emulsification. We encountered much difficulty in trying to analyse the emulsions produced. Only with the help of Jan-Willem Groenendaal of Gist-Brocades, were we able to produce stable emulsions, ready for analysis. Although not entirely as planned, good results were obtained. Both the work of Anne-Mieke and Alexander were presented at the Second World congress on Aerosol Science in Kyoto, Japan in 1990 (*Meesters et al.* 1990^a).

Paul Vercoulen followed, producing liquid droplets in air from the liquid cones as first performed by Anne-Mieke. Because of the high charge we were not able to measure the droplet size of the aerosols produced from the cones until, partly by coincidence but mostly because of the help of Rein Roos from the École Supérieur d'Électricité of Paris, we were able to discharge the droplets. The whole device was developed into an aerosol generator, called the DAG (Delft Aerosol Generator). The DAG provoked much interest from all over the world, especially after presentations at the European Aerosol Conferences of 1990 and 1991 as well as the British Aerosol Conference of 1991. This work is published in the Journal of Aerosol Science (*Meesters et al.* 1990^c, 1992).

The work of Prof. M. Goldman of the École supérieur d'Électricité of Paris gave us insight into the world of corona discharge. With the help of Prof. Goldman and Rein Roos, much of the electrical behaviour of the liquid cones could be explained. Also the experiments carried out in Paris at Prof. Goldman's laboratories were of great

importance to the results presented in this thesis.

Through our visit to Prof. Sakai in Japan in 1986, we became interested in the field of jet break up. After the development of our own rig it was Maria Onderwater who started the first experiments in jet breakup by forced oscillation of the liquid. Uniform regions of jet breakup were measured and with the use of a newly developed computer programm called PASTIFIT, the regions of uniform jet breakup were described by more general equations. These equations were obtained by dimensional analysis. Later more measurements completed the general description of these regions. This work was presented at the World Conference on Particle Technology in Kyoto Japan in 1990 (Meesters *et al.* 1990^b). Maria also performed the measurements on the break up length of the jets. These results will be published in the near future.

After the development of a high pressure rig, Marnix van Woerden started his graduate project. Marnix studied the breakup of more viscous liquids from which solid particles could be obtained. He automated the high pressure rig, thus being able to produce, 'tailor-made', size distributions. This was possible through knowledge of the regions of uniform jet breakup. Marnix wrote an excellent literature survey on the breakup and stability phenomena of liquid jets.

It was Edgar van Asperen who benefitted from all the previous research. Edgar carried out his graduate research at the faculty of Mining Engineering. He used the liquid cones as well as the high pressure jet breakup rig to produce water-in-oil emulsions which were needed for further research at his Faculty. He tested the limits of the high pressure apparatus and was able to produce droplets of about 10 µm at pressures of 15 bar.

All this work is collected into this thesis. I hope that you will find it interesting. Also I would like to thank you all for making this thesis possible.

1.2 References

- Levebvre, A.H., (1989) Atomisation and Sprays, Chemisphere Publ. Corp. New York
- Meesters, G.M.H., Reedijk A.M.E., Krekel A.P.C., Scarlett B., (1990^a) *Proc. 3rd Int. Aerosol Conf. Kyoto Japan* Ge60, 259
- Meesters, G.M.H., Onderwater, M.F.J., Scarlett, B., (1990^b) *Proc. 2nd World Congr. Particle Technol., Kyoto, Japan*, p.397
- Meesters, G.M.H., Vercoulen, P.H.W., Marijnissen, J.C.M., Scarlett, B. (1990^c) *J. Aerosol Sci.*, 21 S1, 669
- Meesters, G.M.H., Vercoulen, P.H.W., Marijnissen, J.C.M., Scarlett, B. (1992) *J. Aerosol Sci.*, 23(1), 37
- Sakai T., Hoshino N., (1980), *J. Chem. Eng. Japan*, 13(4), 263
- Sakai T., Sadakata M., Saito M., Hoshino N., Senuma S., (1982), *Proc. Int. Conf. Liquid Atomisation and*

Chapter 1

Spray Systems, ICLASS-82, Japan, 2-1, 37

Sakai T., (1985), *Proc. Int. Conf. Liquid Atomisation and Spray Systems, ICLASS-85, London, VII-13(b)2,*
¹

Taylor, G.I. (1964) *Proc. Roy. Soc. A280*, 383

Rayleigh, Lord F., (1878), *Proc. London Math. Soc.*, 11, 4

Weber C., (1931), *Z. für Angew. Math. Und Mech.*, 11, 136

PART ONE

**Dispersion of liquids
by exposure to high electric fields**

Corpus vero dicit ipsum manifesto in aquae globola gutta posita supra siccum: nam succinum appositum in conuenienti distantia, proximas conuelliit partes, et educit in conum.

It plainly attracts the body itself in the case of a spherical drop of water standing on a dry surface; for a piece of amber held at suitable distance pulls towards itself the nearest particles and draws them up into a cone.

William Gilbert, (1600), De Magnete

2 Electrostatic spraying of liquids

2.1 Introduction

The first part of this concerns the breakup of a liquid droplet, exposed to a strong electric field, as it slowly flows from a nozzle. This droplet emits droplets in the micron size range.

This phenomenon has often been referred to as the Taylor cone. This name refers to the fact that the droplet hanging from the nozzle is no longer round, but conically shaped. It was Sir Geoffrey Taylor who in 1964, was the first to describe the phenomenon mathematically. Later it was shown that his analysis was only valid for one extreme case. Many researchers tried to describe the phenomenon of these liquid cones, under the more commonly used operating conditions, but without much success. Especially in the field of liquid metal ion sources (LMIS), much interest in the dispersion of liquid metals, using the Taylor cones, was shown by Cutler and co-workers in the 1980s.

Our interest lies in the dispersion of semi-conducting liquids using the Taylor cone. This interest is based on the fact that spraying these semi-conducting liquids leads to the formation of small uniformly sized droplets. Also Bailey, Balachandran and Hyati in England, at the University of Southampton did work on liquid cones. In France Cloupeau also worked on the dispersion of semi-conducting liquids. Nevertheless much remains unknown about the mechanism of the phenomenon itself. Our purpose is to perform accurate measurements on the sizes and size-distributions of the droplets produced and to get more insight into the electric behaviour of the

liquid cones. Already some very rough qualitative results are known about the sizes of the droplets produced, but much better results are required.

Also the behaviour of the cones during operation and its changing shape with changing potential, as reported by others, is investigated. The changing shape of the liquid cones, with changing applied potential, contradicts the description of Taylor, who concluded that only one single cone shape can exist.

In particular the electric behaviour of the cones will be reported on. The space charge formed near the apex of the cone is shown to be crucial in explaining some of the features.

Not only the phenomenon of the liquid cones is researched, but in keeping with the engineering tradition, two practical applications of the phenomenon are also developed.

First an aerosol generator was built. This device makes use of the liquid cones, producing highly charged droplets. These droplets are electrically discharged almost immediately after formation. The highly charged droplets are difficult to manipulate and are attracted to all kinds of earthed objects. Thus by discharging them, an aerosol of uncharged droplets is formed, enabling us to easily transport them to the any desired place.

The second application describes the production of emulsions through the use of liquid cones. These emulsions are made by submerging the liquid cones into another immiscible liquid. The droplets coming from the tip of the cones are directly dispersed into the continuous phase, producing the emulsion. Compared to conventional emulsification techniques, this electrostatic technique has several advantages, these are described.

In both cases various liquids are used.

2.2 Electrostatic spraying of liquids

When a liquid flows from a capillary nozzle at such a flow rate such that the liquid is dripping, the frequency of drop emission is about a half to a few per second. In this case the liquid forms a pendant drop which hangs from the nozzle and grows until its weight overcomes the vertical component of the surface tension. When the nozzle is raised to a higher electric potential, the frequency of droplet emission increases. A liquid droplet, exposed to an electrostatic field, accumulates induced charges on it surface. The drop formation rate is enhanced by the electric force acting on these charges. The sum of electrical and gravitational force act to counteract the surface tension. When, however, the liquid flow rate is kept constant, smaller droplets are formed. This type of drop breakup is the so-called Field Enhanced Dripping (FED) mode. The droplets formed are quite uniform in size. When, in addition to the DC-potential, an AC-potential is added, with a frequency equal to the drop emission rate, the droplets produced are even more uniform in size (Takamatsu *et al*, 1981-1983).

After the spraying process is synchronised with AC-potential, the emission frequency of the spraying process can be altered within certain limits above and below the natural spraying frequency (Sato, 1984). The droplets produced this way are typically in the size range of about one millimetre to about one tenth a millimetre.

By increasing the DC-potential even more another spraying mode is established, the so-called Harmonic Electrical Spraying (HES) mode (Sample and Bollini, 1972). The transition occurs suddenly at a certain potential. This transition is marked by a sharp increase in frequency of droplet emission. In this mode the residual meniscus which remains attached to the nozzle after droplet emission is usually larger than the emitted drop, whereas in the FED mode this residual meniscus is so small that it appears as though the droplet is pulled directly off from the nozzle. Ogata (1976) published descriptions of many experiments about the transition from FED to HES. The specific charge of the droplets increases in both modes with increasing potential and gradually approaches to one-half of the Rayleigh limit (Hendricks, 1962).

At even higher potentials and when spraying semi-conducting liquid a special phenomenon can be seen. A hemi-spheric droplet can be deformed into a stable conically shaped surface. From the tip of this cone very small droplets are formed at frequencies much higher than in the first described regimes. It was Taylor in 1964 who showed that for a special configuration this phenomenon could be explained theoretically and mathematically. These cones are therefore often referred to as Taylor cones.

In 1984 Sato reported on a jet breakup process where the drop production frequency is synchronised by an AC-frequency as well. A liquid jet issuing from a nozzle was exposed to a non-uniform electric field. By synchronising an AC-potential to the jet breakup frequency, mono-sized droplet were produced. The big advantage over the previous breakup processes is the higher flow rate that can be used. Sato produced droplets between 122 and 88 μm at frequencies of, respectively, 10 and 27 kHz at a flow rate of $9.55 \cdot 10^{-9} \text{ m}^3/\text{s}$, using a capillary of 53.3 μm inner diameter. From these results an apparatus was developed to produce larger amounts of droplets by applying the jet breakup to a spinning disk. Dietz and Miller (1982) patented a similar apparatus for producing metal droplets from a molten metal. Balachandran and Bailey (1981) reported on measurements and calculations using electrostatic fields with centrifugal atomisers. They concluded that the atomisation process was enhanced by the electrostatic field and narrowed the size distributions obtained.

The applications for all these electrostatic spraying processes are manifold. Surface coating techniques using electrostatic spray painters are already widely used. The deposition of the droplets is greatly enhanced by the charging the paint droplets (Meesters *et al.* 1990). The same is true for electrostatic crop spraying. Many applications can also be considered in electrostatic printing, electrostatic emulsification, fuel atomisation in combustion systems and in space vehicle propulsion systems.

Taylor cones can be used as ion emitting devices, but can also be used to spray small

amounts of liquid metal. Perel *et al.* (1981) sprayed many molten metals and alloys using several spraying modes.

Electrostatic emulsification of wax was reported on by Hughes *et al.* (1981, 1984). Also non-conducting liquids like kerosine and hexane were sprayed by charge injection.

In spite of these laboratory results, large scale production processes using electrostatic forces during atomisation are not yet established. This is probably due to the fact that much still is not sufficiently well understood as to what causes the drop to be of a particular size. The liquid properties governing the breakup process have to be further investigated. For these reasons small scale production units have been built. These units use only liquids with a high value are sprayed to manufacture small amounts of expensive products. Especially for producing standard materials for testing and calibration purposes these liquid cone techniques are presently of great interest (Scarlett *et al.* 1990).

2.3 References

- Bailey, A.G., Borzabadi, (1978), IEEE Trans. Ind. Appl. 1A-14(2), 162
Bailey, A.J., Balachandran, W. (1981) *J. Electrostatics* 10, 99
Bailey, A.G., (1986) *Atomisation and Spray Techn.* 2, 95
Cloupeau, M., Prunet-Foch, B. (1989) *J. Electrostatics* 22, 135
Chung, M., Cutler, P.H., Feuchtwang, T.E., Miskovsky, N.M., (1984) *J.Physique*, 45 C9, 146
Chung, M., Cutler, P.H., Feuchtwang, T.E., Kazes, E., Miskovsky, N.M., (1984) *J.Physique* 45 C9, 153
Chung, M., Cutler, P.H., Feuchtwang, T.E., Kazes, E., (1985) *Appl. Phys.* A36 171
Chung, M., Cutler, P.H., Feuchtwang, T.E., Miskovsky, N.M., Sujatha, N., (1984) *Scanning Electron*
Hendricks, C.D., (1962) *J. Colloid Sci.* 17, 249
Hayati, I., Bailey, A.I., Tadros, Th. F. (1986) *Nature* 319, 41.
Hayati, I., Bailey, A.I., Tadros, Th. F. (1987) *J. Colloid Interface Sci.* 177(1), 205
Hayati, I., Bailey, A.I., Tadros, Th. F. (1987) *J. Colloid Interface Sci.* 177(1), 222
Hughes, J.F., Pavey, I.D., (1981) *J. Electrostatics* 10, 45
Hughes, J.F., Pavey, I.D., Arimoto, M., (1981) *IEEE Conf. Rec. LAS Ann. Meeting*, 1031
Hughes, J.F., Roberts J.M.C., (1984) *Int. J. Cosmetic Sci.* 6, 103
Meesters, G.M.H., Zevenhoven, C.A.P., Brons, J.F.J., Verheijen, P.J.T. (1990) *J. Electrostatics* 25, 265
Ogata, S., Kawashima, T., Nakaya, O., Shinohara, H., (1976) *J. Chem. Eng. Japan* 9(6), 440
Perel, J., Mahoney, J.F., Kalensher, B.E., Mehrabian, R., (1981) *Advances in Metal Processing* Plenum
Publ. Corp. New York, pp. 79-89
Sample, S.B., Bollini, R., (1972) *J. Colloid Interface Sci.* 41(2), 185
Sato, M., (1984) *J. Electrostatics* 15, 237
Scarlett, B., Merkus, H.G., Meesters, G.M.H., (1990) *Liquid Particle Size Measurements, ASTM STP 1083*
Vol. 2, Philadelphia pp. 9-18
Takamatsu, T., Hashimoto, Y., Yamaguchi, M., Katayama, T., (1981) *J. Chem. Eng. Japan* 14, 178
Takamatsu, T., Yamaguchi, M., Katayama, T., (1982) *J. Chem. Eng. Japan* 15(5), 349
Takamatsu, T., Yamaguchi, M., Katayama, T., (1983) *J. Chem. Eng. Japan* 16(4), 267
Taylor, G.I. (1964) *Proc. Roy. Soc. A280*, 383
UK Patent No. GB2111536A (1982) by Dietz P.W and Miller R.S.

*Living things grow upwards but are not free
The highest branches trap air and light
but only feed endless grindings of earth
Growth itself is without meaning*

3 History

3.1 History of the research on liquid cones

The theory of the Taylor cone was first developed by G.I. Taylor (1964), but others had already reported the phenomenon. Zeleny (1914, 1915, 1917) and Drozin (1955) observed, that a liquid droplet assumed a conical shape when issuing from a nozzle and when subjected to a high electric field. Both researchers observed that an aerosol was formed which emerges from the tip of the cone, but neither could scientifically explain the phenomenon. However the very first observation was given in 1600! In his book *De Magnete*, William Gilbert writes that '... for a piece of amber held at suitable distance pulls towards itself the nearest particles and draws them up into a cone....', He refers to a drop of water becoming cone shaped when attracted by a amber stick charged by rubbing it with a piece of cloth. The real research on liquid droplets and liquid films, exposed to high electric fields, started much later, in the early part of this century.

Wilson and Taylor (1925) and Mackey (1930) carried out experiments with hemispheric soap bubbles exposed to electric fields, and Nolan (1926) and Mackey (1931) carried out experiments with uncharged drops falling through uniform fields. As a function of the drop radius they determined the smallest electrical field in which falling droplets disrupted. Later Zeleny (1935) also did experiments on the onset of the cones. He found that, for a voltage only slightly greater than that necessary for making the surface unstable, the drop at the end of a small tube assumes a nearly

conical form. From this conical drop a continuous thread of liquid issues from the apex. The filament breaks up into innumerable and individually invisible droplets. When illuminated with a strong light source Zeleny (1917) had previously found that a coloured mist could be seen. When spraying water he observed that occasionally fine filaments of liquid were ejected. After this the meniscus relaxed back into the more rounded off shape. This was a repetitive process, which was seen in a small potential range just before a stable cone was formed. A gaseous discharge was also observed which remained at higher potentials when the stable cone was established. Zeleny measured roughly that approximately $\frac{1}{6}$ of the current was carried by the droplets formed and $\frac{5}{6}$ by the ions from the glow discharge.

Only much later Vonnegut and Neubauer (1952, 1953) also described that a liquid disperses into very small droplets when subjected to a high electric field. When the droplets produced were illuminated with a beam of parallel light, higher-order Tyndall spectra were created (the coloured mist of Zeleny (1917), proving that the aerosol was relatively uniform in size and that the droplet diameters were of the order of $1 \mu\text{m}$. Further work on the electrical atomization of liquids using cones has been reported by Bailey (1974, 1988), Kelly (1976), Joffre (1982), Hyati *et al.* (1987) and Cloupeau (1989).

However, it was Taylor who first explained the phenomenon theoretically and described it mathematically. Although this occurred in 1964, Taylor had earlier been working with Wilson (1925) on the electrical break up of liquid surfaces. Taylor studied the conditions under which a conically shaped liquid surface could exist, considering the influence of the electric field and the surface tension. He balanced the outward electrostatic pressure with the inward pressure caused by the surface tension, as shown in Figure 3.1. Mathematically:

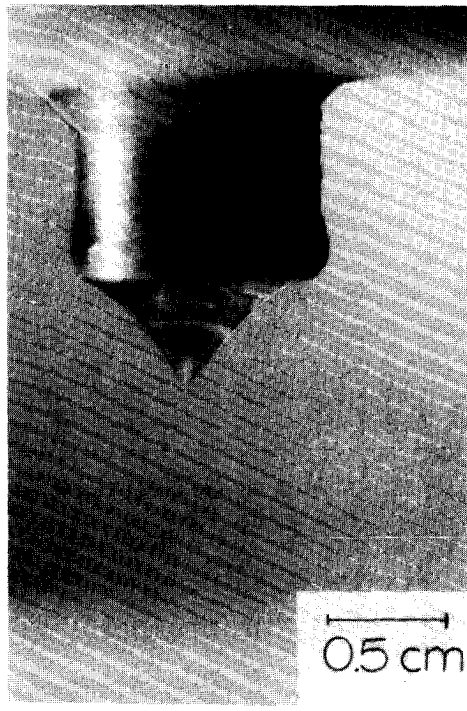
$$\frac{1}{2}\epsilon_0 E^2 = \frac{\sigma_s}{r \tan\alpha} \quad (1)$$

where E = electric field strength at cone interface [V/m]

$r \tan\alpha$ = a radius of curvature of a cone [m]

σ_s = surface tension of the liquid [N/m]

ϵ_0 = permittivity of free space [F/m]



(b)

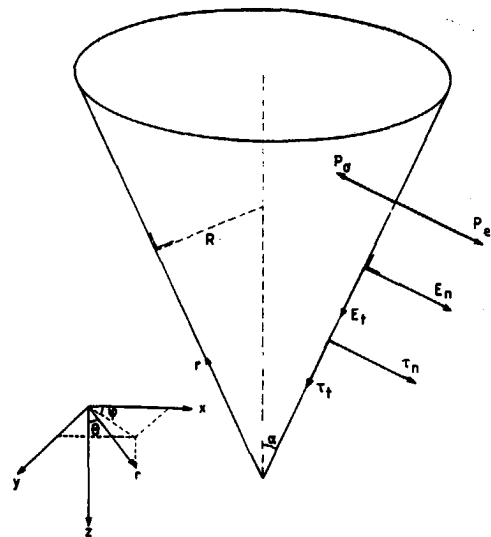


Figure 3.1 A photograph (a) and a schematic drawing (b) of the Taylor cone.

The potential distribution for a conical surface is (in spherical coordinates) is given by

$$V = V_0 + A\sqrt{R} \cdot P_{1/2}(\cos\theta) \quad (2)$$

with R =radial distance from apex [m]

V_0 =potential at the base of the cone [V]

$P_{1/2}(\cos\theta)$ =Legendre function of order $1/2$

θ =angle from horizontal axis

A = constant, depending on geometry and surface tension [$V/(m^{1/2})$]

Taylor calculated the field between a conical surface and a special counter electrode. He assumed an equipotential cone surface, $V=V_0$ (Eq.2), and assumed no pressure difference to exist over the liquid surface.

With E given as (cylindrical coordinates)

$$E = -\frac{1}{R} \frac{\partial V}{\partial \theta} \quad (3)$$

and with Eq.2, Eq.3 becomes:

$$E = -AR^{-\frac{1}{2}} \frac{\partial}{\partial \theta} (P_{\frac{1}{2}}(\cos \theta))_{\theta=\theta_0} \quad (4)$$

which satisfies (1) when (4) is rewritten into

$$E = \sqrt{\frac{2\sigma}{\epsilon_0 R \tan \alpha}} = R^{-\frac{1}{2}} \sqrt{\frac{2\sigma}{\epsilon_0 \cdot \tan \alpha}} \quad (5)$$

The Legendre function has only one value for zero between 0° and 180° . By assuming an equipotential surface ($V=V_0$), so that $P_{\frac{1}{2}}(\cos \theta)=0$ Eq. 4 can only be true for one value of θ , namely for $\theta=130.7^\circ$ (Gray 1953). Thus the cone half angle must be $\pi - 130.7^\circ = 49.3^\circ$.

The value of the factor A in Eq. 4 must have an appropriate value. Taylor calculated that this value must be $A = 4.53 \cdot 10^5 (\sigma_s)^{\frac{1}{2}}$. Taylor made several assumptions. He did not attempt to calculate the field between a cone and a plate, the usual configuration used, but looked instead only at the case of a conical surface and a special counter electrode. In Taylor's case an appropriately shaped curved counter electrode is used, causing the field lines to be perpendicular to the conical surface. Therefor Eq.(2) can be largely satisfied. Due to surface tension the pressure inside a liquid drop is normally higher than outside. A pressure head over the nozzle may increase the pressure inside a pendant drop. This causes a pressure difference to exist over the liquid gas interface. Taylor, however assumed no pressure difference across the surface. No pump or reservoir was used for liquid supply to the nozzle. His reason was that he looked at the point where the surface tension just balanced the electric pressure just before electrically charged drops are ejected from the cone. Therefor the assumption that the pressure difference over the surface of the cone is zero is a reasonable. Taylor also did not have to correct for any charge lost from the system, which otherwise has to be supplied by the power source.

Because of all these assumptions Taylor's theory has often been scrutinised. Furthermore it is too simple and not applicable to simple nozzle to plate configurations, especially in the field of the Liquid Metal Ion Sources (LMIS). It was however never the intention of Taylor to derive a equation like Eq.(1) to be applied

to all possible systems. He only proved that the observed cone could under certain assumptions be mathematically explained. In a series of papers, Cutler and co-workers (Chung, Miskovsky) (1983-1985) concluded that Taylor's theory was incorrect and too simple to describe liquid metal ion sources (LMIS), which are in fact Taylor cones of liquid metals. They objected to the field configuration assumed by Taylor and to his employing only a single Legendre function in the analysis. Allen (1985) correctly pointed out that Taylor did not describe the point to plane configuration as was used by Cutler *et al.*. Those authors stated that the assumption that pressure difference is equal to zero cannot be correct. In the case that the cone ejects droplets this is true. Liquid must be continuously supplied. In that case the surface of the cone is not a surface of constant pressure (Meesters *et al.* 1990^a).

Smith (1986) investigated the breakup of resistive liquids when subjected to high electric fields, thus producing aerosols. The influence of the various liquid properties, like conductivity, viscosity and surface tension were investigated and an approximate measurement of sizes was performed. No significant influence of the surface tension was found. By increasing the viscosity, the mean droplet size is increased and by increasing the conductivity the mean droplet size is decreased. This is in accordance with findings of Kelly (1976), who investigated the breakup of molten copper. The mean particle size from this conducting liquid was approximately 12 nm. This experiment demonstrates the possibility of producing very small nanometer range particles by using the Taylor cone, even when highly conductive liquids, like molten copper, are sprayed. Although highly conducting liquids are not usually easily sprayed making use of liquid cones, many reports on spraying of molten metals exist (Cutler *et al.* 1983-1985). The cones established using these metals are much smaller in size than the one described by Taylor and others, using semi-conducting liquids. The size of these metal cones is usually in the range of 10 to 100 nm, and of the semi-conducting liquids in the range of 1 to 15 mm. It might be possible that the viscosity and surface tension of the molten metals play an important role in stabilising the cones. Also, often those metals are sprayed in vacuum, where electric discharges leading to spark breakdown, often accompanying irregular breakup, do not occur.

Cloupeau and Prunet-Foch (1989) and Joffre and Cloupeau (1982, 1986) also reported experiments using the Taylor cone in which droplet size decreased with increasing conductivity. They also found that when the potential of the cone was increased, the electric current supplied to the cone also increased. At the same time the droplet diameter decreased. Another regime, the cone-jet regime, was defined by Cloupeau *et al.* (1989). This cone-jet regime was found to exist at higher flow rates. A small liquid jet is now formed, coming from the tip of the cone and breaking into drops of about 1 μm at frequencies up to $2 \cdot 10^7$ Hz.

Joffre *et al.* (1982) calculated the shape of an electrified meniscus by a numerical method. They balanced the hydrostatic pressure, the pressure caused by surface tension and the electric pressure of every point on the surface assuming a point to plate configuration. The droplet raised to a certain potential, was formed at the end

of a capillary tube. An earthed plate was placed perpendicular to the capillary axis. The researchers calculated the pressure balance, not of conically shaped menisci, but of liquid menisci of rounded shape. Nevertheless their calculations were in good agreement with their experimental results. They found that the space charge exerts a regulating effect on the field, but could not yet find a charge emission equation to model the charges emitted from the tip of the cones. Like many others they considered stable liquid menisci but not the dynamic situation of spraying drops from the apex of the cone. The apex was assumed to have a rounded-off shape, while the meniscus is pointed near the apex.

Hayati *et al.* (1987) proved the existence of a tangential shear in cones of semi-conducting liquids. He did this by photographing cones while spraying liquid. Lycopodium powder was suspended in the liquid. The direction of the liquid motion could thus be easily seen from the movement of the lycopodium particles. From streak pictures taken a symmetric axial circulation could be seen inside the cones. The direction of the fluid motion was seen to go down the surface of the cone and reverse upwards at the centre of the cone. From our own observations (unpublished) it was seen that the velocity was high near the tip of the cone and slow when the particles move upwards. The movement was also seen near the cone surface, where the liquid is strongly accelerated. There is a low speed back flow of liquid in the centre of the cone which means that not all the liquid is stripped off from the surface. This velocity profile is almost the complete opposite of the laminar flow seen in pipes, where the flow is highest in the centre and zero at the edges.

The origin of this motion was explained by Melcher and Taylor (1969). They combined the fluid motion to the electric field, since there is an interaction between the electric field and the fluid motion. These researchers explained this liquid flow inside the cone by stating that there must be an electrohydrodynamic shear stress. Such a shear stress is only possible when an interface simultaneously supports surface charge and has a discontinuity in the electric field. Thus this surface is subject to a tangential electric field. With liquids having sufficient electric charge, these charges will move towards the surface of the drop. The speed with which this charge accumulation takes place depends on the relaxation time τ of the charges in the liquid according to:

$$\tau = \frac{\epsilon}{\kappa} \quad (6)$$

with $\epsilon = \epsilon_R \cdot \epsilon_0$

ϵ_R = relative permittivity [-]

ϵ_0 = permittivity of free space [F/m]

κ = conductivity of the liquid [$\Omega^{-1}m^{-1}$]

The charges at the surface of the liquid give rise to a normal electric field causing a

normal electric stress τ_n (Figure 3.1^b) given by:

$$\tau_n = \frac{1}{2}\epsilon_0 E_n^2 - \frac{1}{2}(\epsilon - \epsilon_0)E_t^2 \quad (7)$$

with E_n = normal component of the electric field [V/m]

E_t = tangential component of the electric field [V/m]

It is this normal field stress which opposes the pressure caused by the surface tension, $\tau_{\text{surf.tension}}$ given by:

$$\tau_{\text{surf.tension}} = \frac{\sigma_s}{r \tan \alpha} \quad (8)$$

for a cone shaped meniscus (Figure 3.1^b).

For non-conducting liquids the speed with which the charges move towards the liquid gas interface is too slow. Therefor the shape of the hanging drop does not change to a conically shaped drop. Instead the drop will migrate up the nozzle to the highest field intensity (Hayati *et al.* 1987). This phenomenon is called dielectrophoresis.

For conducting liquids the surface will be charged to the Rayleigh limit causing. The surface to disrupts accordingly, although reports are found discussing the possibility of spraying highly conducting liquids (molten copper (Kelley (1976), LMIS (Cutler and Miskovsky *et al.* (1983-1985)).

The liquids of interest for this research are found in the intermediate region of conductivity, the so called semi-conducting liquids. Conductivities range roughly from 10^{-10} to $10^{-4} \Omega^{-1}m^{-1}$.

As explained by Melcher and Taylor (1969) and later used by Hayati *et al.* (1987) to explain the fluid motion, the cones must simultaneously carry surface charges and be subjected to a tangential electric field. Because of the semi-conducting nature of the liquids, both conditions are satisfied. When the potential is raised to a certain value, the drop will elongate. At a certain potential the drop changes into the conical shape, at the same time creating a very high field near the apex of the then formed cone. The high field causes charges to be emitted from the cone. Because of loss of charge from the cone a conduction current flows through the cone to compensate for the charges lost by the emission of the drops. The liquid, a semi-conductor, will act as a resistor to this current, causing a potential drop over the surface of the cone. This potential drop causes the tangential field at the surface of the cone. Depending on the conductivity of the liquid, new charges move in a certain time to the cone surface. At a certain potential the speed with which the charges move towards the surface of the cone is equal to the speed with which they are removed by the stripping of the liquid. The cone becomes stable at this value at the applied potential.

There thus exists a potential difference between the base and the tip of the cone. This

potential drop causes the tangential field given by;

$$E_t = \frac{dV}{dl} \quad (9)$$

with dV = potential difference [V]
 dl = distance along cone surface [m]

This tangential field gives rise to a tangential electric stress given by;

$$\tau_t = \epsilon_0 E_n E_t \quad (10)$$

It is this shear stress which also causes a downward longitudinal force which stabilises any perturbations on the surface, thus smoothing the surface of the cone.

When using a highly conducting liquid, where almost no tangential field exists, but only a normal field, unstable breakup occurs because of the lack of the stabilising tangential shear. This is seen when, for example, water is used as the sprayed liquid; here it looks as though Rayleigh-like breakup occurs.

Hayati *et al.* (1987^a) published extensive work done on the factors affecting the formation of stable jets and the break-up of these jets. They also published (1987^b) on the mechanisms of the jet formation and electric forces acting on semi conducting cones. The researchers concluded that the liquid conductivity plays a major role in the electric disruption of the liquids and that stable jets can only be produced using semi-conducting liquids. They used a finite element method to calculate the potential drop over the cone surface by solving the Poisson equation given as:

$$\nabla \cdot (\epsilon \nabla V) = \rho \quad (11)$$

The cone was divided into ten sections for which the potentials were calculated. From this the normal and tangential fields were calculated, so that the stresses could be derived. Hayati *et al.* found that the normal field strength E_n was almost constant over the cone surface (about $3 \cdot 10^6$ V/m), while the tangential field strength E_t increased with distance, increasing in the direction of the cone tip.

Smith (1986) tried unsuccessfully to calculate the filament diameter issuing from the cone by calculating the thickness of the surface which is stripped off because of the tangential shear.

3.2 References

- Allen, J.E. (1985) *J. Phys. D: Appl. Phys.* **18**, L59
Bailey, A.J. (1988) *Electrostatic spraying of liquids*, John Wiley & Sons, New York
Bailey, A.J., Balachandran, W. (1981) *J. Electrostatics* **10**, 99.
Bailey, A.J. (1974) *Sci. Prog. Oxf.* **61**, 555.
Cloupeau, M., Prunet-Foch, B. (1989) *J. Electrostatics* **22**, 135.
Chung, M., Cutler, P.H., Feuchtwang, T.E., Miskovsky, N.M., (1984) *J. Physique*, **45 C9**, 146
Chung, M., Cutler, P.H., Feuchtwang, T.E., Kazes, E., Miskovsky, N.M., (1984) *J. Physique* **45 C9**, 153
Chung, M., Cutler, P.H., Feuchtwang, T.E., Kazes, E., (1985) *Appl. Phys.* **A36171**
Chung, M., Cutler, P.H., Feuchtwang, T.E., Miskovsky, N.M., Sujatha, N., (1984) *Scanning Electron Microscopy IV*, Chicago SEM Inc. p.1547
Cross, J.A. (1987) *Electrostatics: Principles, Problems and Applications*, Adam Hilger, Bristol.
Drozin, V.G. (1955) *J. Colloid Sci.* **10**, 158.
Fernandez de la Mora J., Navascues J., Fernandez F., Rosell-Llompart J.,(1990), *J. Aerosol Sci.* **21(s1)**, 673
Garton, C.G., Krasuchi Z., (1964) *Proc. Roy. Soc. London*, **A280**, 211
Gilbert, W., *De Magnete*, (1600), p55, Translated by P.F. Mottelay, Dover Publ. (1958) p.89
Goldman, M., Goldman, A. (1978) *Gaseous Electronics Vol. I*, p219, Academic Press, edt. M.N. Hirsh and H.J. Oskam.
Gomez S., Kaqi T.,(1990), *Western state meeting of the combustion Institute*, La Jolla California, October 1990
Gray, (1953) *Quart. App. Math.* **11**, 311
Hayati, I., Bailey, A.I., Tadros, Th. F. (1986) *Nature* **319**, 41.
Hayati, I., Bailey, A.I., Tadros, Th. F. (1987^a) *J. Colloid Interface Sci.* **177(1)**, 205
Hayati, I., Bailey, A.I., Tadros, Th. F. (1987^b) *J. Colloid Interface Sci.* **177(1)**, 222
Joffre, G., Cloupeau, M. (1986) *J. Electrostatics* **18**, 147.
Joffre, G., Prunet-Foch, B., Berthomme, S., Cloupeau, M. (1982) *J. Electrostatics* **13**, 151.
Kelly, A.J. (1976) *J. Appl. Phys.* **47**, 5264.
Mackey, W.A. (1930) *Proc. Camb. Phil. Soc.* **16**, 421
Mackey, W.A. (1931) *Proc. Roy. Soc. A133*, 565
Meesters G.M.H., Reedijk A.M.E., Krekel A.P.C., Scarlett B., (1990^a) *Proc. 3^d Int. Aerosol Conf. Kyoto Japan* Ge60, 259
Melcher, J.R., Taylor, G.I. (1969) *Rev. Fluid Mech.* **1**, 111.
Miskovsky, N.M., Cutler, P.H., Feuchtwang, T.E., (1984) *Appl. Phys.* **A33**, 205
Miskovsky, N.M., Cutler, P.H., Kazes, E., (1985) *J.Vac.Sci.Technol.* **B3**, 202
Moriya, S., Adachi K., Kotaka T. (1986) *Langmuir* **2**, 155
Nolan, J.J. (1926) *Proc. Roy. Irish Acad* **37A**, 28
Robinson, M. (1961) *Trans. Am. Inst. Elec. Engrs.* **80**, 143.
Sherwood, J.D. (1988) *J. Fluid Mech.* **188**, 133.
Smith, D.P.H. (1986) *IEEE Trans. Ind. Appl.* **IA-22** (3), 527.
Sujatha, N., Cutler, P.H., Kazes, E., Rogers, G.P., (1983) *Appl.Phys.* **A32**, 55
Taylor, G.I. (1964) *Proc. Roy. Soc. A280*, 383.
US Patent No. 4,829,996 (1989) by T.J. Noakes, ICI, England
Vereshchagin, I.P., Gonik, A.E. (1980) *Izvestiya Akademij Nauk SSSR. Energetika i Transport* **18 (4)**, 95.
Vonnegut, B., Neubauer, R.L. (1952) *J. Colloid Sci.* **7**, 616.
Vonnegut, B., Neubauer, R.L. (1953) *J. Colloid Sci.* **8**, 551.
Wilson, C.T.R., Taylor, G.I. (1925) *Proc. Camb. Phil. Soc.* **22**, 728
Zeleny, J. (1914) *Phys. Rev.* **3**, 69.
Zeleny, J. (1915) *Proc. Camb. Phil. Soc.* **18**, 17.
Zeleny, J. (1917) *Phys. Rev.* **10**, 1.
Zeleny, J. (1935) *J. Franklin Inst.* **219(6)**, 659

*We light the deepest oceans, send photographs of Mars
We are so enchanted by how clever we are.
Why should one baby feel so hungry;
She cries!
Saltwater wells in my eyes....*

Julian Lennon (1991), Help yourself

4 Experiments based on visually seen phenomena

The liquid cones exhibit certain typical phenomena, which were observed. These observations are discussed in this next chapter. The shape of the cones change with changing applied potential. At onset the cones vibrate, accompanied by liquid ejection. Above this potential the cones become stable. At even higher applied potentials more cones are formed at the rim of the nozzle. Around the apex of the cones a gas discharge can be seen.

It will be shown that much of these phenomena are similar to corona discharges around solid needles. Simulation of the electric fields around liquid cones help to explaining some of the phenomena.

4.1 Visual observations of cone processes

The Taylor cone is a phenomenon seen when a liquid is exposed to a high electric field. The configuration used in the following experiments is the nozzle to plate configuration shown in Figure 4.1.

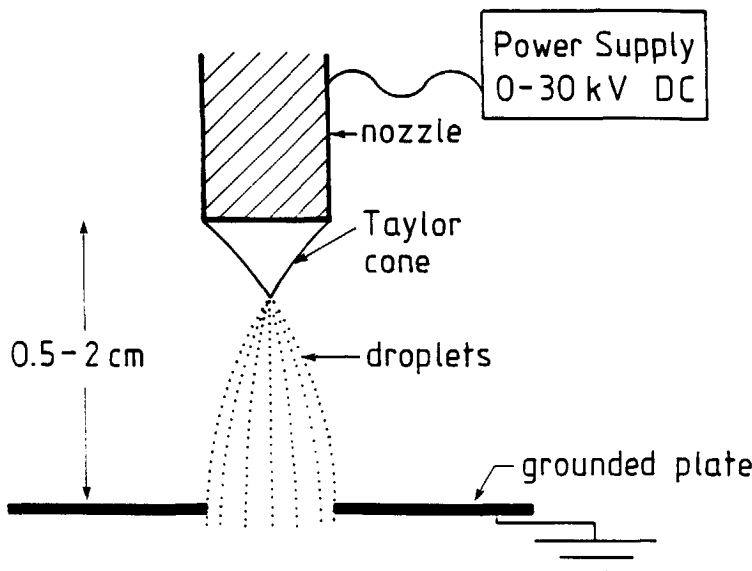


Figure 4.1 Configuration of experimental set up (outer nozzle diameter is 1.6 mm).

A semi-conducting liquid, with a conductivity roughly between 10^{-10} to $10^{-5} \Omega^{-1}\text{m}^{-1}$, flows slowly from the nozzle. The potential difference between the nozzle and plate is increased until at a certain potential the rounded off drop hanging from the nozzle will change into a conically shaped volume of liquid. This process however, is not yet completely stable. The cone pulsates for several seconds, after which the drop relaxes back to a more rounded off shape. The drop then grows again, and after a few seconds the pulsation is again seen. This process repeats itself. By increasing the potential on the nozzle just slightly, the frequency increases too, but the amplitude of the pulses decreases. Smith (1986) also reported on the pulsating mode of the cone. The highest frequency observed by Smith is about 300 Hz.

Visually two menisci are seen superimposed onto each other as is shown in Figure 4.2. One cone shaped and one more rounded off shaped drop can be seen, and a long jet-like filament is seen going downwards.

By increasing the potential on the nozzle even slightly more, a stable cone is formed producing a constant flow of small droplets, seen as a mist coming from the tip of the cone. The droplets coming from the tip are highly charged and disappear quickly to any earthed object available. Visually no pulses can be seen. This cone is now stable, and on increasing the potential even more it still remains stable, although the volume

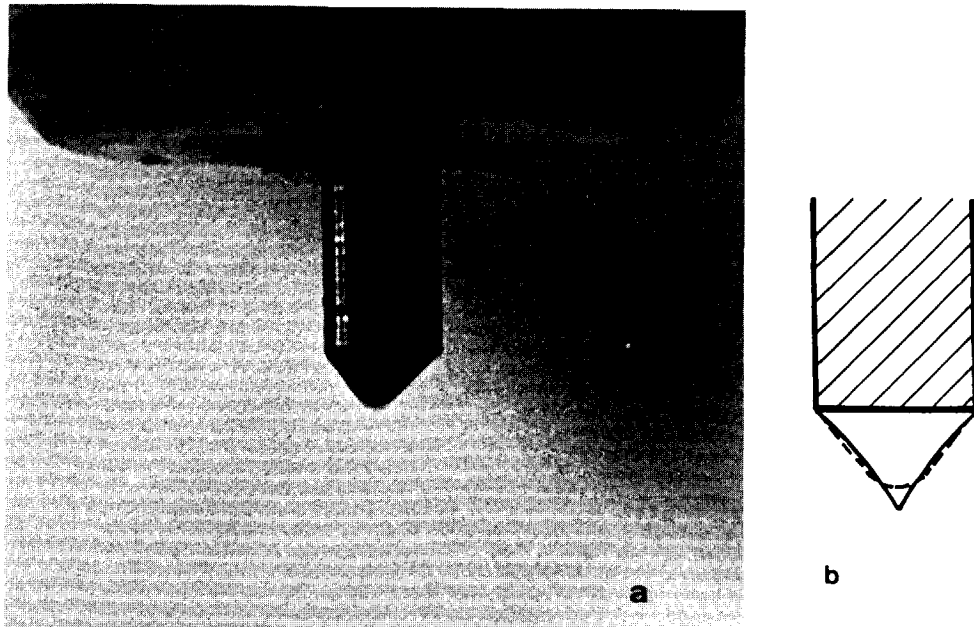


Figure 4.2 The shape of the cone as seen just at its threshold, a) = photograph, b) = schematic drawing.

of the cone decreases. Figure 4.3 shows photographs at five successive stages of the cone with increasing potential.

The cone angle increases with increasing potential.

At a certain potential the cone will become skew, and at even higher potentials the whole cone will be flattened, having an angle of almost 180° . By increasing the potential even more, several small cones are seen to form at the rim of the nozzle. With increasing potential even more cones are added to the rim; up to ten to fifteen can be seen.

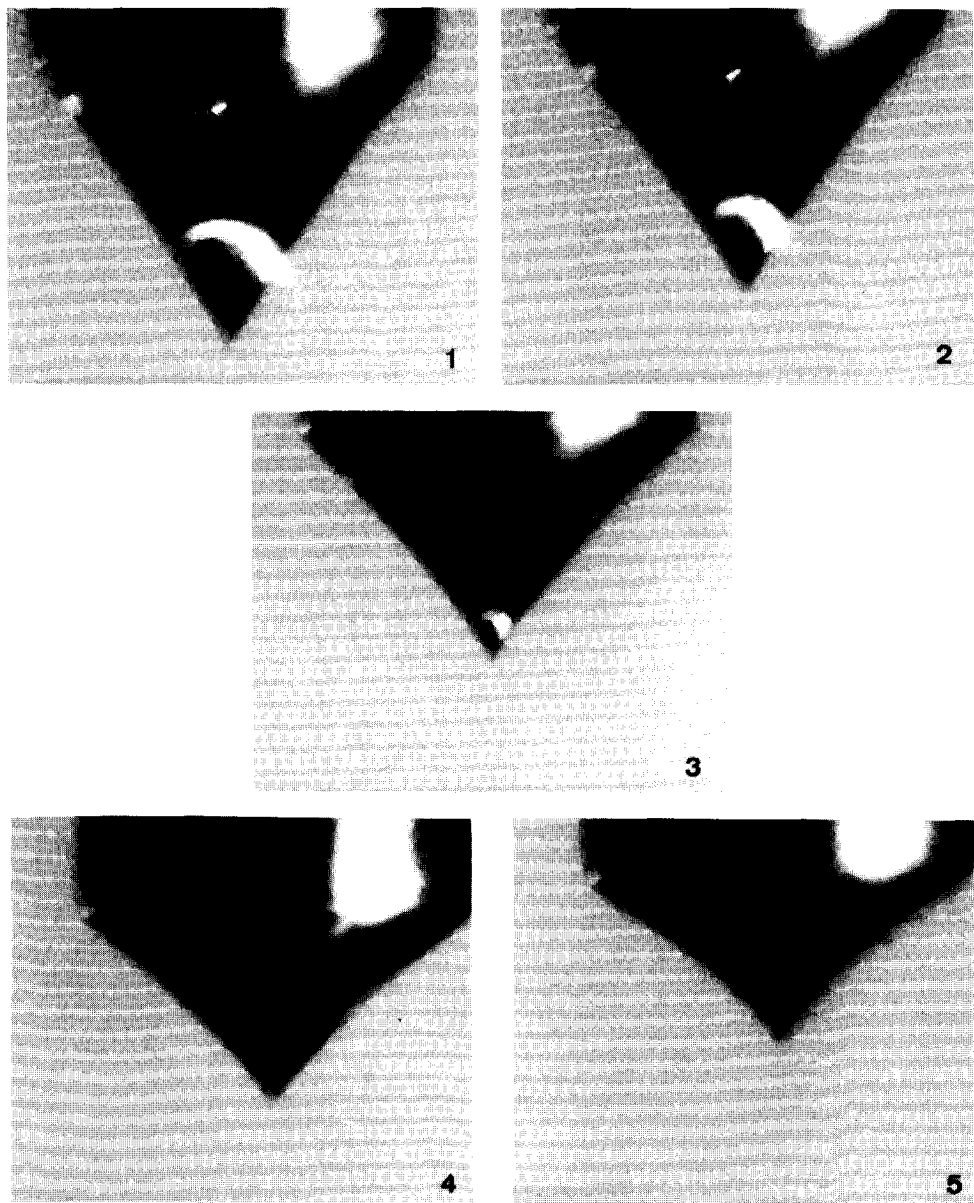


Figure 4.3 *Photographs of five successive shapes of the cones seen with increasing potential (1: $V=11.2\text{ kV}$, 2: $V=12\text{ kV}$, 3: $V=13\text{ kV}$, 4: $V=14\text{ kV}$, 5: $V=15\text{ kV}$)
Liquid used is ethylene glycol, $\sigma=46\text{ mN/m}$, $Qm=0.97\text{ mg/s}$*

4.2 Measurement of the current pulses of the cone

At a certain potential the drop hanging from the nozzle will pulsate between a more rounded off and conical shape. At a certain threshold potential the average current increases from about 10^{-10} to about 10^{-5} A. At this point the drop hanging from the nozzle is pulled into a cone shape, while simultaneously emitting droplets. After the droplet emission it relaxes back into the more rounded off cone shape. The frequency with which this occurs lies between 20-150 Hz. This frequency can be measured by observing the current-time behaviour. The pulses are detected on the average current measured, as is shown in Fig 4.4^a.

From the shape of the curve and the amount of charge released, one can conclude that these pulses are due to a space charge moving away from the droplet.

Space charge is an amount of charge in a space, in this case produced around the cone tip, consisting of charged droplets, clusters of charged molecules and ions. Due to the electric field these charges will move away from the tip of the cone. At the same time the space charge, inducing an electric field of its own, adds this field to the externally imposed field, reducing the field strength around the tip according to Poissons law;

$$\nabla \cdot (\epsilon \nabla \phi) = \rho \quad (12)$$

with $\nabla \phi$ = potential gradient (E) [V/m]

E = field strength [V/m]

ρ = charge density [C/m³]

ϵ = permittivity [F/m]

The pulses are not due to discharge phenomena like the discharge of a capacitor. In that case the curves would have shapes as drawn in Figure 4.4^b, resembling the discharge from a capacitor. The potential drop measured on the oscilloscope was too small to resemble a capacitor discharging (only a few volts (Fig 4.4^b)). By increasing the potential on the nozzle more, curves shaped as shown in Figure 4.4^c are seen. Again space charge is removed, but a small extra peak is seen. This process is stable in time and gives the highest frequencies of around 150 Hz.

By increasing the potential on the nozzle even more, a stable cone is formed producing a constant current in time without any pulses.

The shape of these measured current pulses are not unique. They are also seen in systems called corona discharges.

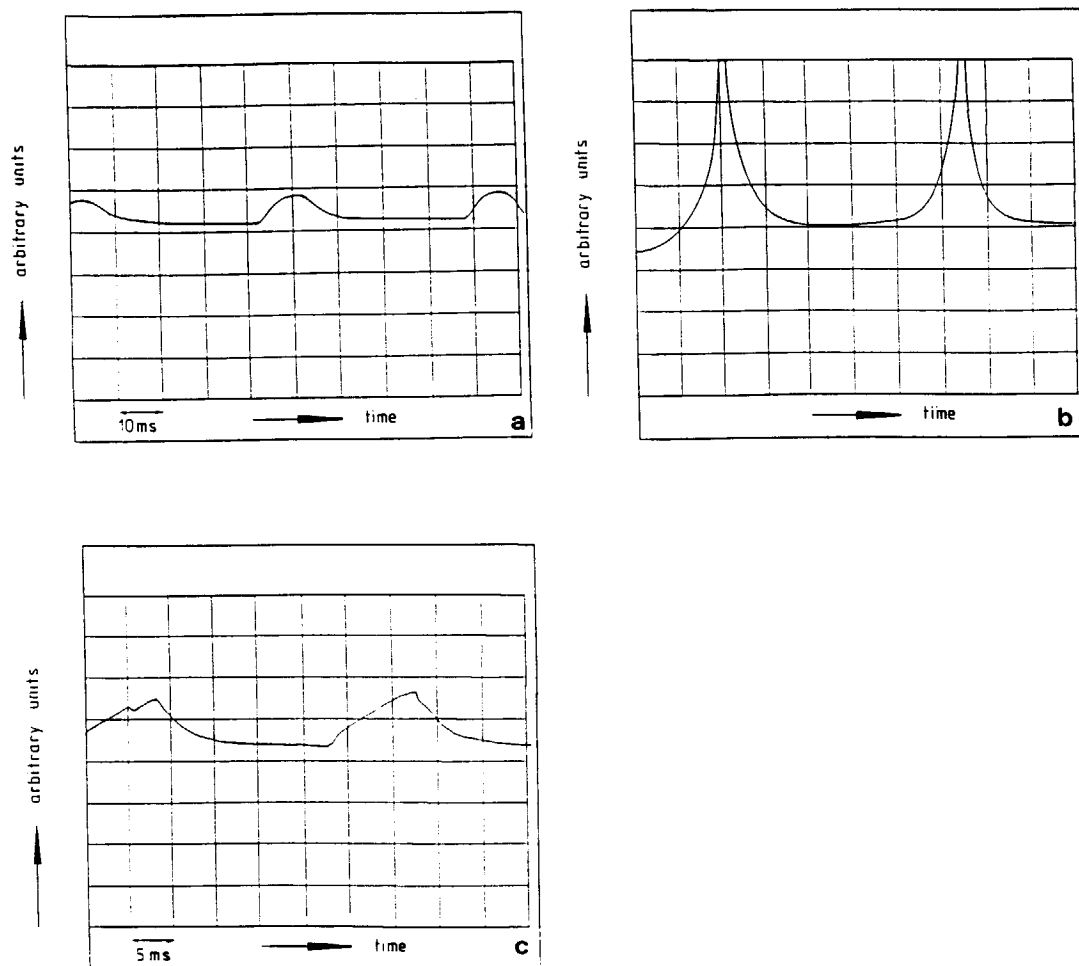


Figure 4.4 a:) Current pulses as measured when the liquid drop is just before its threshold becoming a cone, vibrating between cone and drop
b:) Current pulses from a capacitor, releasing its charge
c:) Current pulses as measured when the cone is just at its threshold state

4.3 Measuring corona discharge

4.3.1 Corona discharge

The production of cold plasmas at atmospheric pressure usually involves corona discharges. Corona discharges can be seen in the gas phase at high electric fields, usually where the field is strongly non-uniform. At these areas the gas is partially ionised.

The threshold of the corona discharge is characterised by an abrupt increase in the current between the electrodes and the appearance of a glow in the vicinity of the pointed electrode.

Below this potential the measured current is due to the collection of ions and charged particles from the air ($I \approx 10^{-14} A$) caused by cosmic rays and radiation of radioactive compounds. This is the so called Townsend regime.

The corona discharge is initiated by an electron which causes an avalanche of charged ions (Goldman and Goldman, 1978). In a point to plane configuration the avalanche develops near the pointed electrode. At a positive electrode the avalanche begins, in air at normal pressure and if free electrons are present, at a field strength of about $3 \cdot 10^6 V/m$. The discharge will now stabilise into a glow discharge if the potential on the pointed electrode is high enough. This discharge is called a streamer.

A streamer is, in the case of a positive corona, a channel of positive ions formed between the corona and the counter electrode. The space charge adds its field to the externally imposed field and facilitates the flow of positive ions through the channel. Streamers are formed before breakdown of the field. Figure 4.5 shows the current as a function of time, with the main stages of discharge, leading to a spark breakdown of the field (Marode *et al.*, 1979). The pulses are caused by the space charge released from the corona region. The extra peak seen on the pulses (2 in Figure 4.5), is caused by the streamer reaching the counter electrode. After this a constant current is seen without pulses. Still later the field breaks down through sparking.

In the electric field an electron, which is liberated from a gas molecule, moves towards the positive point. In its path it will excite and ionise more molecules. At the point of the streamer the electrons combine with the positive ions and give a photo-illumination effect. If the potential on the tip is not high enough the space charge releases itself from the tip and moves towards the counter electrode. This causes a current pulse as shown in Figure 4.4^a and 4.5¹. The space charge which forms during an impulse reduces the local field to a value insufficient to permit further multiplication. The space charge will have to move away before a new multiplication takes place. The time between those pulses determines the frequency of the corona and varies with potential up to a few kHz. This regime is called the autostabilisation or burst pulse regime. At the moment that the streamer reaches from the pointed electrode down to the counter electrode an extra peak is seen on the current, as shown in Figure 4.4^c and 4.5².

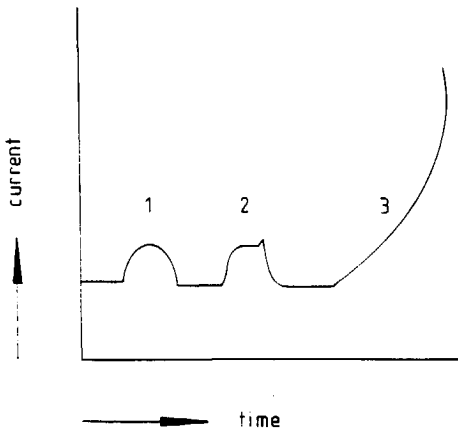


Figure 4.5 Schematic drawing of the current as a function of time, with the three main stages of discharge leading to spark breakdown (Olivier (1977), Marode (1977)) 1=streamer development, 2=streamer reaches counter electrode, 3=spark breakdown

Thus the current pulses seen at the threshold of the cones are similar in shape to those seen for coronas at the autostabilisation regime.

By increasing the potential even more the second regime, the pulseless glow regime, is entered. No pulses are detected any more because a fully developed channel of positive ions will be found which will reach down from the tip of the corona to the counter electrode. Because of the higher potential the whole active zone will have to reduce the high field at the tip to a field strength of about $3 \cdot 10^6$ V/m.

During the propagation of the streamer, the small zone which is the active site where the ionisation takes place, is illuminated (Marode 1977). This illuminated region can visually be observed as it glows, emitting light.

When liquids are sprayed corona discharges are observed too, as reported by Hayati (1986,1987), Bailey (1988), English (1948) and Zeleny (1917). Because the cones show a similarity with corona dischargers, photographs were taken of the cone in the dark. By regarding a system with a positive potential on a nozzle from which a liquid flows, at increasing the potential the drop will become conical and will start pulsating back into a more rounded off shaped cone. These pulses cause current pulses. Streamers are formed at the tip at the same time releasing droplets. By a slight increase in potential the streamer is powerful enough to reach the counter electrode to give a pulse as is shown in Figure 4.4c. As the potential is increased even more a stable

regime is reached where positive streamers and burst pulse coronas generate a positive space charge. By increasing the potential the pulseless glow regime with the characteristic surface glow occurs, increasing in area over the point surface of the cone with increasing potential.

As can be seen in Figure 4.6 there is a glow around the discharging needle, below, as is to be expected, but around the tip of the cone a glow can also be seen. When the potential is increased to a level that more small cones are established at the rim of the nozzle, the same glow is still seen (Fig. 4.7). However, more light emitting sites are seen as well; these occur at the places where the small cones are seen at the rim of the nozzle.

Hayati *et al.* (1986) investigated the difference seen in the discharge when different liquids were used. For conducting liquids like water and glycerol, glow discharge was observed at the surface of the cone. With insulating liquids like oils, the discharge occurred at the metal nozzle from which the liquid was flowing. They also found that the gas breakdown potential is very important. If the gas breakdown potential is lower than required for liquid instability, e.g. when He or Ne are used, electrostatic breakup will not occur. In gases with a breakdown potential higher than that required for liquid instability, e.g. air and N₂, spraying could occur.

The ionisation growth process leading to spark breakdown has been studied by many (Marode (1977, 1979), Hartmann (1975, 1978), Loeb (1965), Goldman (1978)).

Especially the space charge controlled growth, the streamer process, and the glow discharge is of special interest in this research. After the initial streamer phase the space charge generally leads to a further spark discharge development. This is of lesser importance in this research and is not discussed further.

In a point to plane gap in N₂ or air, most of the energy is used to ionise or excite the gas molecules. It is well established that in N₂ the main part of the electron energy goes into excitation of vibrational N₂-levels. Since the relaxation time of this stored energy is very short (0.01 to 1 μ s), only a small fraction of the energy is transferred into neutral heating of the gas. Most of the energy manifests itself as emission of light quants, causing illumination of the discharge area (Hartmann (1975), Vedenov *et al.* (1976)).

Ionisation means that molecules dissociate into positive and negative ions and electrons. But because there are also many free electrons in this regime they will collide with free gas molecules (A). This leads to loss of kinetic energy of the electrons (e⁻) and possible excitation of the gas molecules (A*) according to;



The electrons will be accelerated in the electric field, enabling them to excite more gas molecules. This will continue until the field strength becomes too low to sufficiently accelerate the electron. The excited molecules will remain so for only 0.01-1 μs (Cobine, 1958) and return to a lower energy level while simultaneously emitting a light quant:



If their kinetic energy is high enough, the electrons are also able to ionise the gas molecules, giving:



But ionised molecules can also recombine with electrons giving:



while at the same time releasing a light quant. Thus one electron can excite or ionise many molecules. This occurs because every time its kinetic energy is (partly) lost it will repeatedly accelerate in the electric field. This process stops only when the field strength is not strong enough.

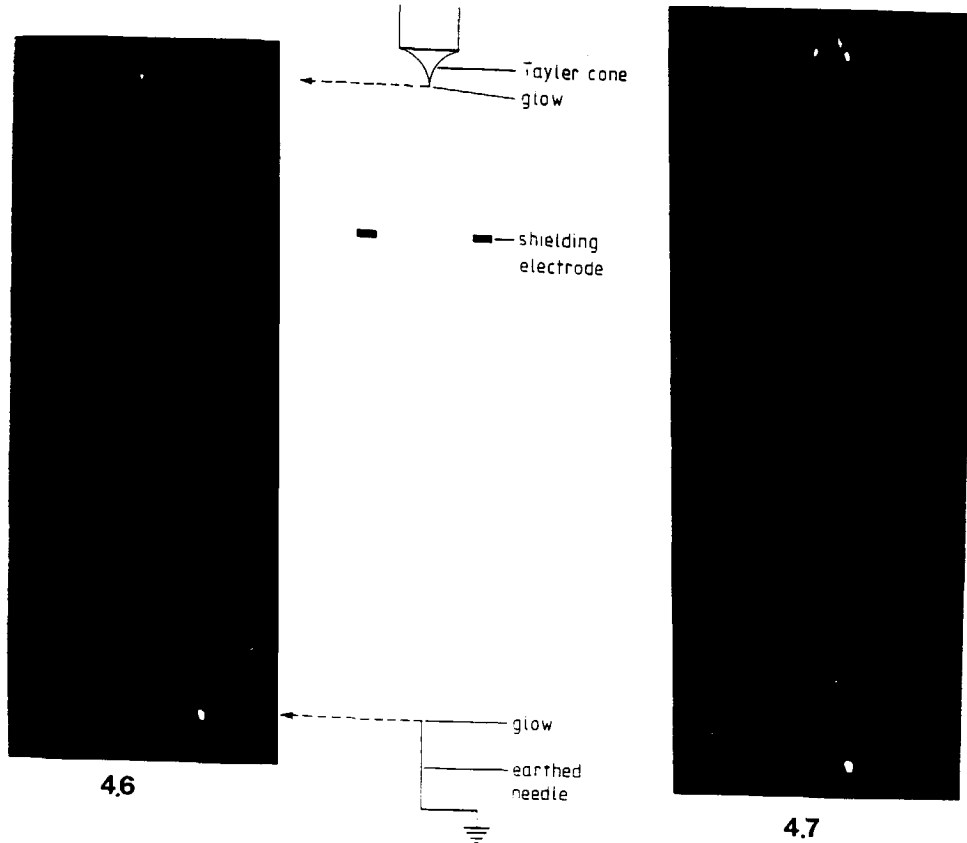


Figure 4.6 Photograph taken in the dark, of the DAG when working, showing the discharge areas. A schematic drawing of the whole setup is drawn along side the picture.

Figure 4.7 Photograph taken of the multi cone regime, showing several glow discharges

4.3.2 Measurements of light emission from the corona glow

In order to establish whether or not the liquid cone takes part in the discharge, or that the observed light comes only from the gas discharge around the tip of the cone, measurements were carried out to find the wavelengths of the emitted light. A mixture of Di-Octyl-Phthalate (DOP) and methanol 1:1 (v/v) was sprayed during the experiments, to determine wavelengths of the light coming from the tip of the cone. In gas discharge processes the electron energy is mainly used for bringing N₂ into the excited vibrational levels. Table 4.1 gives the measured and theoretical wavelength of the N₂ excited states, the N₂ C³Π_u-B³Π_g second positive systems, and an ionisation state called the first negative system of N₂.

The results of the measurements are shown in Figure 4.8. Table 4.1 give the wavelength of the peaks detected.

The only strong bands detected were the N₂ bands, namely several second positive bands (N₂^{*} → N₂ + hν) and the first negative band (N₂ + N₂⁺). Also the O-H, C-H and C-O bands were measured. Only a very weak signal of the O-H band ($\lambda=306.30$ nm) could be detected. This is very likely caused by the water molecules present in the ambient air. The O-H band, originating from the DOP or methanol, C-H and C-O band were also to be expected in the spectrum; these, however, could not be detected. This also leads to the conclusion that the phenomenon of the emitted light around the tip of the cone is caused by a gas ionisation process. This is similar to what is seen with coronas around solid needles, where there can only be a gas ionisation surrounding the tip of the solid needle. Because what is measured is the same as for coronas around solid needles, and since no C-O and C-H bands could be detected when using the liquid cone, the cones are not involved in the ionisation process.

Table 4.1 The measured and literature values (Hartmann and Johnson, 1978) of the first negative and several of the second positive band of N₂ of the glow around the tip of the cone.

band	$\lambda_{\text{measured}}(\text{nm})$	$\lambda_{\text{lit}}(\text{nm})$
N ₂ ⁺ (0-0)	391.44	391.4
N ₂ (3-6)	389.46	389.5
N ₂ (3-2)	311.60	311.7
N ₂ (3-1)	296.20	296.2
N ₂ (2-5)	394.30	394.3
N ₂ (2-1)	313.60	313.6
N ₂ (2-0)	297.68	297.7
N ₂ (1-4)	399.84	399.8
N ₂ (1-0)	315.93	315.9

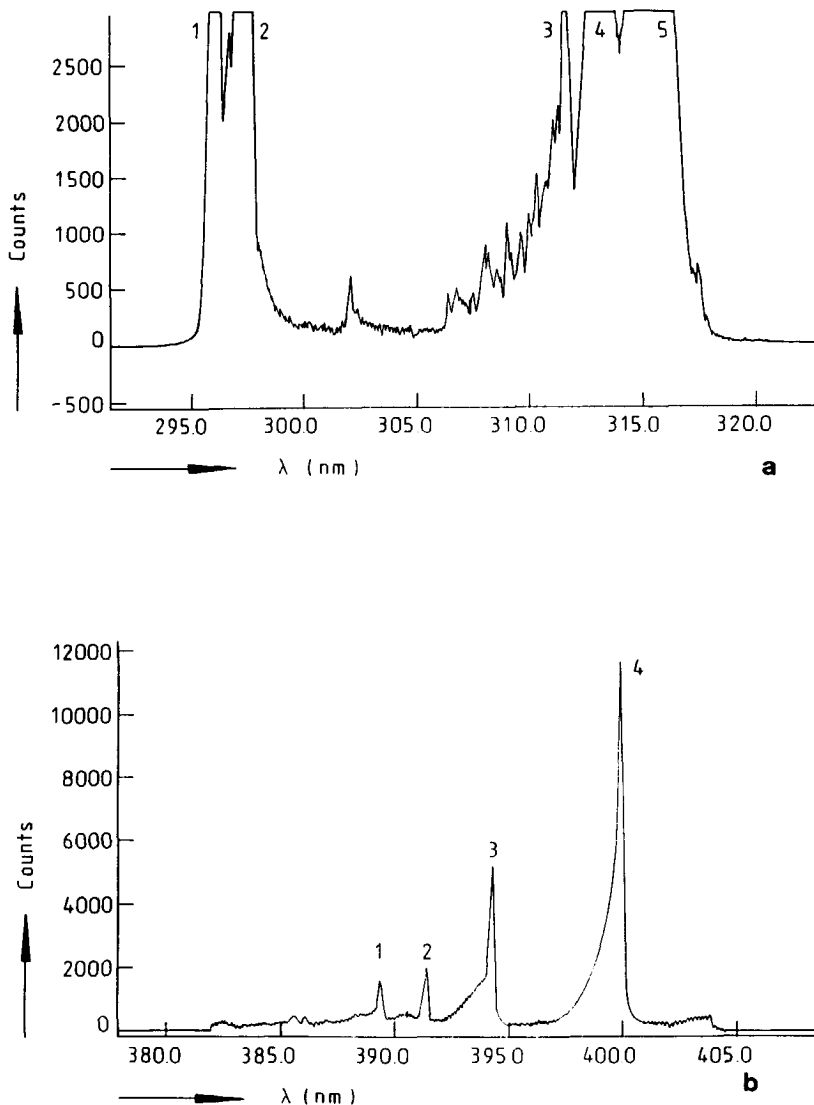


Figure 4.8 Measured spectrum coming from the cone when a glow discharge is established. (a: 1=(3-1), 2=(3.0), 3=(3-2), 4=(2-1),
5=(1-0). b: 1=(3-6), 2=(0-0), 3=(2-5), 4=(1-4) see also Table 4.1)

4.4 Current voltage characteristics

When looking at the whole current voltage characteristic of the cone and comparing this with the current voltage characteristic of a solid needle discharge, a remarkable difference is seen. We next discuss this.

4.4.1 Current voltage characteristic of solid needles

First the current-voltage characteristic of a solid needle is discussed. By increasing the potential of a needle in a point to plane configuration, the current measured is low (10^{-10} A). In the zone between the needle and the plate, charged particles are collected from the ambient air. At a certain point the potential on the tip of the needle becomes so high that charges are emitted from the needle. Because of this the average current increases to 10^{-6} to 10^{-5} A. The high field causes a space charge to develop around the apex of the needle. A streamer is formed which develops away from the apex. This space charge will add its field to the externally imposed field and will facilitate the flow of the ions formed between corona and electrode. Due to the space charge the field around the apex will decrease, causing the development of the streamer to stop. When the space charge has moved away from the apex the field will increase again and at its threshold cause a new discharge. This repetitive process causes the pulses on the measured current. This regime is called the autostabilisation or burst pulses regime. The corona is unstable on its threshold. The fluctuations vary in frequency up to a few kHz with increasing potential.

By increasing the potential on the needle more the second corona regime is entered. This regime is called the pulseless glow regime. A steady glow discharge is established. The glow can be seen existing at the apex. The field at the apex is constant. The space charge reduces it, causing it to remain constant at increasing potential. When the potential is increased more the current still continues to increase, as Figure 4.9^a shows. This process is stable, meaning that current pulses can no longer be detected. By increasing the potential even further, the third corona regime occurs. This is called the stable impulsive discharge regime and is also characterised by current pulses.

4.4.2 Current voltage characteristic of the cones

In order to compare the cones with the solid needle discharge the current voltage characteristic of the cone is measured. When measuring the current voltage characteristic of the liquid cone, the following is seen. At low potentials (Fig. 4.9^b) only the charges collected from the ambient air are captured. At a certain threshold potential the average current increases from around 10^{-10} to around 10^{-5} A. At this point the drop hanging from the nozzle is pulled into a cone shape, while at the same time it emits droplets, but relaxes back into the more rounded off cone shape after the droplet emission.

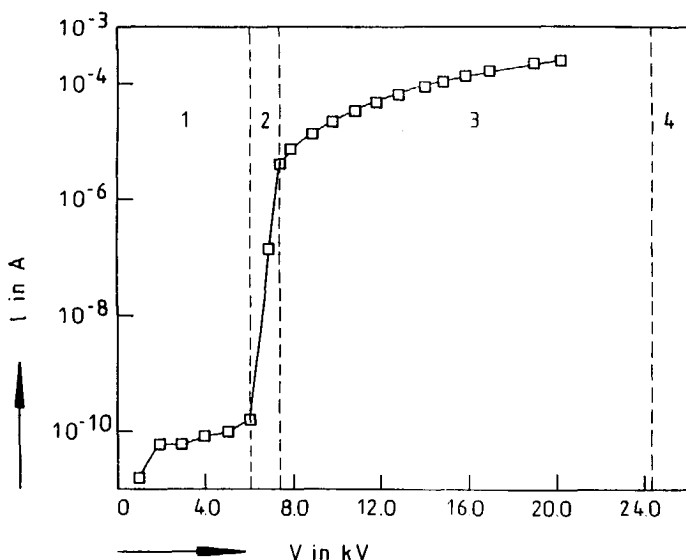


Figure 4.9^a Current voltage characteristic for a corona discharge at a positive needle. (1=pre-corona-onset regime, 2=autostabilisation regime, 3=pulseless glow regime, 4=impulsive discharge regime)

This last regime is similar to the first corona discharge regime, the burst pulses regime. Space charge is built up around the tip of the cone, but it moves away due to the electric field. This space charge mainly consists of charged drops. It reduces the field around the apex of the cone, causing the droplet to relax back, due to the surface tension, into a more rounded shape. When the space charge has moved away and the drop has regrown, the field is able to pull the drop into a cone shape, after which the process repeats itself. The frequencies of these pulses is much lower than

the pulses measured using solid needles. This difference can be explained as follows. If one compares the electrical mobility of a positive ion to the mobility of a positively charged droplet of about $1 \mu\text{m}$, the following is found. The electrical mobility Z_p of a single charged positive ion is $1.4 \cdot 10^{-4} \text{ m}^2/\text{Vs}$ (Davies 1966, Hinds 1982). In the strong electric field E (about $3 \cdot 10^6 \text{ V/m}$) this leads to a terminal electrical velocity v_{TE} of about 364 m/s according to;

$$\bar{V}_{TE} = Z_p \bar{E} \quad (17)$$

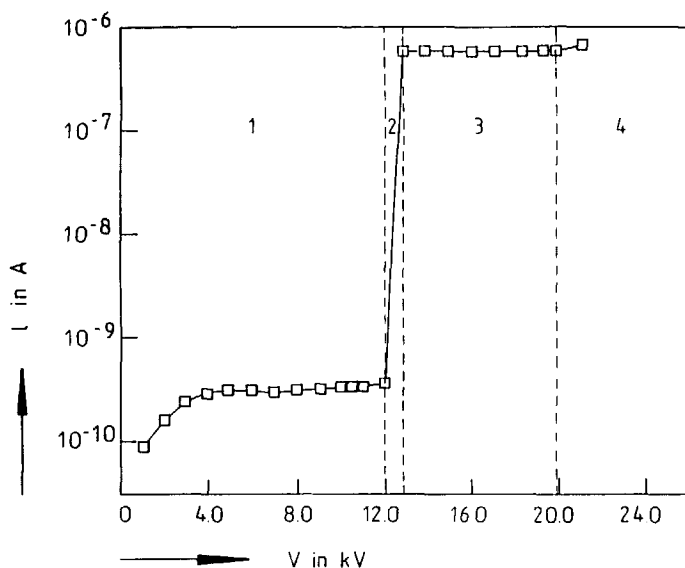


Figure 4.9b Current voltage characteristic of the liquid cone (1=pre-cone-onset regime, 2=autostabilisation regime, 3=pulseless glow regime, 4=multiple cone regime)

The electrically charged droplet mobility is determined from our own measurements. At a flow rate of 13.7 ml/h , an electric current $I=0.6 \mu\text{A}$, and an average droplet diameter $d_v=1.58 \mu\text{m}$, the average charge/drop is $3.26 \cdot 10^{-16} \text{ C}$, assuming that all the charge is carried by the droplets produced. This is only 1.35% of the Rayleigh limit. The Rayleigh limit is the limit to which a liquid droplet can be charged. At this limit

the mutual repulsion of electric charges within the droplet exceeds the confining force of the surface tension (σ_s). The limiting charge per drop is given by:

$$(ne)_{\text{Rayl.}} = \pi \sqrt{8 \epsilon_0 \sigma_s d^3} \quad (18)$$

with $(n e)_{\text{Rayl.}}$ = maximum charge per drop according to the Rayleigh criterium [C/drop]
 d = droplet diameter [m]

$(n e)_{\text{Rayl.}} = 2.4 \cdot 10^{-14}$ C/drop for the previously mentioned drop. To determine v_{TE} , the factor Reynolds squared times the drag coefficient, i.e $C_D Re^2$, has to be calculated using;

$$C_D Re^2 = \frac{8 n e E \rho_g}{\pi \eta^2} \quad (19)$$

with ρ_g = gas density [kg/m^3]
 η = gas viscosity [$\text{Pa} \cdot \text{s}$]

By calculating the terminal electrical velocity, v_{TE} , of a droplet of this size and charge in a field of about $3 \cdot 10^6$ V/cm, $C_D \cdot Re^2 = 9.5$, giving $Re = 0.4$ (Hinds, 1982), from which v_{TE} can be calculated as $v_{TE} = 3.4$ m/s. This is about a hundred times as slow as the terminal electrical velocity of positive ions.

The frequency of positive streamers is in the order of a few kHz. The frequency of the current pulses measured when using the liquid cone varied from 25 to 150 Hz. This is a factor of about fifty to a hundred lower than the frequency of pre-onset streamer pulses. This difference is the same order of magnitude as the difference in mobility.

Thus the lower frequency of the current pulses can be explained by the difference in the mobilities of the formed species. More accurate measurements must be done. This is a difficult because one has to compare two systems, a solid needle with known dimensions and a liquid cone with varying dimensions.

By increasing the potential on the nozzle even more, a stable cone is formed producing a constant current in time without any pulses. Nevertheless a difference can be seen in the current voltage characteristic between the needle and the liquid cone. Unlike the needle corona discharge, the current does not increase much when increasing the potential on the nozzle. This can be explained by the fact that the space charge formed around a solid needle corona discharge adjusts itself to the potential and the configuration of the system. This is necessary to keep a constant field strength around the needle tip with increasing potential. The area with the critical field strength moves further away from the needle with increasing potential,

causing the area to increase too. Because of the increase in area the flux of charges through this area can increase as well, which explains the increase of current with increasing potential.

Looking at the cone, something different is observed and measured. The current does not change much with increasing potential. There is corona discharge, as was proven by taking pictures of the cone in the dark. These showed a glow around the apex of the cone, caused by the discharges. When the potential on the nozzle is increased a little the current first increases too but within a few tenths of a second, it falls back to the previous level; simultaneously the cone hanging from the nozzle changes in shape. The cone angle increases with increasing potential, thus decreasing the surface area, as shown in Figure 4.3, where pictures of the cones at different potentials are given. This is explained by the fact that when the potential on the cone increases, the local field around the cone also increases. A solid needle corona discharge would increase the amount of space charge, thus reducing the local field strength. A cone starts to emit more droplets, causing the space charge to increase too. However, because at the same time the electric field stresses also increase, in particular the tangential stress τ_t , the cone surface will be stripped off faster. Because the liquid flow rate is kept constant, the volume of the liquid cone will decrease, increasing the cone angle. Because of this the electric surface stress will decrease again, decreasing the space charge to a lower level. Thus a new steady state is established, which is essentially the same as the previous one. The only thing changed is the shape of the liquid cone. The tangential surface stress remains the same, causing the same amount of charge to be released from the cone for reducing the local field. The effect of increasing the potential is mainly compensated for by changing the shape of the cone; the amount of space charge remains equal, as can be seen from the current voltage measurements. This whole process is only possible because the stripping off of the cone surface is caused by the tangential stress τ_t , which exists because of the semi-conducting nature of the liquid.

So if the potential on the cone is increased the cone angle will increase too, causing the amount of charges removed to remain almost constant. A corona discharge around a solid needle can not change its shape; thus the amount of charge released must change.

4.5 Mobility of charged particles

From the equation of Townsend given as:

$$I = C Z_p V (V - V_s) \quad (20)$$

with I = current [A]

V = potential [V]

V_s = potential where corona discharge starts [V]

C = constant which depends on the geometry of the space charge [C/Vm^2]

one can get an idea about the mobility of the charged particles. This is done by plotting I/V against the applied potential V , and by rewriting equation (20) into

$$\frac{I}{V} = C Z_p V - C Z_p V_s \quad (21)$$

From the slope of the line one gets the value of CZ_p , and from the interception with the I/V axis the value for $CZ_p V_s$. The meaning of these plots is to establish if the velocity of the space charge removed from the system is removed at a constant velocity, independent of the applied potential. In that case the slope of the plotted line has to be constant in order to be able to conclude that the mobility is constant in the potential range examined. When two slopes are seen in the plot, the mobility changes at a certain potential, as can be seen in Figures 4.10 and 4.11.

In Figure 4.10 the I/V versus V plot is given for the regime for which the current pulses are measured, the burst pulse regime.

The slope of the curve is calculated as being $-5.2 \cdot 10^{-15} A/V^2$ and the constant $CZ_p V_s$ as $9.17 \cdot 10^{-11} A/V$. A straight line is obtained, proving that the mobility of the charged particles is constant with increasing applied potential.

Figure 4.11 shows the I/V versus V plot of the second corona regime, the pulseless glow regime. Here the slope is $-1.7 \cdot 10^{-14} A/V^2$ and the constant equals $4.37 \cdot 10^{-10} A/V$. Between 7.5 and 8 kV the slope differs from the rest of the curve. This means that between 7.5 and 8 kV the space charge is removed at a speed different from that in the region from 8 to 11.2 kV.

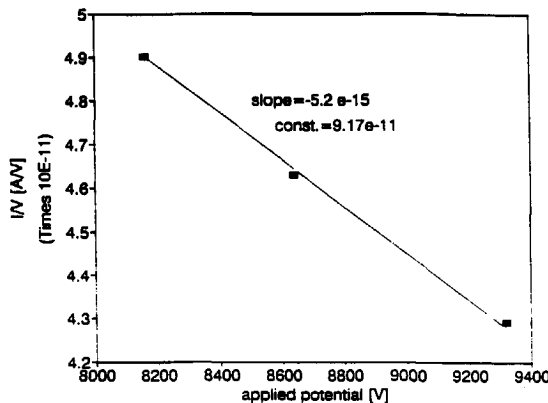


Figure 4.10 I/V as a function of the applied potential for the burst pulses regime

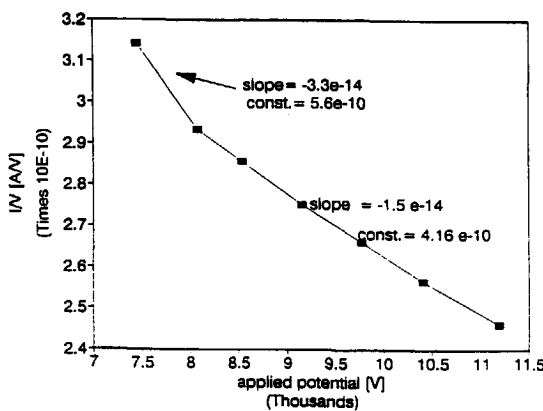


Figure 4.11 I/V as a function of the applied potential for the pulseless glow

4.6 Cone angle

A software package called Ansoft by Maxell is used to calculate the potential distributions over the cone surface. Detailed description of the simulation process is given later. The potential distribution over the cone surface is calculated by solving the Poisson equation for the whole problem space, consisting of the nozzle, liquid cone, earthed ring and surrounding medium. The problem space consists of about two to three thousand mesh points. A finite element method is used to solve the problem. In the early beginning of the research we noticed that the cone angle (α in Figure 3.1^b) was not a constant as described by Taylor (1964). The cone angle changed with changing potential applied to the nozzle. Figure 4.12 shows the cone angle as a function of applied potential at different liquid flow rates using two different liquids. The liquids used are ethylene glycol ($\sigma = 0.046 \text{ N/m}$, flow rate between 0.42 and 1.18 mg/s = 1.36 to 3.83 ml/h) and a mixture of ethylene glycol and water 2:1 (v/v) ($\sigma = 0.059 \text{ N/m}$, flow rate = 0.878 mg/s = 2.70 ml/h). It is clear that the cone angle is not a constant but a linear function of the applied voltage. The slope of all the curves is identical. The curves for the pure ethylene glycol do not change with increasing flow rate. The position of the curve changes when another liquid is used, although again the slope remains constant. Hayati *et al.* (1986) also found that the slope remained constant with varying flow rate, but the same cone angle was found at higher potentials when using higher flow rates. These researchers used flow rates of 12.3 and 60 ml/h. As mentioned above, in our experiments, however, no difference was found using different flow rates. This is probably caused by insufficient variation in flow rates.

The slope of the line is roughly constant and also does not change much when using another liquid, as can be seen in Table 4.2.

From the results presented in Table 4.2 we see that the average cone angle per kV for pure ethylene glycol equals 4.3, and for the mixture of ethylene glycol and water equals 4.5. For a mixture of Isopar with butanol Hayati *et al.* (1986) found a slope of about 4.5 °/kV.

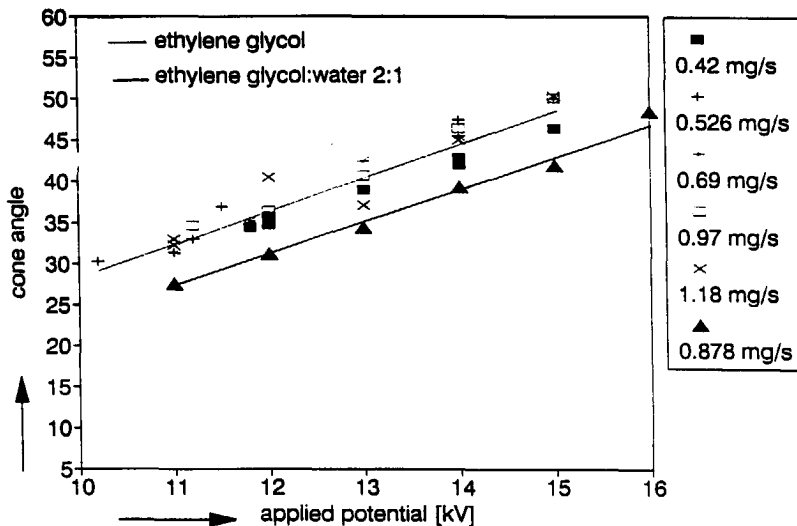


Figure 4.12 Cone angle as a function of applied potential, using different flow rates and two different liquids

Table 4.2. Slope of the cone angle line as a function of applied potential

liquid	flow rate [ml/h]	slope [$^{\circ}$ /kV]
ethylene glycol	1.36	4.2
	1.71	4.5
	2.24	4.6
	3.15	3.9
	3.83	4.4
ethylene glycol : water (2:1 w/w)	2.95	4.5
Isopar + butanol (Hyati <i>et al.</i>)	12-60 ml/h	4.4

4.7 Potential drop over cone surface

A remarkable feature is seen when the potential drop over the cone surface is plotted as a function of the potential applied to the nozzle. When the potential is increased the cone angle also increases, thus decreasing the base-apex distance. However, but the potential drop over this base-apex distance remains the same, also at different flow rates; this is shown in Figure 4.13.

When the potential is increased the cone regulates its shape such that the potential drop over the cone surface remains constant. Because the current measured coming from the cone remains the same, and the flow rate is kept constant using a syringe pump, and the drop size does not change, we must conclude that the shear stresses must remain almost the same with increasing potential.

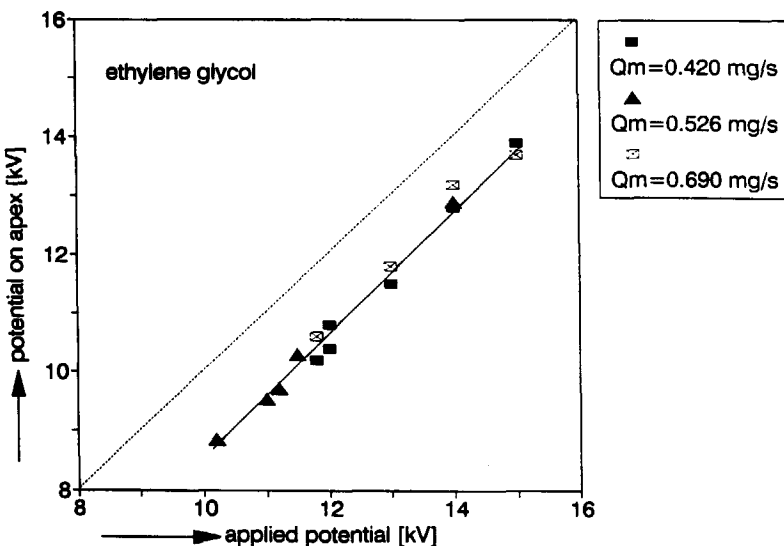


Figure 4.13 Potential drop over the cone surface as a function of applied potential, at several flow rates.

4.8 Multiple cone regime

At increasing potential, the cone angle continuously increases more and more, eventually causing the liquid cone to reach an angle of almost 180° .

At this point two or three cones are formed. These are necessary to remove all the space charge, this in order to keep the field strength at about $3 \cdot 10^6 \text{ V/m}$. The cone can not change its shape any more. Furthermore charges have to be removed to get a larger space charge, in order to reduce the local field strength. This can only be done by creating more cones, at the same time creating more glow discharges for supplying more charge. These cones formed at the rim of the nozzle are much smaller than the first cone. By further increasing the potential, more cones are formed at the rim of the nozzle. This can also be seen on the current voltage characteristic of the cone to plane measurements (Fig. 4.14). Every time a new cone is added onto the rim of the nozzle the current increases to a higher plateau. The average droplet diameter of the droplets produced remains the same. The values of the current plateau are dependent on the liquid flow rate (Figs. 4.14 and 4.15).

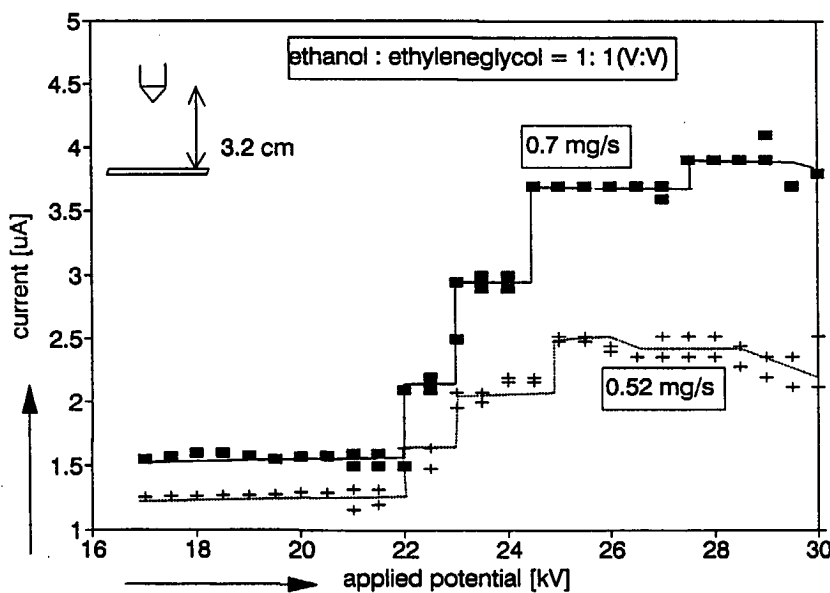


Figure 4.14 V-I characteristic of the cone regime extending into the multiple cone regime for two liquid flow rates.

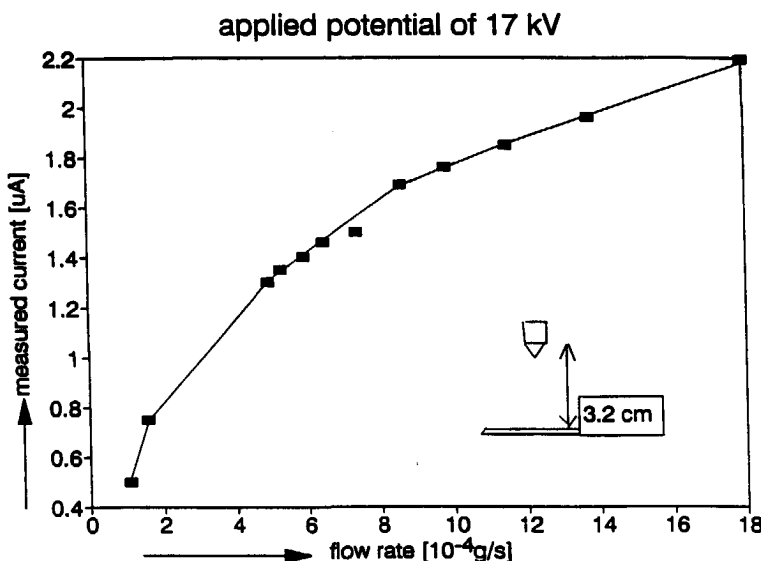


Figure 4.15 Measured current of a single cone as a function of the liquid flow rate.

The cones on the rim move around when a new one is added, but become steady when the potential is increased a little more. This is a well-known effect of coronas placed close together, each one at its turn takes over the emitting process. When going from one current plateau to another, usually one cone is added, but soon disappears again, coming back and disappearing etc. This fluctuating effect is easily explained by the fact that one cone extra at that certain potential causes too much current to be removed from the system, causing the cone to disappear again; but then not enough charge is removed and one extra cone is needed, and so on.

Due to limitations of the high voltage source used, which can apply a maximum of 30 kV to the nozzle, the maximum potential used was 30 kV. Up to this limit no pulses on the current could be measured. The third corona regime, the stable impulsive discharge regime, could not be found when operating the cone.

4.9 Hysteresis in the current voltage curve

The current voltage characteristic of the liquid cone exhibits hysteresis. At a certain threshold value V_1 , the hanging drop changes abruptly into a cone shaped drop. It remains so when the potential is increased. However, when the potential is decreased again, at a potential V_2 , the cone shaped droplet relaxes back into the drop shaped drop. The value of V_2 is lower than V_1 , as shown in Figure 4.16. This is a

phenomenon for coronas known, but not yet well investigated. In this area the system is in a metastable region.

The hysteresis can be explained as follows. By increasing the potential from $V=0$ to $V=V_1$ the current remains low (about 10^{-10} A). Here the surface stress exceeds the electric stress over the liquid surface. At $V=V_1$ the surface stress balances the electric stress exactly. A slight increase in V destroys this equilibrium, and the cone-like structure develops. The tangential stress is initiated by the fact that the first charges are removed by several large drops. Because new surface charges have to be supplied by the system, the tangential stress is induced, and stabilises the cone structure. In this emitting mode the electric and surface tension stresses are out of balance, as is shown in Figure 4.17.

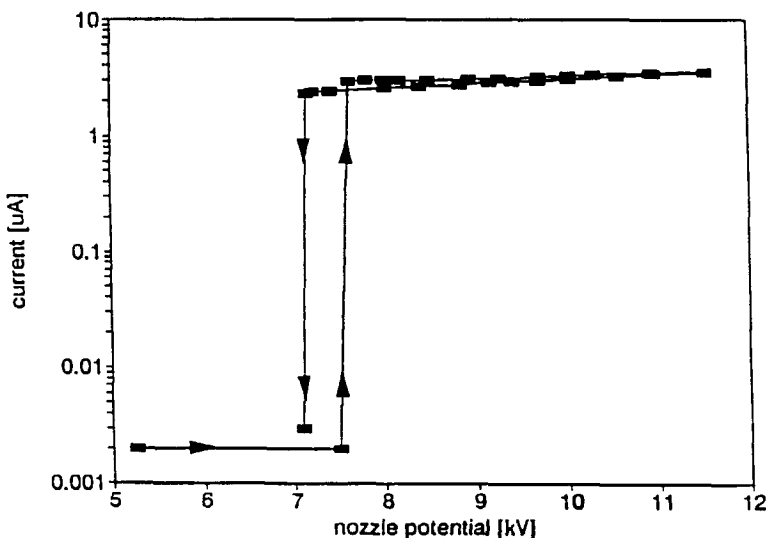


Figure 4.16 Hysteresis in the current voltage characteristic near the threshold of the cone

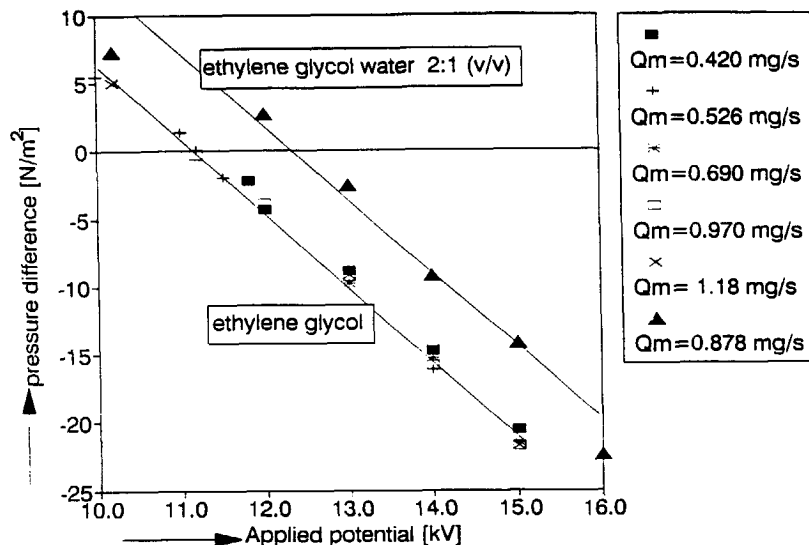


Figure 4.17 The difference between the surface stress and the electric stress as a function of the applied potential.

The liquid is under tension by an excess pressure equal to the amount by which the electric stress exceeds the surface tension stress. If the voltage is now reduced to $V_2 < V < V_1$ the cone structure still remains, still emitting charged droplets and ions. It is because charges are still emitted that the ohmic resistance remains, causing the tangential field to uphold the tangential shear stress. Also the sharp point of the cone is already established, keeping the high field near the tip. The ohmic resistance declines with declining potential. At $V=V_2$ the current and the flow of charged droplets fall simultaneously to zero; here the true Taylor cone is established. The electric and surface tension stresses balance each other exactly and no charge is emitted. The surface is thus equipotential, which Taylor assumed while deriving his theory. At a potential slightly lower than V_2 , the rounded off droplet is seen again. This occurs because the electric stress is no longer capable of upholding the cone shape.

4.10 Visualisation of the cone apex through a microscope

In order to view what is happening in the vicinity of the apex, i.e. the tip of the cone, a long distance microscope was used. A commonly used microscope has an object to lens distance of 1 cm to a few millimetres. The long distance microscope has a resolution of $1.1 \mu\text{m}$ at a distance of 15 cm from the object. It is thus very suitable for our purpose, because in this configuration it does not influence the electric field near the tip of the cone. Nevertheless it remains difficult to observe individual droplet of $1.5 \mu\text{m}$ travelling at high speeds. What we had in mind was to clarify droplet trajectories and the shape of the cone near the apex.

The long distance microscope, a Questar, was zoomed in on the apex of the cone. The result is seen in Figure 4.18.

What is seen clearly is that the tip of the cone is cusp shaped.

If a photograph is taken not only of the apex but also of a part of the droplet formed, it is seen that the stream of droplets forms a conically shaped volume, as is shown in Figure 4.19.

When a stroboscopic light is used to photograph the same area, it can be clearly seen that the droplets follow a spirally shaped track away from the tip of the cone. This is shown in Figure 4.20.

If the droplets are produced one by one, at a production rate of 10^8 to 10^{12} per second, this would mean that the velocity of the droplets, just after detachment, is over 2300 m/s, which is supersonic (about seven times the speed of sound).

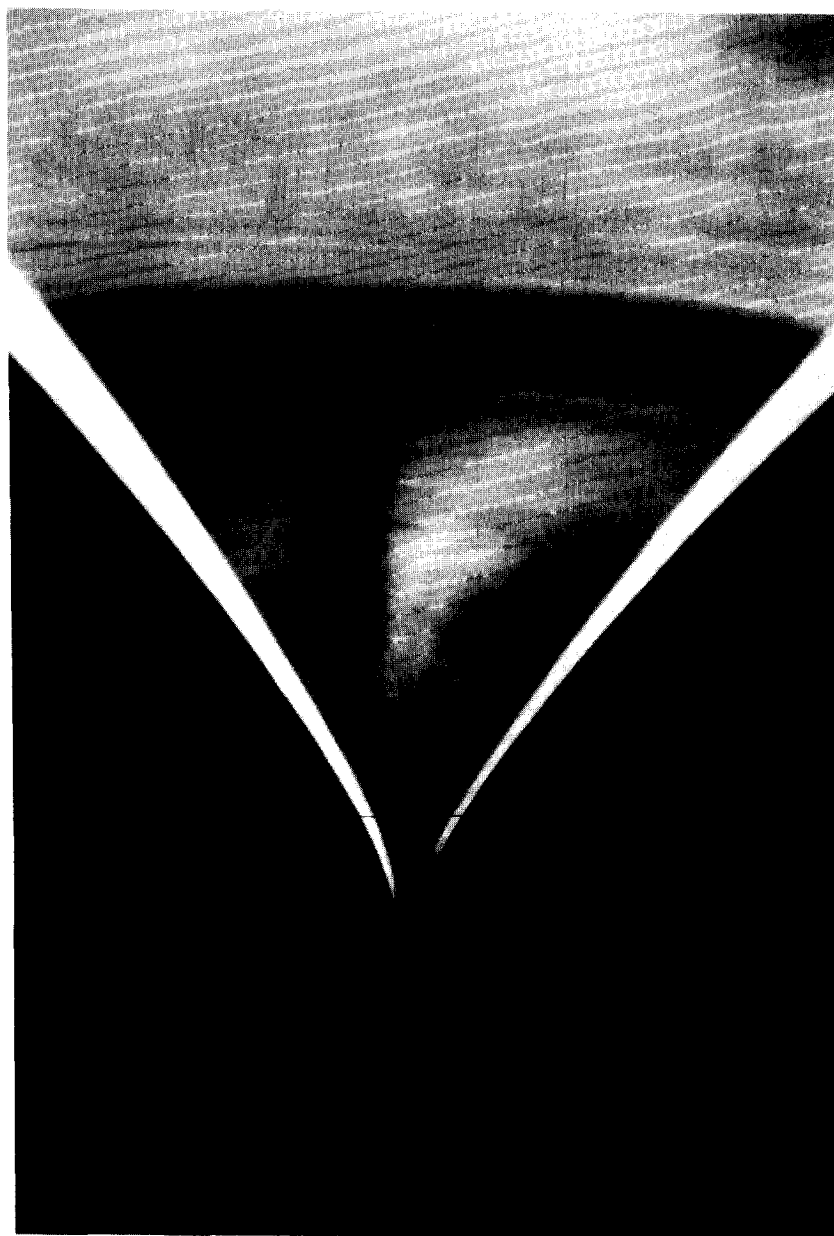


Figure 4.18 Photograph of the apex of a liquid cone of ethylene glycol, using a high intensity light source.

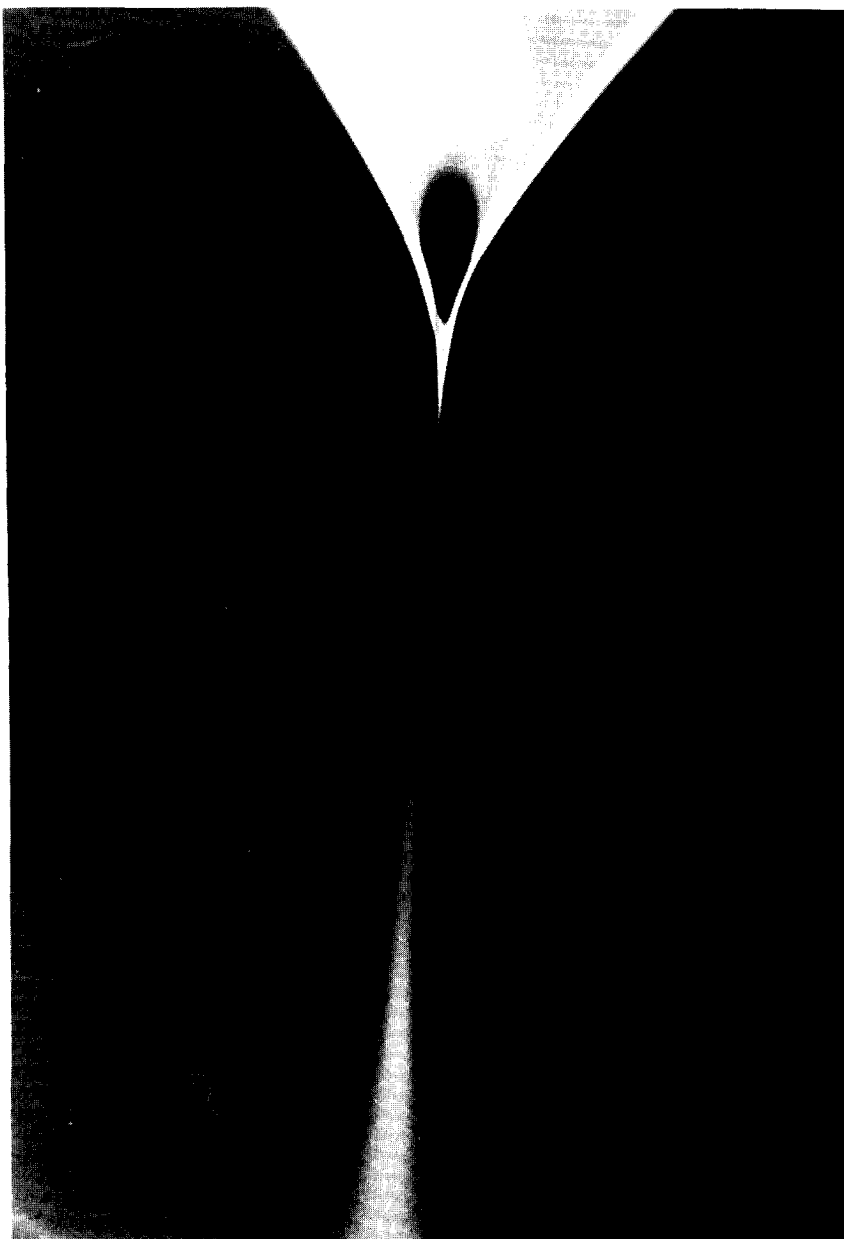


Figure 4.19 Photograph of the apex of the cone and the stream of droplets coming from the cone, using a high intensity light source.



Figure 4.20 *Photograph taken of the stream of droplets coming from the cone, using a stroboscopic light, showing the path which the droplets follow when coming from the cone.*

4.11 Electric wind

4.11.1 Theory of electric wind

When an ion is created in the corona region it moves due to the electric field. The mean free path of an ion in air at NTP is approximately $2 \cdot 10^{-7}$ m. Because the mass of an ionised gas molecule is about the same as the mass of a neutral gas molecule, the momentum is partly transferred to the neutral molecule when the two collide. After the collision the ion is accelerated again by the electric field and then it collides again; this repeats itself until it reaches the opposite, usually earthed, electrode. As a result of many such collisions the neutral molecules acquire a velocity in the direction of the electric field. This phenomenon is called the electric wind, ion wind or sometimes the corona wind. It is called the ion wind not because it is a movement of ions but because it is generated by the energy transfer from ions (Cross, 1987). The electric wind velocity was found to be proportional to the square root of the current, according to:

$$v = A\sqrt{I} \quad \text{where } A = g\sqrt{\frac{I}{\kappa\rho B}} \quad (22)$$

where v = electric wind velocity [m/s]

g = function of geometry [$\text{m}^{1/2}$]

κ = loss coefficient [-]

ρ = air density [kg/m^3]

B = ion mobility [m^2/Vs]

4.11.2 Electric wind measurements

Measuring wind velocities is very easy, but measuring wind velocities in a high electric field is something completely different. The best method to measure this velocity is probably the laser-doppler method (Welling 1982). First a glass pitot-tube was used, because a metal pitot-tube would give some problems with the electric field.

Experiments were done in which the electric wind velocity was measured as a function of the applied potential. The normal nozzle-to-plate configuration was used, but first without liquid coming from the nozzle. A metal needle was placed in the center of the nozzle. The velocity was measured 5 mm under the tip of this needle, which was hanging from the nozzle.

It proved to be impossible to measure the electric wind velocity with the pitot-tube when a liquid cone was "working". The electric field was influenced too much, and the liquid droplets were attracted by the glass pitot-tube.

In the nozzle/needle-to-plate configuration the wind velocity was measured as a

function of the applied voltage. Simultaneously the electric current was measured. The results can be seen in the Figures 4.21 and 4.22, where the velocity, v , is plotted against the square root of the electric current, and the electric pressure is plotted as a function of the applied electric field strength. The electric field strength was calculated according to the method of Jones and Thong (1971).

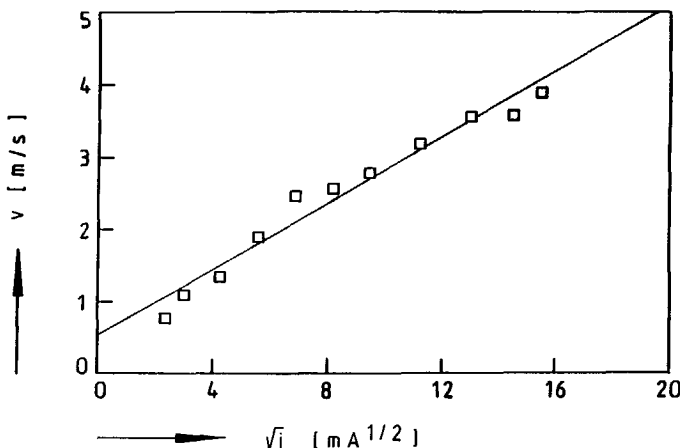


Figure 4.21 Velocity of the air flow caused by the electric wind versus the square root of the current I . Nozzle-ring distance is 30 mm.

It can be concluded that equation 22 is valid for the system used. It can also be concluded that near the field breakdown value of $3 \cdot 10^6 \text{ V/m}$, the pressure caused by the electric wind is in the order of 10 N/m^2 .

The wind velocity during operation of the liquid cones was measured using the laser-doppler method. It proved to be very difficult to get accurate values of the wind velocities near the cone surface. One centimetre below the apex of the cone, and five millimetres out of the center line, velocities of a few meters per second were measured, which are the same order of magnitude as for the nozzle-to-plate system measured above.

The movement of smoke and particles introduced near the cone clearly showed the downward movement of the air around the cone, as drawn in Figure 4.23.

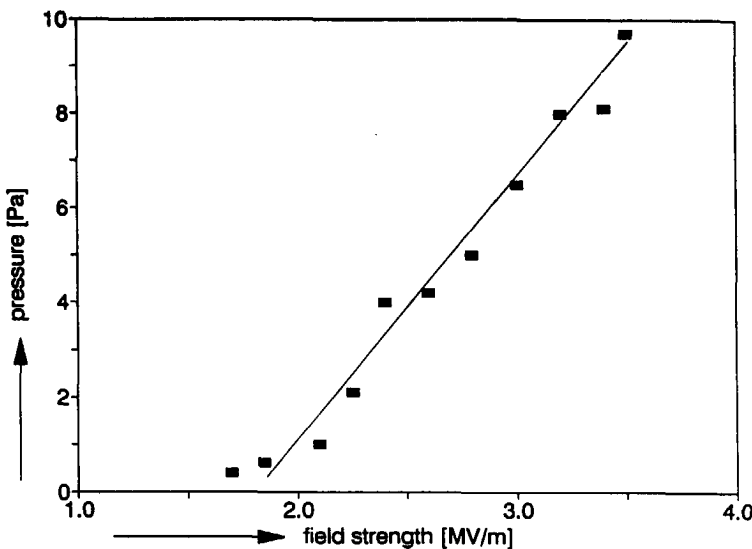


Figure 4.22 Pressure cause by the electric wind as a function of the applied field strength. Nozzle-ring distance is 30 mm.

What can be concluded from these measurements and observations is that the same electric wind exists around the liquid cones, which also exists for corona discharges around sharp needles. The absolute value of the electric wind around the cone is in the same order of magnitude. When setting up a pressure balance over the cone surface, as done by Taylor (1964), the pressure caused by the electric wind also has to be accounted for.

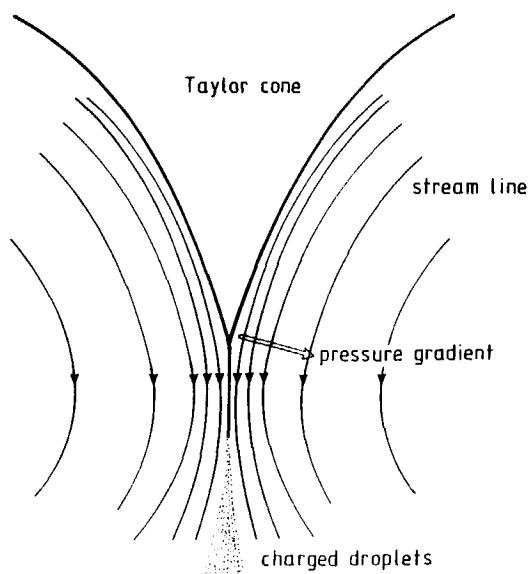


Figure 4.23 Schematic presentation of the liquid cone with the streamlines of the electric wind drawn next to the cone.

4.12 Ansoft Computer Simulations

4.12.1 Solving Routines

The software package Ansoft by Maxwell (1989) is used to simulate the field configurations around the nozzle cone-to-plate configuration. To solve a problem a mesh has to be created using the Meshmaker module. First the configuration is drawn, as is shown in Figure 4.24.

From this a finite element mesh is created. This is done by creating triangles in the problem space. The triangles are being refined around sharp points like the cone as is shown in Figure 4.25, until the amount is such that the solution no longer alters. A very fine mesh is established.

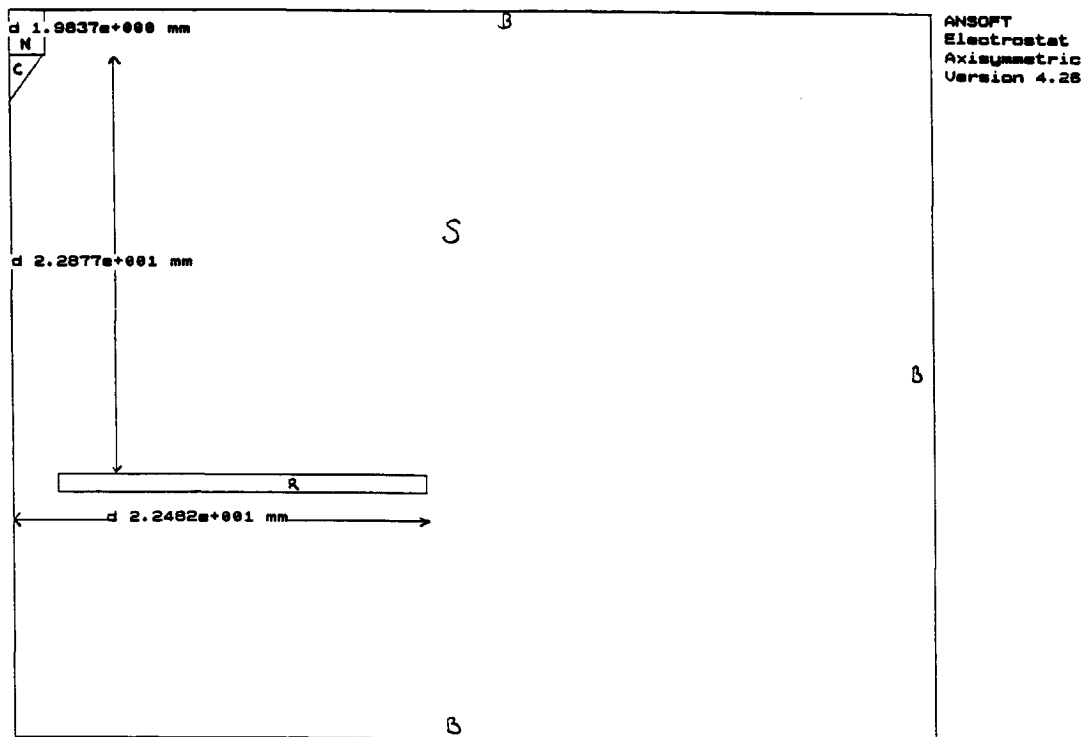
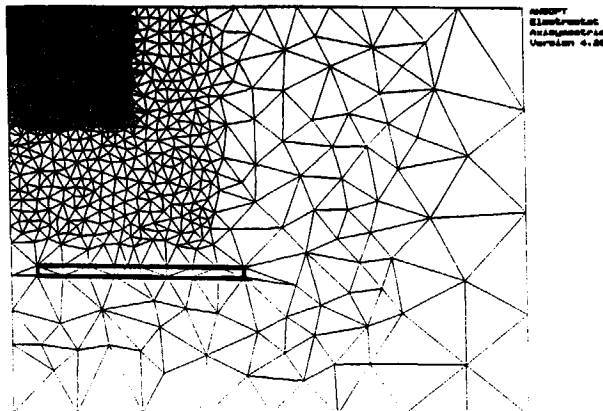
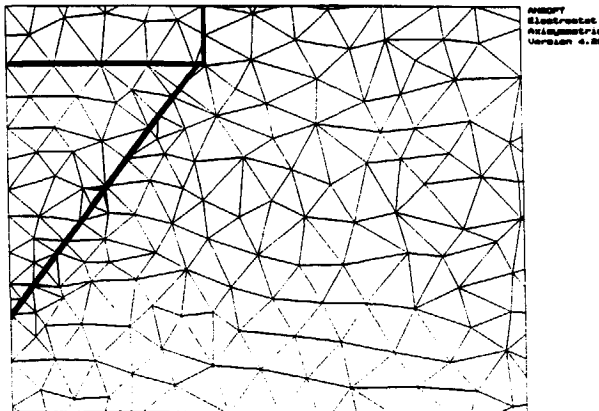


Figure 4.24 Configuration analysed using the Ansoft simulation package. N=metal nozzle, C=liquid cone, R=metal grounded ring, S=surrounding medium (air), B=ballooned edges

Normally it is assumed that the two dimensional geometry being modelled represents a cross section of a system that extends in the z-direction perpendicular to the screen. However, in the simulations performed a special option was used by which axisymmetric problems can be solved. There a r-z section of a r-θ-z cylindrical coordinate system is solved.



(a)



(b)

Figure 4.25 Mesh created of the problem space (a), zoomed in around the nozzle and cone (b).

Before being able to calculate the solution, the boundary conditions have to be set. The edges of the field shown on the screen are ballooned. Ballooned boundaries are the outer boundaries that separate the meshed problem space from the nothingness beyond. They indicate that the background extends to infinity and that the field goes to zero potential at infinity. This allows charges to exist at infinity in order to ensure zero potential. The axis of symmetry (z-axis) is chosen automatically so that the field lines are perpendicular to this line. The liquid cone is seen as a body with a given relative permittivity. Metal objects, like the nozzle and the grounded metal ring, are declared as non-existent. This way the solver module will not attempt to solve the problem created in the portion of the mesh associated with these objects. Declaring an object as non-existent is equivalent to declaring it to be a conductor under static conditions; the entire conductor will thus be seen to be at the same potential. This potential is a boundary condition to be set as well. In this way the Ansoft Electrostat RZ solver module allows the analysis of static electric fields arising for charge distributions and potential differences. The Poisson equation given as;

$$\nabla \cdot (\epsilon \nabla \phi) = \rho \quad (23)$$

where $\rho = \rho(r,z)$ = charge distribution [C/m³]

$\epsilon = \epsilon(r,z)$ = permittivity [F/m]

is solved for every created mesh point.

The finite element method used solves a function which is minimised. This function is given as

$$F = \int_V \epsilon (\nabla \phi)^2 dV \quad (24)$$

where F is an energy function to be minimised.

The residual is a normalised measure of how close the solution comes to satisfy the field equation. The residual ($\nabla \cdot D - \rho$) is equivalent to a fictitious charge. The energy associated with this fictitious charge is the energy calculated from equation 24.

After each iteration the solution is put back into the field equation that is being solved. If the solution is exact the residual is zero. Otherwise the residual is non-zero and a small correction is added to the solution. The residual is then recalculated and the iterative process continues until the residual is less than the preset target value.

If an object is a conductor, charges have already flowed to the surface of the object and forced the field inside the conductor to be zero. Objects that are not conductors are assumed to be lossless insulators in which no current flows. For all the materials defined in the problem space, the permittivity must be given as a constant value or a function of place. After the problem is solved in the Electrostat RZ module, the potential $\phi(r,z)$ is known in every mesh point in the problem space. A special calculator now enables one to calculate the field strength $E(r,z)$ or displacement

$D(r,z)$, where $D = \epsilon E$. From $E(r,z)$ the normal E_n and tangential E_t field strength along the cone surface can be calculated. These can then be used to determine the normal shear stress τ_n and the tangential shear stress τ_t induced at the cone surface. These are given as;

$$\tau_n = \frac{1}{2} \epsilon_0 E_n^2 + \frac{1}{2} (\epsilon - \epsilon_0) E_t^2 \quad (25)$$

and

$$\tau_t = \epsilon_0 E_n E_t \quad (26)$$

The stresses can be plotted as a function of place along a defined line, in our case the cone surface.

By integrating the shear stresses over the cone surface the normal, F_n , and tangential force, F_t , acting on the cone surface can be calculated according to;

$$F_n = \int_A \tau_n dA \quad (27)$$

and

$$F_t = \int_A \tau_t dA \quad (28)$$

This is done by a line chosen (the cone surface) in the r,z section on the screen to be swept around the $r=0$ axis, to form the desired cone surface.

The calculations were made for several different cone configurations at different potentials. The tangential field component calculated for these configurations is performed as if the cone does not eject charge and as if there is no liquid flow inside the cone. Thus as if the current is carried by conduction. The conduction current density J passing through each section of the cone is therefore given by:

$$J = \kappa E \quad (29)$$

where κ = conductivity of the liquid $[\Omega^{-1}m^{-1}]$

and the conduction current I is given by:

$$I = JA \quad (30)$$

where A equals the steradian area of the cone given as:

$$A = 2\pi(1 - \cos\alpha)r^2 \quad (31)$$

with α =cone half angle

r =spherical radius of the cone [m]

Combining equations 29 to 31 gives the tangential field strength as:

$$E_t = \frac{I}{2\pi r(1 - \cos\alpha)} \frac{1}{r^2} \quad (32)$$

For calculating the normal field strength E_n the potential distributions, calculated using the ansoft simulation program, is used. The tangential field strength is calculated using equation 32. Here the current is measured and the cone half angle determined from photographs

4.12.2 Results of simulations

The configurations analysed are like the one shown in Figure 4.24. The nozzle was declared as non-existent with a certain set potential. The liquid cone hanging from the nozzle was defined as a body with a set relative permittivity (37.7 for ethylene glycol). The ring was defined as being non-existent, with a potential of zero volts (grounded ring). The surrounding medium was defined as having a relative permittivity of unity. The boundaries of the problem space were ballooned. The cone was taken as a real conically shaped body. The shape, cone angle and length of the cone were obtained from photographs pictures taken at different potentials and different liquid flow rates.

A typical number of triangles for our simulations is between 1500 to 2000. The mesh is such created that the whole field of interest is calculated by refining to a high mesh point density generated around the cone and nozzle.

From the potential distribution obtained from the Ansoft simulations the field strength is calculated. Figure 4.26 shows an example of a calculated potential distribution along the cone surface.

The field strength at the apex of the cone was found to exceed the critical field strength for electric break down in air ($3 \cdot 10^6$ V/m) as shown in Figure 4.27. This can be explained by the fact that the Ansoft program does not take into account the space charge generated at the apex of the cone. The space charge reduces the field strength around the cone apex to the value of $3 \cdot 10^6$ kV/m.

From the electric field strength the shear at the surface can be calculated (Figure

4.28). Again near the apex the value calculated will be too high. This is why the value is reduced to that where the field strength is near the break down value. From the stresses the net forces on the surface can be calculated using the values as calculated by the program. The error caused by the high values of the field near the apex is small because of the surface integral taken. The surface area near the apex is small compared to that near the base of the cone.

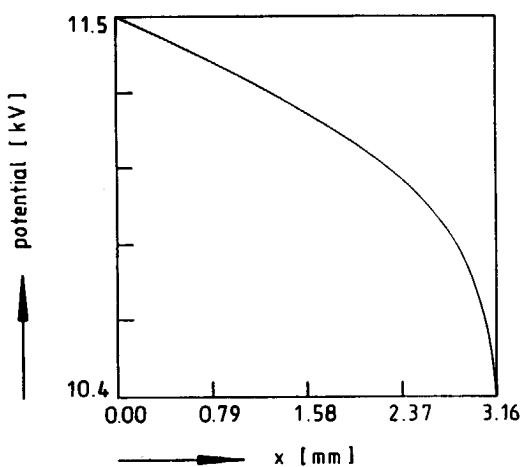


Figure 4.26 Potential along a ethylene glycol cone surface as a function of the distance along the cone surface; $x=0$ is the cone base. $Q_m = 0.526 \text{ mg/s}$, $\sigma = 46 \text{ mN/m}$

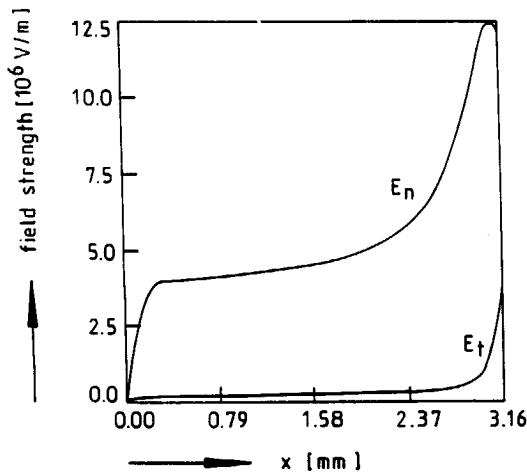


Figure 4.27 Field strength E_n and E_t as of the distance from the cone base ($x=0$), along the surface. $Q_m = 0.526 \text{ mg/s}$, $\sigma = 46 \text{ mN/m}$.

A remarkable feature is seen when the potential drop over the cone surface is plotted as a function of the applied potential to the nozzle. When the potential is increased the cone angle decreases too, thus decreasing the base-apex distance. However the potential drop over this base-apex distance remains the same, also at different flow rates as is shown in Figure 4.13.

From Figure 4.29 it is seen that the calculated forces do not change much as the potential is increased or the flow rate is changed.

The normal electric force acting on the cone surface, are almost of the same value,

increasing slightly with increasing potential, but independent on the liquid flow rate. The tangential shear forces are about ten times lower than the normal forces acting on the cone, not changing much with applied potential.

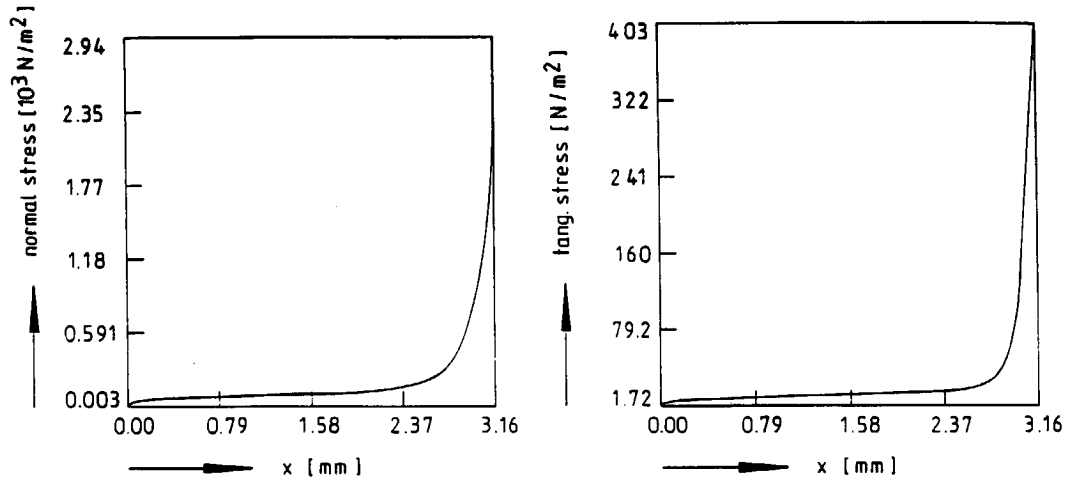


Figure 4.28 Normal and tangential stresses as calculated from the Ansoft potential distribution ($x=0$ is the base of the cone).

These results are almost equal to those found by Hyati *et al.* (1987). They assumed that a jet was coming from the cone tip. We did not, this because we did not see a jet during our experiments.

The calculations and simulations show that the normal electric field strength is around the field breakdown value of $3 \cdot 10^6$ V/m, increasing to about 10^7 V/m and higher near the apex of the cone. This is due to the fact that the program does not take space charge into account which, in reality, is formed just below the point of the cone. This space charge consists of charged droplets and ions from the corona discharge. The fact that the calculations show a value of higher than $3 \cdot 10^6$, indicates that space charge has to diverge the field to a lower value. The tangential field strength is much lower, about 10^5 V/m, at the cone surface, increasing to a value of about $1-4 \cdot 10^6$ V/m near the apex of the cone. This is in accordance with the visual observations of the increase of the liquid velocity inside the cone. This is visualised by introducing particles in the liquid.

The liquid accelerates strongly near the tip of the cone pulling it downwards and causing it to become cusp-shaped at the tip. The liquid is then dispersed into droplets. This is not taken into account during the simulations.

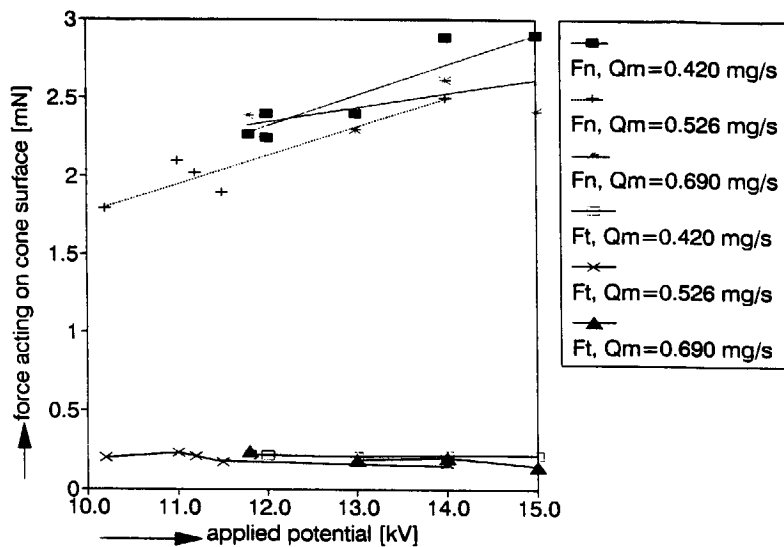


Figure 4.29 Normal F_n and tangential F_t forces as a function of applied potential for several flow rates.

4.12.3 Conclusions

From the simulations it is clear that a space charge must reduce the field strength around the tip of the cone, to prevent break down of the field. This is concluded because the values calculated for the electric field strengths are above the field breakdown value of $3 \cdot 10^6 \text{ V/m}$.

These values are also high enough to cause a corona to form around the sharp point of the cone.

By calculating the electric fields and stresses around the liquid cones, it is clear that the shape of the cones play a very important role in regulating the field around the cones.

The stresses are seen to increase rapidly in the vicinity of the apex. This causes the liquid to be accelerated strongly near the tip. At the same time this explains the liquid flow inside the cone, especially the fact that the liquid velocity is largest at the liquid-gas interface and low inside the cone. The stresses are largest near the apex of the cone, causing the liquid to be accelerated strongly near the tip, as was clearly

observed.

From the stresses the net forces acting on the cone surfaces can be calculated. The normal forces are seen to be almost constant, slightly decreasing with increasing potential. This could well explain the fact that the drop size does not change much with increasing potential. The tangential forces were calculated to be about a decade smaller in size than the normal forces calculated. This was also found by Hyati *et al.* (1986).

A remarkable feature was seen when calculating the potential drop over the cone surface. This potential drop was found to be a constant with increasing potential and liquid velocity.

Due to the limitations of the simulation process a next step will have to be a further development of the simulation procedures. The simulations performed are all of a static process. What will have to be incorporated are the space charge formed below and removed from the liquid cone. This space charge consists of the charged droplets and ions. Also the liquid flow caused by the tangential stress have to be accounted for as well. Refinement of the shape of the liquid cones into cusps near the apex will probably make the calculations slightly more accurate. After this recalculating is done the above will show us if the conclusions drawn from the static process still hold for the dynamic realistic process.

4.13 References

- Bailey, A.J., (1988) *Electrostatic spraying of liquids*, John Wiley & Sons, New York
- Cobine, J.D., (1958) *Gaseous Conductors, Theory and Engineering Applications*, Dover Publ. Inc., New York
- Cross, J.A., (1987) *Electrostatics: Principles, Problems and Applications*, Adam Hilger, Bristol UK
- Davis, C.N., (1966) *Aerosol Science*, Academic Press, London & New York
- English, W.N., (1948) *Phys. Rev.* 74(2), 179
- Goldman, M., Goldman, A. (1978) *Gaseous Electronics Vol.1*, p219, Academic Press, edt. M.N. Hirsh and H.J. Oskam.
- Hartmann, G., Gallimberti J., (1975) *J. Phys. D.* 8, 670
- Hartmann, G., Johnson, P.C., (1978) *J. Phys. B: Atom. Molec.Phys.* 11(9), 1597
- Hayati, I., Bailey, A.I., Tadros, Th. F. (1986) *Nature* 319, 41.
- Hayati, I., Bailey, A.I., Tadros, Th. F. (1987) *J. Colloid Interface Sci.* 177(1), 205
- Hinds, W.C., (1982) *Aerosol Technology: Properties Behaviour and Measurement of airborne particles*, John Wiley & Sons New York
- Jones, A.R., Thong, K.C., (1971), *J. Phys. D. Appl. Phys.* 4, 1159
- Loeb, L.B., (1965) *Electrical Coronas* Univ. California Press, Berkley USA
- Marode, G., (1977) *Thesis Univ. of Paris Centre d'Orsay*, No. 1783, 2/2/1977
- Marode ,G., (1979) *J. Appl. Phys.* 50(1), 140
- Maxwell (1989), *Maxwell users guide*, Ansoft corp. Pittsburg USA

- Olivier, B.F., (1977) *Thesis Univ. of Paris Centre d'Orsay*, No. 1871, 1/7/1977
Robinson, M., (1961) *Trans. Am. Inst. Elec. Eng.* **80**, 143
Smith, D.P.H. (1986) *IEEE Trans. Ind. Appl.* **1A-22** (3), 527.
Taylor, G.I. (1964) *Proc. Roy. Soc. A280*, 383.
Vedenov, A.A., Vitdhas, A.F., Gerts, V.E., Naumow, V.G., (1976) *High Temperature* **14**, 403
Welling, A., (1989) *Pt/Werktaulgouw* **37**(12), 72
Zeleny, J. (1917) *Phys. Rev.* **10**, 1.

Nothing is impossible for people who do not have to do it themselves

5 Practical applications of liquid cones

5.1 Generation of micron sized droplets from the Taylor cone (Meesters et al. 1992)

5.1.1 Introduction

Aerosol generators are widely used for the calibration of instruments, in testing procedures, as applicators and manufacturing processes. The requirements are usually for a controlled droplet size and often narrow size distributions or at least a readily identifiable modal value. The production of droplets which have a diameter of order one micron is inconvenient to attain by the commonly used mechanical breakup methods, like the vibrating orifice and the spinning disc. In order to produce such droplets, larger droplets are produced and subsequently reduced by evaporation. This paper reports the development and study of an aerosol generator from which droplets of about one micron are produced directly. The device is particularly attractive because it combines the features of high production rate, small droplets and easy operation with no clogging of the nozzle. The generator uses an electrostatic field to assist the breakup.

The droplets carry, initially, a high charge. The charge must be partially or completely neutralised so that the droplets can be collimated into a stream. If charged droplets are required, the degree of neutralisation can be controlled.

The only previous report of a similar aerosol generator which has been brought to our attention is a patent application of 1989 (US patent 1989).

We believe that the device deserves much wider study and application and we have taken the liberty of naming it the Delft Aerosol Generator (DAG).

5.1.2 Delft Aerosol Generator design

A schematic diagram of the aerosol generator is shown in Figure 5.1. The Delft Aerosol Generator, DAG, is based on the principle of the Taylor cone. From the tip of this cone the droplets are produced. The liquid is fed to a nozzle whose inner diameter can vary between 1 and 0.1 mm. This relatively large opening ensures that there are no problems of small particles clogging the nozzle, whilst the droplets produced are two to three decades smaller than the nozzle opening. The outside diameter can vary from 1 to 0.1 cm. The nozzle is constructed from a conducting metal. Constant flow is maintained by using either a syringe pump or a constant pressure feed. The liquid flow is in the range of 0.1 to 30 ml/h. The aerosol generator itself consists of three functional parts, namely the nozzle and spraying system, the metal needle acting as the discharger and a metal ring which has the function of a shielding ring. The apparatus is easy to scale up to a system of multiple nozzles if a larger production rate is required.

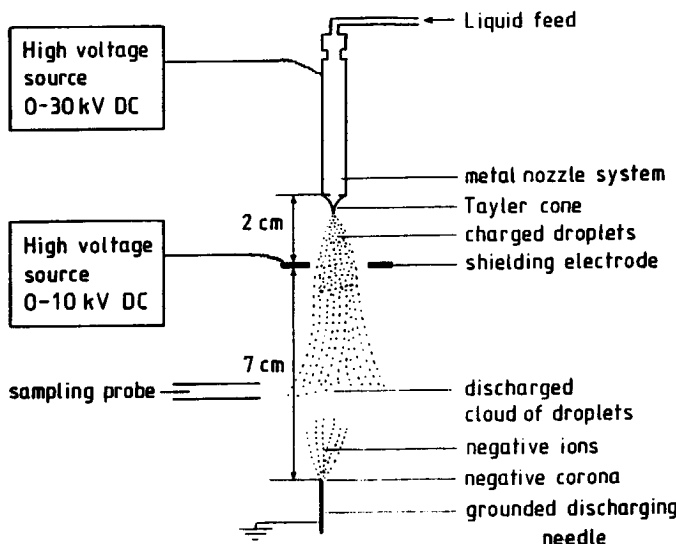


Figure 5.1 Basic design of the Delft Aerosol Generator (DAG)

The nozzle is connected to a high voltage source variable in the range of 0-30 kV DC and which may either be positive or negative. In order to create the cone in this configuration (Fig. 5.1) and with liquids of modest conductivity, a potential difference of 5-12 kV is usually required between the nozzle and the ring. The discharge electrode consists of a metal needle which is earthed. The third component, the shielding ring, is maintained at the same polarity as the nozzle. The field created between the shielding ring and needle causes a corona discharge supplying neutralising ions of opposite polarity to the droplets. The neutralisation ions combine with the charged droplets.

The shielding ring is essential to the satisfactory operation of the generator. Without the shielding ring the liquid cone is very unstable.

This shielding ring with a voltage of 0-10 kV DC, has two functions. It creates a strong electric field causing a corona discharger on the needle and also stabilises the field between nozzle and ring which gives a more stable liquid cone and a more concentrated stream of droplets.

Since the discharge of the droplets occurs below the shielding ring, it must be large enough for the droplets to enter the discharge region. If, on the other hand, it is too large the shielding and concentrating function is diminished. The shape of the cloud of droplets coming from the Taylor cone is also conically shaped. This is because the droplets are highly charged when they are formed and this charge prevents the droplets from coalescing. The expanding cloud of droplets collides partially with the shielding ring if the opening is too small. In the configuration of Figure 5.1, the outside diameter of the shielding ring is 47 mm and the inside diameter is 37 mm, Meesters *et al.* (1990^b). The potential difference between the shielding ring and the needle determines the degree of charge remaining on the droplets produced, thus enabling the creation of charged aerosols. A specific value causes the aerosol to be completely neutralised, making it manageable in subsequent processes or measuring devices. The arrangement shown in Figure 5.1 is 15 cm high and has a diameter of 5 cm, thus making it very easy to fit into an apparatus.

The experimental parameters which have been investigated in this work are the nozzle-ring and the ring-needle distances and the potentials applied to both nozzle and ring.

There is only a limited range of potential differences which can be applied. If the potential difference between the nozzle and ring is too low there is no Taylor cone and if it is too high, the cone becomes skew or several tiny cones appear at the rim of the nozzle. These cones still produce droplets, but outside the intended regime of operation of the device. A potential difference of 5-12 kV between nozzle and ring is usually sufficient for the single cone regime, above 12 kV, the multiple cone regime occurs. If the potential difference between the ring and the needle is too low the droplets are not discharged and, if it is too high, the droplets are negatively charged. For optimal discharging a potential difference of 6-8 kV is required between the ring and needle. Within this limited range the mean droplet size varies only slightly with

the potential difference.

The DAG can be built directly into a duct, as shown in Figure 5.2. In this case it is more convenient to operate with the nozzle and the needle connected to the electrodes of the voltage source and to maintain the shielding ring at earth potential.

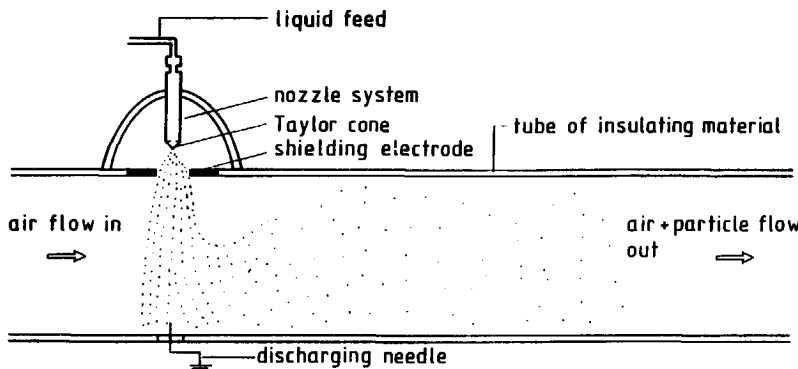


Figure 5.2 The proposed Delft Aerosol Generator (DAG) build into a ducting system

5.1.3 Delft Aerosol Generator operation

In many respects, the phenomenon which occurs at the tip of a cone are similar to those occurring in a corona discharge which occurs at the tip of a needle. The difference is that, in the case of the liquid cone, the surface is liquid and thus unstable. The stream of emitted droplets are thus responsible for carrying some of the effective current flow through the tip. In other respects, however, the cone behaviour exhibits regimes of behaviour similar to those of a needle corona and can be compared with it.

The region which is chosen for the operation of the aerosol generator is the pulseless glow regime. In this regime the current is almost constant and thus it is easy to detect, a voltage which is either too high or too low. The emission of the droplets is also constant. The actual values of potential which define the regime are specific to each fluid. The fourth regime where current pulses reappear is not found operating the cones, but might reappear at higher potentials

5.1.4 Droplet production

The droplets produced by the DAG were measured using a white light particle counter, the CLIMET CI1000/CI226. This instrument was chosen for this purpose of its active range of 0.3 to 3 μm and its response curve consisting of 2770 size classes. Calibration was achieved using samples of standard latex particles.

The device was first tested with ethylene glycol. A typical recorded droplet size distribution is shown in Figure 5.3. The distributions were not perfectly mono-sized but they have a readily identifiable modal value and a small standard deviation.

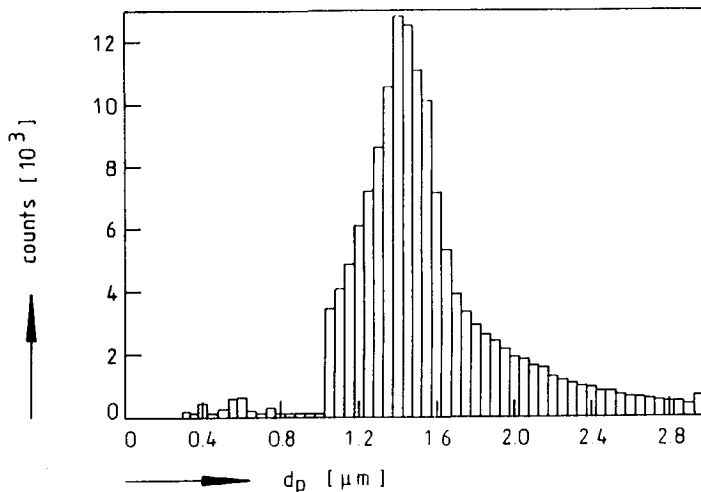


Figure 5.3 Size distribution of ethylene glycol sprayed with the DAG and analysed with the CLIMET

The droplet size is only slightly dependent upon the field applied between the nozzle and the shielding ring. This is illustrated by the results in Table 5.1.

Table 5.1. Ethyleneglycol modal droplet sizes and arithmetic standard deviations as a function of the nozzle-ring potential difference, at two nozzle-ring distances, measured using a CLIMET particle sizer.

distance nozzle-ring (mm)	ΔV nozzle- ring (kV)	d_{droplet} modal value [μm]	d_{droplet} st.d. [μm]
20	10	1.55	0.20
	9	1.40	0.21
	8	1.40	0.21
	8	1.30	0.23
	7	1.30	0.28
	7	1.33	0.30
10	8.8	1.56	0.16
	8.6	1.50	0.20
	7.6	1.44	0.20
	6.6	1.40	0.20

The field was varied by changing both the distance between the nozzle and the ring and also the applied voltage. The modal value of the distribution can be reduced only slightly by increasing the voltage. The standard deviation of the distributions is consistently small. The consequence of this is that the device is stable in operation so long as it is maintained in the pulseless glow regime. The rate of production of droplets is high, for example for the $1.44 \mu\text{m}$ droplets (table 5.1) at a flow rate of 15 g/h of ethylene glycol, calculated to be equal to $2.4 \cdot 10^9$ droplets per second.

Variation of the potential between the shielding ring and the neutralising needle does not have any significant effect on the modal value of the droplet diameter as shown in Table 5.2. Variation of the potential between the shielding ring and neutralising needle does, however, have a dramatic effect on the number of droplets counted, as shown in Table 5.3.

Table 5.2. Ethylene-glycol mean droplet sizes and arithmetic standard deviations as a function of the ring-needle potential difference for two different ring-needle distances

distance ring-needle (mm)	ΔV ring- needle (kV)	d_{droplet} mean value [μm]	d_{droplet} st.d. [μm]
70	10	1.33	0.30
	9	1.30	0.30
	8	1.30	0.28
	7	1.30	0.23
80	10	1.38	0.28
	9	1.40	0.28
	8	1.40	0.29
	7	1.44	0.25
	6	1.44	0.40
	5	1.36	0.30
	4	1.45	0.30
	3	1.45	0.30

Table 5.3. Number of ethylene-glycol droplets counted by a CLIMET, distance nozzle-ring=10 mm (distance ring-needle=80 mm, ΔV nozzle-ring=7.6 kV).

ΔV (kV) ring- needle	number of counts (-)
10	7000
9	10000
8	13000
7	13000
6	13000
5	4000
4	6000
3	4000

We interpret this Table to imply that the maximum number of droplets is counted when neutralisation of the initial charge is achieved. If the potential between the shielding ring and needle is too small the droplets retain a charge, if it is too high they

to collect in the analyzer.

The droplet size produced is dependent upon the properties of the liquid, namely the viscosity, surface tension and conductivity. It is difficult to vary these parameters independently but their collective effect can be illustrated by a set of experiments in which mixtures of Di-Octyl-Phthalate, DOP, and ethanol were atomised using the DAG. The ethanol evaporated after atomisation leaving behind droplets of DOP. The droplet sizes which can be achieved are, consequently, considerably smaller but are still of narrow distribution. This is illustrated in Figure 5.4, which shows a typical particle size distribution which has a modal size of $0.104 \mu\text{m}$. In this case the droplet size distributions were measured using a Differential Mobility Particle Sizer combined with a Condensation Particle Counter (DMPS-CPC) manufactured by TSI.

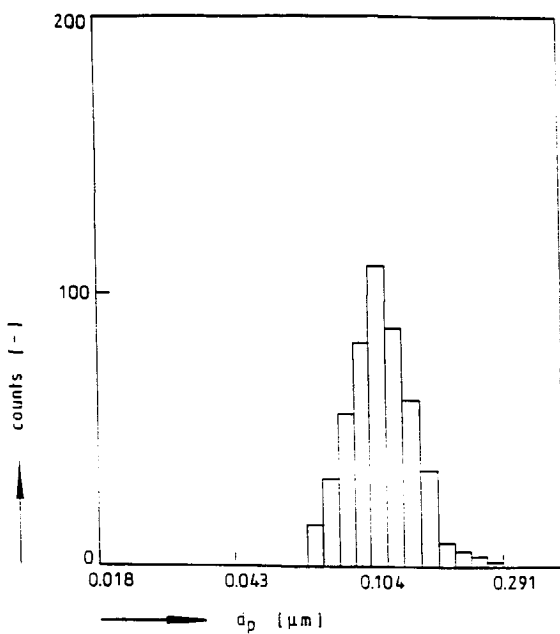


Figure 5.4 Size distribution of a mixture of DOP and ethanol (50/50 V/V%) measured with a DMPS-CPC

The results are shown in Figure 5.5 where the modal droplet diameter by number is plotted as a function of the DOP concentration. This droplet diameter increases with concentration but can be translated back to the mean diameter produced by the DAG. This line is also shown in Figure 5.5. The modal droplet diameter decreases

considerably as the DOP concentration is increased upto the value of 50%. In this region there is a decrease of the viscosity a constant surface tension and increase in size in the conductivity.

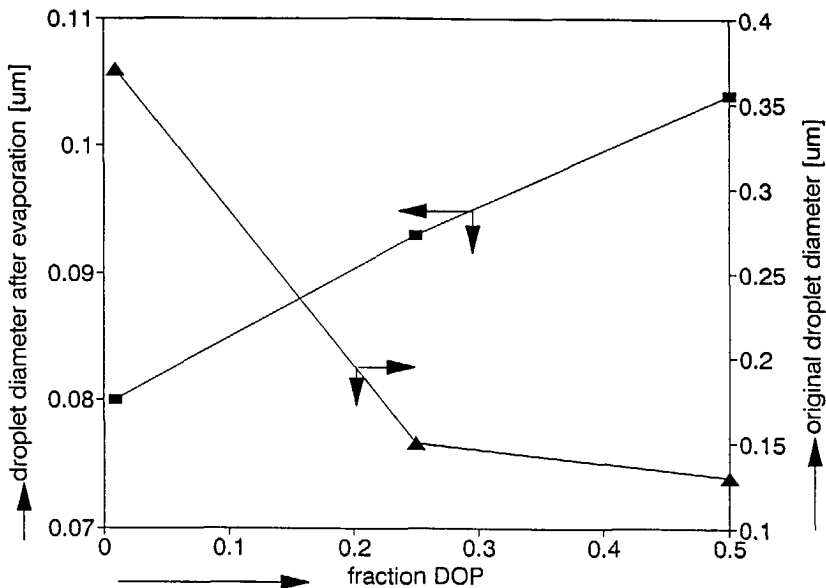


Figure 5.5 Calibration curve of DOP-ethanol mixtures with the resulting model diameters of the DOP and of the originally formed droplets as a function of the DOP concentration

5.1.5 Conclusions

The droplets which are emitted from the tip of a liquid cone have a diameter of the order of magnitude of $1 \mu\text{m}$. The mechanism can be used to produce droplets of this size directly and, by suitable dilution and evaporation, at least an order of magnitude smaller. The droplets are initially highly charged but can be neutralised by a suitable corona of opposite polarity. These features can all be incorporated into an aerosol

corona of opposite polarity. These features can all be incorporated into an aerosol generator which is more convenient than conventional ones for producing droplets in this size region. The droplet size distribution is narrow and the generator stable in operation.

The electrical phenomena of the liquid cones show much resemblance with the corona discharge on solid needles. The first three regimes from the current voltage characteristics of the solid needle are similar with the first three regimes of the liquid cones, the fourth regime was not found for the cones.

5.2 Electrostatic Emulsification

5.2.1 Introduction

All existing emulsification processes rely on the application of high shear rates to two immiscible liquids. The simplest method often used is by mixing the liquids violently. With this method emulsions with an average droplets size of about 5 μm can be produced. For smaller droplets a homogeniser is used in which the emulsion is forced through a small orifice at high velocity, thus producing droplets of about 1 μm or less. (Sherman, 1968)

The first attempt to use electrostatics to emulsify one liquid into another is reported by Nawab and Mason (1958). They produced an emulsion with a droplet size of about 3 μm . Watchtal and La Mer (1962) tried to improve the process, but their results were disappointing. It was not until the late seventies and early eighties that the first satisfactory attempts were reported on by Watanabe *et al.* (1978). They reported on a system consisting of a needle from which the liquid to be dispersed flowed. This needle was immersed into another liquid, the continuous phase, which is immiscible with the liquid flowing out of the needle, the dispersed phase. The phenomenon they observed is similar to the phenomenon of electrostatic spraying into the air, leading to the formation of liquid cones. They applied a potential to the needle, relative to a counter electrode, placed a few centimetres below the needle. The whole needle-counter electrode system is immersed into the continuous phase. The counter electrode was grounded to earth. A small amount of surfactant was added to stabilise the emulsion formed. The system worked as follows. At a constant liquid flow rate and at a needle potential $V_{\text{needle}}=0$ V the liquid flows slowly from the needle at a low drop formation frequency, producing droplets in the emulsion in the millimetre range. By increasing the potential the frequency of droplet emission also increases, and, because of the constant flow rate, the droplets produced are smaller. At a certain potential, called the onset potential, V_{onset} , the process abruptly changes from the field enhanced drop formation into the emulsification mode, producing droplets at very high frequencies. At this point a clearly visible cloud of fine droplets is seen as if

this cloud originates straight from the needle tip. The droplets produced are now in the micrometer range. The size distribution of the emulsions formed this way is reported to be narrow and the emulsion stability to be high. Watanabe *et al.* (1978) stated that when the emulsification process occurs, the interfacial tension between the continuous and disperse phase, near the needle tip, is reduced to zero, thus causing the spontaneous emulsification. Here they mean that the apparent interfacial tension is reduced to zero due to the electrostatic force counteracting the interfacial tension force. They found that the onset potential for emulsification depends on the liquids used, especially the ionic strength of the two liquids. When the ionic strength of the two liquids approach each other, the onset potential of emulsification increases. The liquids they used were water, with different concentrations of KCl, dispersed into methyl-iso-butyl ketone.

The big advantage of the described emulsification process is that there is a very low power input necessary, compared to the usual emulsification processes (less than a Watt per needle). The emulsions produced this way have usually very narrow size distributions.

The process as described by Watanabe *et al.* (1978) is similar to the spraying of a liquid in the air. They observed a changing in shape of the droplet curvature hanging from the needle submerged into another liquid. This is as described for the Taylor cone processes when spraying liquids in the air.

It is also possible to collect the droplets produced from the Taylor cone, by spraying liquid above a second liquid in which the droplets produced are then mixed, thus producing an emulsion. Hughes *et al.* (1981,1984) reported on an electrostatic spray system in which the dispersed phase particles are produced before coming into contact with the continuous phase. Due to gravity and the electrostatic force, the thus produced charged aerosol is transported to the continuous phase. They sprayed molten wax, which solidified in the air soon after being sprayed, from a sprayer head consisting of several coaxial annular slits raised to a potential of about -25 kV. The continuous phase in this case was water. The emulsion is produced by mixing the two phases together and is stabilised by a surfactant. The counter electrode was chosen to be the continuous phase, the water, in which an earthed metal plate was placed, thus directing the charged wax particles in the desired direction. The emulsions produced this way had the majority of the droplets in the range between one and three microns, with only a very small amount of droplets larger than ten microns, those were probably caused by coalescence or coagulation. The results are similar to the results obtained from our Taylor cone experiments.

5.2.2 Emulsification setup

In our laboratory we used a set up similar as described by Watanabe *et al.* (1978) to produce emulsions. The system used is exactly the same as used for spraying liquids in air from the liquid cones. The only difference with the spraying in air is that the whole nozzle-earthed ring system is immersed into the continuous phase. Figure 5.6 shows a schematic drawing of the configuration used.

From the nozzle, which has an outer diameter of 5 mm and an inner diameter of 0.5 mm, the disperse phase flows at a constant flow rate, using a constant flow syringe pump. The nozzle is facing a ring shaped counter electrode ($d_{inner} = 38$ mm, $d_{outer} = 43$ mm), placed two centimetres below the nozzle and connected to earth.

Before the emulsion becomes so dense as to become opaque, a conically shaped droplet can clearly be seen hanging from the nozzle. Only the cone, established this way, is much smaller than when spraying in air.

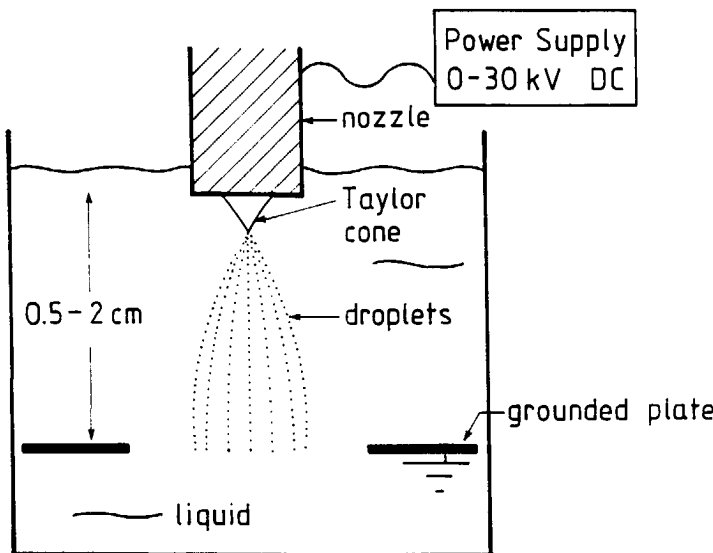


Figure 5.6 Schematic drawing of the experimental set up used for producing emulsions.

A Malvern 2600 C particle sizer was used to determine the size distributions of the emulsions produced. The size distribution of the emulsions is calculated from the forward scattered light distribution measured.

Several liquids were used as the dispersed phase. Ethylene glycol (chemical grade), water (demineralised) and a mixture of ethylene glycol (40 wt. %) and water (60 wt. %). A paraffin oil was used as the continuous phase. As reported by Watanabe, the conductivity of the liquids dispersed influences the dispersion process. Not only the onset potential for emulsification, but also the size distributions were reported to be influenced. To determine this influence of conductivity, several amounts of NaCl were added to the pure ethylene glycol (chemical grade), which was emulsified. In order to determine the influence of the applied potential, several potentials were used between 10 and 18 kV. During all the experiments the liquid flow rate was kept constant at 5 ml/hour.

The continuous phase used was a paraffin oil (chemical grade) with a viscosity of $35 \cdot 10^{-3}$ Pa·s. To stabilise the emulsion two surfactants were added to the continuous phase, namely Span-80 (Sigma), a sorbitan mono-oleate, and Span-85 (Sigma), a sorbitan tri-oleate. A 2 wt. % of a 1:1 Span-80:Span-85 mixture in paraffin oil stabilised the emulsion satisfactorally.

5.2.3 Measurements of size distribution using forward light scattering

The Malvern software, used to determine the size distributions of the emulsions produced, assumes the ratio of the real part of the refractive indices of the continuous and dispersed phase to be constant, with a value of 1.17. This is due to the fact that the Malvern software is calibrated using glass beads suspended in water.

In order to verify the reliability of the Malvern measurements the computer program called ROMA, developed at the TU Delft at the Particle Technology group (STM), was used. This program takes the refractive index ratio of the emulsion into account. The real part of the refractive index of the several disperse phase liquids and the continuous phase were determined using a refractometer. This refractometer measures the real part of the refractive index between the pure liquid and air.

The interfacial tension between the two phases was measured using the Ring of Nouy method. In a vessel the paraffin and the liquid to be dispersed were slowly added on top of each other, without causing the liquids to be mixed. The ring was placed under the liquid-liquid interface formed. The interfacial tension between the liquids was obtained by applying an upward force to the ring until it was pulled through the interface. From this force the interfacial tension could be determined.

Table 5.4 shows the measured real parts of the refractive indices, the ratio of the refractive indices between the disperse phases and the paraffin, and interfacial tensions between the liquids used. It is clear that the refractive index ratio is not the 1.17 assumed by the Malvern software.

Table 5.4 Measured refractive indices, calculated ratio between the refractive indices of the liquids and the paraffin and the measured interfacial tensions between the liquids and paraffin.

	ethylene-glycol	ethylene-glycol, water mixture 40:60 wt%	ethylene-glycol with NaCl added	water	paraffin
refract. index	1.432	1.373	1.432	1.334	1.476
r.i. ratio	0.98	0.94	0.98	0.91	1.0
Interf. tension [mN/m]	2.9	2.8	3.6	4.9	--

The program deconvolutes the light scattering pattern coming from the Malvern 2600C, equipped with a 5 mW He/Ne laser ($\lambda=632.8\text{nm}$). All strategies used for deconvoluting in forward light scattering experiment equipment are based on a comparison between a light scattering model and the mean value of the recorded integrated intensity pattern. The particle size distribution is obtained by deconvoluting the scattering pattern using an inversion algorithm. The success of this deconvoluting depends on several data processing steps. An advantage of the ROMA program is that it does not depend on the size distribution models. The procedure used in ROMA incorporates the mean scattering intensity and its standard deviation. Using this standard deviation in the light intensity, confidence intervals for the resulting particle size distribution can be determined.

The ROMA software was used to determine the reliability of the measured size distributions. From the results it was shown that only the water in paraffin oil emulsions have a low reliability. This is due to the fact that these emulsions contain droplets near the lower detection limit of the Malvern particle sizer (1\mu m). Droplets smaller than 1\mu m are probably produced, but these are not measured, although they can give a signal onto the rings of the Malvern, thus influencing the distribution. The emulsion of the ethylene glycol-water mixture in paraffin gave slightly larger droplets, causing the reliability to increase. The droplets of the pure ethylene glycol are measured with a high reliability according to the ROMA software, due to the larger droplets sizes.

The reported size distributions below were all measured using the Malvern software.

5.2.4 Influence of the applied potential on the droplet sizes

In order to establish the influence of the applied nozzle potential on the size distribution, the following results were obtained (Table 5.5). The measured median droplet sizes of the emulsions, $D_{n,50}$, for the three liquids used at different applied nozzle potentials are given. Figures 5.7^a to 5.7^c show three sizes distributions of the produced emulsions as obtained using the Malvern 2600C using the Malvern software. The applied potential does not have a pronounced influence on the median droplet size of the produced emulsions. The only difference seen, when looking at the size distributions, is that some larger droplets are formed at higher potentials.

As can be seen from Figure 5.7^c the size distributions are close to the lower detection limit of the Malvern particle sizer.

Table 5.5 $D_{n,50}$ for the emulsions made applying different potentials at a constant flow rate of 5 ml/h, measured with a Malvern particle sizer (ethylene glycol, ethylene-glycol water mixture 40:60 wt. % and pure demineralised water).

potential [kV]	ethylene- glycol	ethylene- glycol and water	water
	$D_{n,50}$ μm	$D_{n,50}$ μm	$D_{n,50}$ μm
10	4.4	1.4	1.2
12	4.6	1.5	1.2
14	4.2	1.6	1.3
16	5.2	2.1	2.0
18	4.3	2.0	1.3

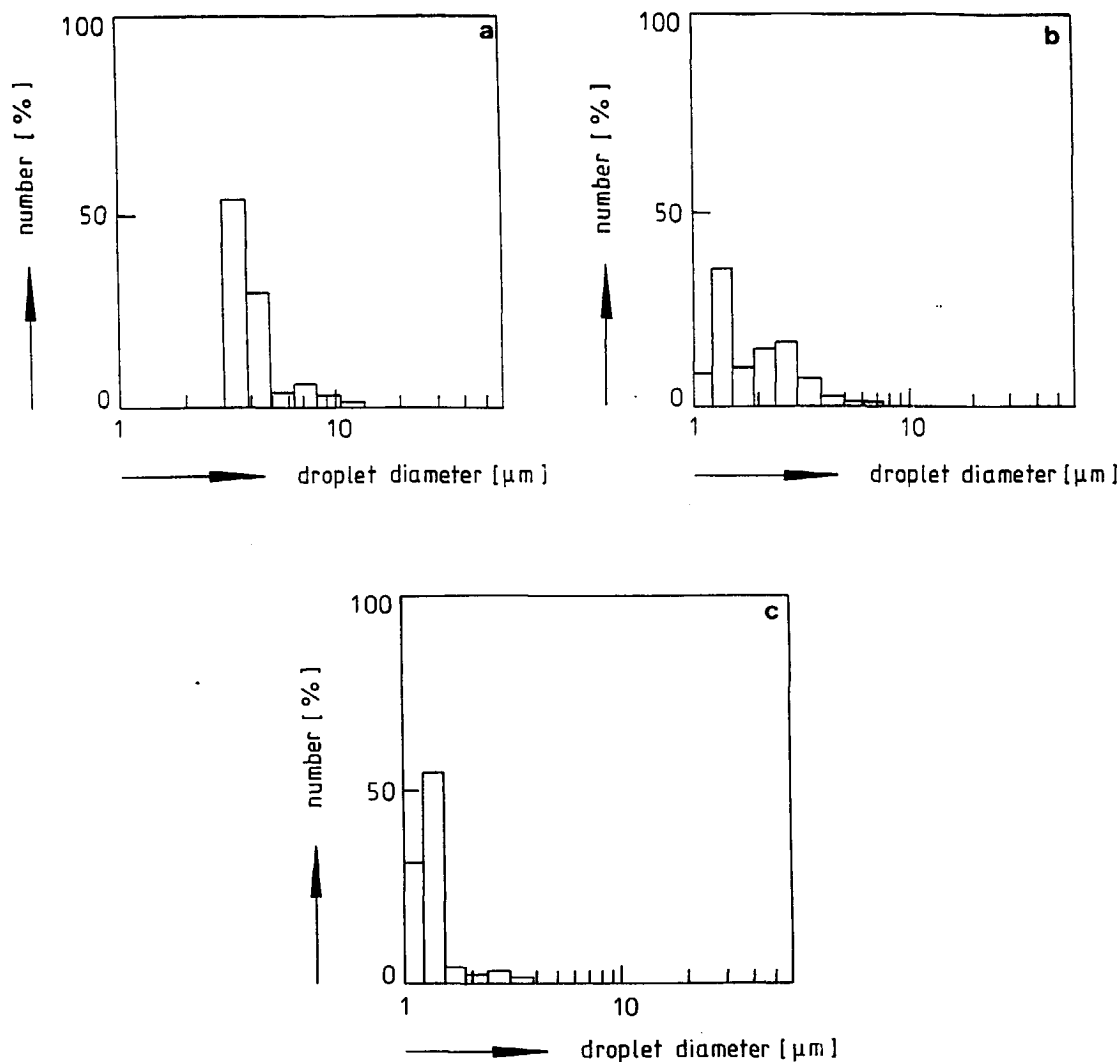


Figure 5.7 Emulsion size distributions as obtained from the Malvern 2600C. a) ethylene glycol in paraffin, b) ethylene glycol water mixture 40:60 wt% in paraffin, c) demineralised water in paraffin. Applied potential is 14 kV.

5.2.5 Stability of the emulsions produced

The emulsions produced were made using the same procedure each time. During three minutes the emulsions were produced at a flow rate of 5 ml/hour. The volume of the continuous phase was 250 ml. Five minutes after the emulsification had stopped the measurement using the Malvern 2600C was performed. This procedure was followed to ensure less time dependent influences. If coalescence or settling of the droplets occurs, the error made due to these is taken to be constant. To establish if coalescence does occur an emulsion of pure ethylene glycol in paraffin was produced, stabilised by the surfactants. The emulsion was measured according to the standard procedure and left standing afterwards. After fifteen and forty five minutes the emulsion was measured again. The results are shown in Table 5.6.

Table 5.6 Measurements of the droplet diameters of ethylene glycol emulsions in paraffin, followed in time.

time [min]	$d_{n,10}$ [μm]	$d_{n,50}$ [μm]	$d_{n,90}$ [μm]
5	3.1	4.4	7.5
15	3.5	4.6	8.2
45	3.4	4.7	8.3

A slight increase in droplet sizes is seen between $t=5$ and $t=15$ minutes, but the droplet diameter distributions stabilise in time. The difference is not very pronounced. Table 5.7 shows, like Table 5.6, the droplet size evolution in time, but now for an emulsion of a mixture of ethylene glycol water (40:60 wt. %) in paraffin.

Table 5.7 Measurements of the diameters of a mixture of ethylene glycol in water (40:60 wt. %) emulsions in paraffin, followed in time.

time [min]	$d_{n,10}$ [μm]	$d_{n,50}$ [μm]	$d_{n,90}$ [μm]
5	0.8	1.4	2.8
15	1.4	2.3	3.9
30	2.2	2.7	3.9

An increase in droplets size is clearly seen, very likely caused by coalescence of the smaller droplets, causing the increase of the $d_{n,10}$ thus not influencing the $d_{n,90}$.

5.2.6 Influence of the flow rate on the droplet sizes

To investigate the influence of the flow rate of the disperse phase into the continuous phase, three emulsions were produced at three different flow rates. The emulsions were made of pure ethylene glycol with 0.5 wt. % NaCl dissolved in it. The results are shown in Table 5.8.

Table 5.8 Three emulsions of ethylene glycol, with 0.5 wt. % NaCl dissolved in it, in paraffin. The applied potential is 18 kV.

flow rate [ml/h]	$d_{n,10}$ [μm]	$d_{n,50}$ [μm]	$d_{n,90}$ [μm]
5	2.7	3.6	6.2
10	3.3	4.2	7.1
15	3.2	4.4	7.3

The increase in flow rate influences the size distribution. Not only does the median droplet size increase, the size distribution is also broadened and shifted to larger values.

5.2.7 Influence of the conductivity on the droplet sizes

To investigate the influence of the conductivity on the emulsification process, NaCl was added to the ethylene glycol in different concentrations. Table 5.9 shows the number and volume D_{50} 's at different conductivities.

The influence of the conductivity is small when looking at the droplet sizes measured. At higher conductivities the $d_{n,50}$ decreases, while the $d_{v,50}$ does not.

Table 5.9 $D_{n,50}$ and $D_{v,50}$ for the emulsions made at different potentials at a constant flow rate of 5 ml/h and an applied potential of 18 kV, measured with a Malvern particle sizer as a function of the conductivity. Between brackets is the weight % of NaCl dissolved in the ethylene glycol.

conductivity [$\Omega^{-1}\text{cm}^{-1}$]	$D_{n,50}$ μm	$D_{v,50}$ μm
0.14 (0)	4.3	6.9
43 (0.1)	4.1	6.8
82 (0.2)	4.0	7.2
154 (0.3)	4.3	6.7
200 (0.4)	3.5	5.8
221 (0.5)	3.6	6.8

5.2.8 Onset potentials of the emulsification

At the onset of the emulsification process it looks as though an emulsion is coming straight from the small liquid cone, hanging from the nozzle.

The onset potentials for emulsification of the different liquids was also measured, as is shown in Table 5.10.

Addition of NaCl to the pure ethylene glycol, which dissolves in the ethylene glycol at low concentrations, does not change the onset potential of emulsification. When looking at the onset potential of the pure water and the water with 2% NaCl, the addition of the salt clearly lowers the onset potential. The addition of the salt almost increases the conductivity three orders of magnitude, from $1.65 \mu\Omega^{-1}\text{cm}^{-1}$ for the pure water to $1.48 \text{ m}\Omega^{-1}\text{cm}^{-1}$ for the water with 0.2 wt% NaCl. The conductivity of the pure water is higher than that of pure ethylene glycol ($0.14 \mu\Omega^{-1}\text{cm}^{-1}$). From this it appears

that the conductivity lowers the onset potential of the water, but no explanation for the high onset potential can be given.

Often at onset already several large droplets are flowing around in the continuous phase. This is due to start up, when the potential is still zero. Because of the high electric field, the continuous phase is circulating round in the vessel. The circulation is as described for the electric wind around the Taylor cones in the air, flowing down from the nozzle and upwards away from the nozzle. We observed that in the vicinity of the nozzle the large droplets are disrupted, producing smaller droplets. This phenomenon was also observed by Watanabe *et al.* (1978), but not further investigated.

Table 5.10 Onset potential for emulsification of several liquids

liquid	Onset potential [kV]
ethylene glycol	3.40
ethylene glycol + water	5.32
ethylene glycol + 0.1 wt% NaCl	3.34
ethylene glycol + 0.2 wt% NaCl	3.36
ethylene glycol + 0.3 wt% NaCl	3.40
water	11.61
water + 0.2 wt% NaCl	4.90

5.2.9 Emulsification by applying high fields to a premixed liquid phase

The following experiments were performed in order to establish if the emulsification can also take place if two liquids are put in the vessel together in bulk. A two phase liquid containing fifteen millilitres of disperse phase and two hundred and fifty millilitres of continuous phase was placed in the setup as described in Figure 5.6. The nozzle was replaced by a solid metal cone-shaped electrode. When applying the high potential, the liquid started to circulate rapidly as described, downwards from the nozzle and upwards near the vessel wall. The disperse phase lying on the bottom of the vessel was emulsified almost immediately. Visually the emulsion looks the same as the emulsions produced when the disperse phase flows from the nozzle at constant flow rate. Two liquids were dispersed this way, results are shown in Table 5.11.

When the liquid is introduced gradually through the nozzle, the disruption process is more constant and less violent, compared to the almost instantaneous emulsification, but this does not influence the size distributions.

Looking at the water emulsion, the droplet sizes of the emulsions produced this way is almost the same as when produced using the nozzle from which the liquid slowly issues.

Table 5.11 Droplet sizes of the emulsions produced by putting both continuous phase (250 ml), paraffin oil, and disperse phase (15 ml) into the vessel before emulsification. Applied potential is 18 kV. Between brackets are the values of the measured diameters, using the nozzle at a flow rate of 5 ml/h.

liquid	$d_{n,10}$ [μm]	$d_{n,50}$ [μm]	$d_{n,90}$ [μm]
ethylene-glycol	2.8 (3.0)	3.7 (4.2)	6.2 (7.0)
demineralised water	0.6 (0.4)	1.4 (1.3)	1.6 (1.5)

The droplet sizes decrease slightly when looking at the ethylene glycol emulsion. The size distributions were found to be a little more narrow when the liquids were pre-mixed.

This deformation and disruption of droplets has been described by others like Garton and Krasuchi (1964), Moriya *et al.* (1986), Scott and Scisson (1988), Sherwood (1988) and Haywood *et al.* (1991). If an emulsion is exposed to an electric field in which droplets are suspended, the droplets will assume an ellipsoidal shape. This is caused by the polarisation of the charges in the dispersed phase due to the externally imposed electric field. The conductivity of the dispersed phase has to be higher than that of the continuous phase. The charges attracted by the electric field will move in the direction of the electrodes and accumulate at the liquid-liquid interface. As a result the external field will cause a force on the poles of the ellipsoidal droplets,

making them even more elongated.

For perfectly conducting droplets, the limiting aspect ratio was found to be 1.83. Dielectric droplets show two distinct behaviour types dependent on the ratio of dispersed to continuous phase permittivities. Systems with large permittivity ratios, > 20.8 (Haywood *et al.* 1991), exhibit behaviour similar to conducting droplets.

A critical field strength exists, at which the elongation of the droplets becomes too high. The droplet then becomes unstable, and sharp points are formed, as seen with cones, which disrupt into smaller droplets. This elongation and breakup is shown in Figure 5.8. The droplets are ejected from the sharp conical tips at the poles of the droplets.

Systems with permittivity ratios below 20.8 will not form conical tips, and consequently there is no critical field strength. The droplets will theoretically accommodate any strength of electric fields by sufficient elongation. In our case ethylene glycol ($\epsilon_r = 37.7$), water ($\epsilon_r = 80$) and a mixture of ethylene glycol and water was used. The permittivity of the paraffin was about 1.5. The ratios of permittivity were all above 20.8.

The steady state behaviour of deforming liquid droplets subjected to electrostatic fields has been thoroughly studied, both theoretically and experimentally.

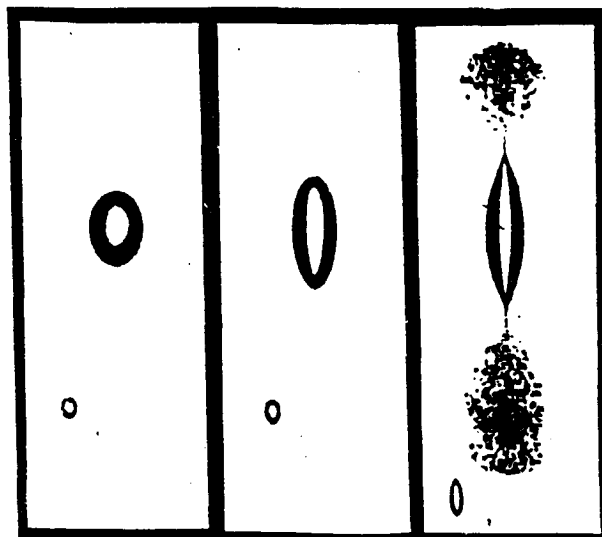


Figure 5.8 Deformation of a liquid droplets suspended into another liquid leading to break up of the droplet at higher potentials (Scott and Scisson, 1988).

A fundamental goal of these studies has been to define the critical field strength and critical permittivity ratio under steady conditions. In many instances however, the results seem conflicting and/or inconclusive.

Haywood *et al.* (1991) concluded from their simulations that the viscosity of the continuous phase predominantly determines the rate of deformation of the droplets. They developed a numerical model able to predict the transient history of deforming liquid droplets in electrostatic fields. The model demonstrates that the critical field strength and critical permittivity ratio during breakup are not necessarily the same as those predicted by steady state theories. The critical permittivity ratio was found to be 18.0.

5.2.10 Conclusions

The electrostatic emulsification process described can produce narrow droplet size distributions. The ethylene glycol dispersed into paraffin showed to be a stable emulsion in time. The water and the mixture of ethylene glycol and water (40:60 wt. %) in paraffin emulsions were found to be less stable, but could still be measured satisfactorily. Both, but especially the water emulsion, produced droplets near the lower detection limit of the Malvern 2600C forward light scattering device.

Using the ROMA program the 95 % confidence interval of the measurement were determined, revealing that near the lower detection limit the measurements were not very reliable. The pure ethylene glycol produced reliable data.

The liquid flowing from the nozzle showed a cone like shape, as described for the liquid cones, used for spraying in air. The difference with the liquid-air systems is seen in the size of the cone hanging from the nozzle, the droplet sizes produced and the onset potential. The cone formed in the liquid-liquid system is much smaller than that formed in the liquid-gas system. This might be due to the lower wettability of the nozzle. In air the whole nozzle ($d_{nozzle} = 0.5$ cm) is wetted by the liquid, and when pulled into a cone the nozzle remained covered by the base of the cone. In the liquid -liquid system the nozzle is not wetted by the liquid flowing from the nozzle, but the droplet is hanging at a slender filament, with a diameter of about the inner nozzle diameter. When a potential is applied a small cone is formed, the base only covering the inner opening of the nozzle.

The onset of emulsification is at much lower potential as in the air. In air, for ethylene glycol, the onset is around 9.5 kV, whilst in the liquid-liquid system the onset is around 3.4 kV, using the same configuration.

The droplets produced when spraying ethylene glycol are different when sprayed in air or in another liquid. The aerosol formed when spraying ethylene glycol in air has a modal aerodynamic mobility diameter, $d_{n,50}$, of about 1.5 μm . In the liquid-liquid system the $d_{n,50}$ is in the order of 4.5 μm , obtained using forward light scattering.

Like in air changing the applied potential does not influence the droplet sizes, neither does the conductivity have an influence on the droplet sizes produced when producing an emulsion. In air it is reported that by increasing the conductivity the droplet size is decreased.

From the measurements with ethylene glycol and NaCl, to determine the influence of the conductivity on the droplet sizes produced during emulsification, it was shown that this does not have an influence. Thus the difference in droplet sizes of the three liquids is probably caused by difference in interfacial tension or liquid viscosity, or by other parameters like the liquid-liquid shear rate or the electric permittivity.

The onset of emulsification was not influenced by the addition of NaCl to the ethylene glycol, but it did lower the onset for demineralised water. The conductivity of demineralised water ($1.65 \mu\Omega^{-1}\text{cm}^{-1}$) is higher than that of pure ethylene glycol ($0.145 \mu\Omega^{-1}\text{cm}^{-1}$) whose onset cannot be lowered. This implies that it is not the

absolute value of the conductivity which is important for the onset of emulsification. Watanabe *et al.*(1978) showed that when the ionic strength of the two liquids approach each other, the onset increases too. The ionic strength of the demineralised water is low as is the ionic strength of the paraffin, explaining the higher onset, but the ionic strength of pure ethylene glycol is also very low, and a higher onset was expected too. The reason for this is still not clear.

The droplet production rate is very high, about $2.9 \cdot 10^7$ droplets per second for ethylene glycol droplets of $4.5 \mu\text{m}$ produced at a flow rate of 5 ml/h.

The mixture of ethylene glycol and water (40:60 wt. %) produced droplets with a $d_{n,50}$ of about $1.6 \mu\text{m}$ and the demineralised water droplets had $d_{n,50}$ of about $1.2 \mu\text{m}$ or less.

It showed possible to create the emulsion just by adding the two liquid together, before applying the high potential. The emulsions formed in this way showed to be quite similar to the ones produced by issuing the liquid from the cone. The disruption process is like the liquid cones sprayed in air, described before. When looking at Figure 5.8, the third frame, the droplet is emitting small droplets from cone shape parts, the same shape is seen when looking at the droplet hanging in the liquid.

Like when spraying in air the drop size produced does not change with increasing potential, even like spraying in air a slight decrease of drop size can be found with increasing potential. This indicates like in air that a space charge regulating system controls the breakup in the emulsion too. Like in air, the surrounding medium is circulating too due to the high electric field and corona discharge. The electric wind was found to be a few meters per second, while the liquid flow rate in the emulsification process was estimated to be only a few centimetres per second.

The energy consumption of this emulsification process is low. At a flow rate of 5 ml/hour a current of about $1 \mu\text{A}$ at a potential of 18 kV is measured. The power consumption being only 0.018 Watt. But as tested the liquids do not have to be introduced gradually. Just a simple premixing of the two liquids can give a good emulsion by just applying a high electric field. An emulsion which has to be broken up further can also be treated in this way. The drop breakup in these cases is established by the high electric field which causes elongation of the droplets, causing small droplets to be ejected from the sharp tips formed at the ends of the elongated droplets.

5.3 References

- Garton, C.G., Krasucki, Z., (1964) *Proc. Roy. Soc. London A*280, 211
Haywood, R.J., Renksizbulut, M., Raithby, G.D., (1991) *AIChE. J.* 37(9), 1305
Hughes, J.F., Pavey, I.D., (1981) *J. Electrostatics* 10, 45
Hughes, J.F., Pavey, I.D., Arimoto, M., (1981) *IEEE Conf. Rec. LAS Ann. Meeting*, 1031
Hughes, J.F., Roberts J.M.C., (1984) *Int. J. Cosmetic Sci.* 6, 103
Meesters, G.M.H., Vercoulen, P.H.W., Marijnissen, J.C.M., Scarlett, B., (1992), *J. Aerosol Sci.* 23(1), 37

Chapter 5

- Moriya, S., Adachi, K., Kotaka, T., (1986) *Langmuir* 2, 155
Nawab, .., Mason, .., (1958) *J. Colloid Sci.* 10, 179
Scott, T.C., Scisson, W.G., (1988) *Sep. Sci. Technol.* 23(12+13), 1541
Sherman, P., (1968) *Emulsion Science*, Acad. Press Inc. London
Sherwood, J.D., (1988) *J. Fluid Mech.* 188, 133
Smith, D.P.H. (1986) *IEEE Trans. Ind. Appl.* 1A-22 (3), 527
Taylor, G.I. (1964) *Proc. Roy. Soc. A280*, 383
US Patent No. 4,829,996 (1989) by T.J. Noakes, ICI, England
Watanabe, A., Higashitsuji, K., Nishizawa K., (1978) *J. Colloid Interface Sci.* 64(2), 278
Watchtal, A., (1962) *J. Colloid Sci.* 17, 531

There can never be a last word in regard to the axioms of any physical theory. All we can ask of them is that they lead to conclusions in agreement with observations. Sooner or later more refined observations will find the weak point in any set of physical axioms.

Nature is far too complicated to be completely described in a few equations.

J.L. Synge (1938), Semi-centenn. Publ. Amer. Math. Soc. 2, 227-69

6 General Conclusions

In the future the phenomenon of the Taylor cone should be referred to as a phenomenon of liquid cones. Only one liquid cone exists that can be called a Taylor cone. That is the liquid cone which exists in the extreme case where the pressure caused by the surface tension is just balanced by the electric pressure. At this point no droplets are emitted, and there is little or no tangential shear stress.

Many different liquid cones, similar to the Taylor cone exist, but in all of these cases the electric pressure is out of balance with the pressure caused by the surface tension. In these cases Taylor's equation is not valid and therefore these liquid cones should not be referred to as Taylor cones.

The liquid cones exist because of the existence of the tangential shear caused by the potential drop over the cone surface. This potential drop results from the use of semi-conducting liquids. These liquids exhibit a conduction resistance to the charges which have to migrate through the cone to the surface, to compensate for the loss of charges due to the emission of charged droplets and ions. At the same time this explains why conducting liquids are not easily kept in a stable cone: then no stabilising tangential shear exists. This tangential shear causes the drop to be stripped of its outer layer of liquid, it is this layer which is dispersed into the droplets formed.

It was seen that the liquid cones change their shape with varying applied potential. This phenomenon was explained by the measurement of the current voltage characteristics. These were seen to be similar to those of coronas around solid needles, but not exactly the same. The difference explains the changing shape. With increasing potential on a solid needle, the amount of space charge must change to

diverge the electric field, in order to prevent breakdown of the field. For liquid cones, changing the potential also results in change in the tangential shear. This regulates the stripping of the cone surface. By increasing the potential the tangential shear increases and strips the cone surface at a higher rate. This causes the cone surface to diminish, causing the tangential shear to diminish. This process continues until the potential drop over the cone surface is almost equal to the previous steady state. Thus the tangential shear is almost equal to its previous state causing the current to be equal too. For the liquid cones it is therefore not the amount of space charge which is changed, but the shape of the liquid cone, cone shape regulates the field around it preventing electric breakdown of the field. The potential drop over the cone surface was found to be constant with increasing potential.

The liquid cones showed more similarities to the corona discharge around solid needles. Two of the characteristic corona regimes, the burst-pulses and the pulseless glow regimes, were found for the liquid cones. The frequency of these burst pulses was found to be a hundred times lower than those of the coronas around the needles. These pulses are caused by the charged droplets coming from the cone at onset. This was explained by the lower mobility of the charged droplets coming from the liquid cones, compared to the ions coming from the needles. The pulses detected on the current were of the same frequency as reported by Smith (1986). The space charge in this regime creates a path, a streamer, facilitating the flow of charges.

The second corona regime, the pulseless glow regime, was found as well for the liquid cones. Then no current pulses were detected. As expected, the liquid cones also exhibit a corona glow in this regime, caused by a gas discharge around the tip. Only the gas molecules around the tip participate in the gas discharge. Exited and ionised states of the surrounding N₂-molecules were measured. Exited states of the vibrational levels of the surrounding N₂ molecules were measured. No exited states of the liquid material could be measured. The cones do not participate in the gas discharge.

Due to this corona and the high electric field, an electric wind was found to be present around the liquid cones as, found around solid needle corona discharges. The pressure caused by this wind should be accounted for as well in the theoretical analysis. We were not able to perform very accurate measurements of the speed of these electric wind and their direction.

By simulation of the potential distributions around the liquid cones the electric fields and the electric stresses could be calculated. Field calculations showed that the space charge must be present to lower the local field around the tip of the cone. It was found that the normal force acting on the cone surface increased slightly with increasing potential. The tangential force, about ten times smaller in value, was found to constant with increasing potential. So the net force acting on the cone surface does not change much with changing applied potential, explaining the fact that the droplet size is almost independent of the applied potential.

The local electric stresses were found to increase enormously near the apex of the

cones, explaining the increasing circulating liquid movement near the apex.

The calculated field strength is much too high near the cone tip. This is caused by the fact that no space charges is taken into account, during the simulations performed. At the same time the high values prove that space charge has to be present to reduce the local field strength.

What really happens at the tip of the cone and how the droplets are formed remains a matter of speculation. Photographs could not reveal much. At the high production rates of 10^8 droplets per second and higher, the droplets can not be formed one by one. The droplets formed were seen to follow a spiralling path down from the cone. When the potential on the nozzle is increased even more, several more cones are formed at the rim of the nozzle. These cones are much smaller in size. One single cone can no longer reduce the field by changing its shape. Now extra space charge is produced to reduce the local field. The current increases every time an extra cone is formed.

The hysteresis in the current voltage characteristic can be explained by the existence of the tangential field. This tangential field causes the tangential stress to remain present still when the applied potential is lower than the onset potential. Thus the cone still remains and remains emitting droplets. When the applied potential decreases the tangential stress decreases as well. At a certain point this tangential stress will no longer be able to cause droplets top be emitted. Now the electric pressure exactly balances the pressure caused by the surface tension. When at this point the liquid flow through the nozzle is stopped too, the one and only real Taylor cone is established.

By being able to discharge the droplets coming from the cones, an aerosol generator, called the Delft Aerosol Generator (DAG), was developed. It was thus possible to measure the droplet sizes and size distributions. Ethylene glycol was seen to be dispersed into droplets with modal sizes of 1.3 to 1.5 μm , size increasing slightly with increasing potential applied. The relative standard deviation was found to be around 10 to 25%. Using mixtures of DOP and ethanol, droplets as small as 0.08 μm were obtained. Changing the concentration of DOP causes the size of the DOP droplets produced to change.

By submerging the system in another liquid, immiscible with the liquid from the cones and of low conductivity, emulsions were obtained. Depending on the liquids used, the droplet sizes changed between about 1 and 5 μm . Little or no influence was found by changing the conductivity of the disperse liquid, or by changing the liquid flow rate. As, when spraying in air, the potential was increased, the median droplet sizes increased slightly too.

The onset potential of emulsification is not influenced by the addition of NaCl when using ethylene glycol. However addition of NaCl to water does lower the onset for emulsification. No explanation was found.

The liquid dispersed does not have to be introduced gradually through a nozzle. In our case, addition of the disperse phase to the continuous phase, without premixing,

gave a similar emulsion, when a high non-uniform electric field was applied to this mixture.

From the work described in this part of the thesis we can conclude that the electrical behaviour of the liquid cones is now better understood than previously. New electric field calculations will have to be done, now accounting for the space charge formed and for the liquid flow inside the cone as the electric wind. This will be difficult. The results from these calculations will show if the above performed static calculations are accurate enough for explaining the phenomenon.

Still little is known about what happens at the tip of the liquid cones, how droplets are formed. A one at a time mechanism for droplet formation seems to be difficult to envisage when the droplets are produced at a rate of 10^8 to 10^{12} per second. More work has to be done on this part as well.

The liquid cones are not only purely of scientific interest, but can be put to use for practical purposes. The size of the droplets produced by the liquid cones can still not be calculated or predicted. We know that the liquid viscosity and the conductivity influence the droplet sizes, but how this influence occurs must still be investigated.

PART TWO

Jet break-up by mechanical vibrations

*Science is nothing without generalisations.
Detached and ill-assorted facts are only raw materials,
and in the absence of a theoretical solvent,
have but little nutritive value.*

Lord Rayleigh (1884), Science 4, 179-184

7 Introduction

The investigations of jet break-up, leading to the formation of droplets, was first described by Savart (1833) and Plateau (1856). They found that a jet is stable to all but axisymmetric disturbances of wavelengths greater than the circumference of that jet. It was Lord Rayleigh (1878) who first described a mathematical analysis of the jet break-up for inviscid liquids. In 1931 Weber included the effects of viscosity and aerodynamic drag into the analysis. These theories still stand as the principles of jet instability. To the present however, close to the point of break-up as well as at higher initial disturbances, observations show an asymmetrical development superimposed on the initial sinusoidal wave.

In practice it was not possible to use the theories of Rayleigh and Weber for all radii and wavenumbers applied ($k \cdot a$ =dimensionless wavenumber, with $k=2\pi/\lambda[m^{-1}]$ and a =jet radius [m]). Often it was seen that satellites accompany the jet break-up, satellites being small droplets formed between the main droplets. This kind of break-up leads to at least two droplets per wavelength which was not explained by the theories. At larger wavenumbers the theories were better able to describe the process of break-up. It was McCormack *et al.* (1964) who extended the theories of Rayleigh and Weber to second order terms and to finite disturbances but it was not until Yuen (1968) described his third order, non-linear theory that satellite formation could also be predicted. Yuen's theory takes into account the non-linear behaviour of jet break-up. Goedde and Yuen (1970) verified the theory experimentally.

main droplets of equal sizes, thus producing uniformly size droplets at a rate of two per wavelength. They calculated that at low wavenumbers, $k \cdot a \sim 0.2$, the volume of the satellites becomes equal or almost equal to the volume of the main droplet. In practise however, at these low wavenumbers the total volume of the satellites consists of at least two droplets. What clearly could be seen from these calculations was that at higher wavenumbers, $k \cdot a > 0.7$, the volume of the satellite becomes zero. Here truly uniformly sized droplets can be expected at a rate of one per wavelength.

In the second part of this thesis the theories of Rayleigh, Weber and Yuen will be briefly reviewed and the satellite formation mechanisms will be qualitatively described. From growth rate calculations it will be shown that, when using liquids of low viscosity, break up into uniformly sized droplets occurs at the higher wavenumbers ($k \cdot a > 0.6$). Disturbances with these wavenumbers were applied to a jet superceeding the random disturbances from the surroundings and causing the jet to break up according to this forced oscillation. By increasing the viscosity of the liquid jet, uniformly sized droplets were produced at wavenumbers between 0.4 and 0.7. The uniformity of these droplets was proven by taken photographs of the droplets just after the jet break-up and also by solidifying the droplets produced. The amplitude and the growth rates of the initial disturbance were determined and compared to the break-up of free jets and to literature values.

It was Sakai *et al.* (1980, 1982, 1985) who described regions of uniform break-up of liquid jets for a longitudinally vibrated jet. The experiments, dealing with the uniform jet break-up, are based on the work by Sakai *et al.*. Uniform regions of jet break-up were determined using different liquids. The limits of these regions were calculated using dimensional analysis.

A practical application of the uniform break-up was tested. By being able to produce uniformly sized droplets it is also possible to produce a desired, tailor made, size distribution by a controlled time cycle. This was achieved by automation of the vibration unit.

7.1 References

- Goedde E.F., Yuen M., (1970), *J.Fluid Mech.*, **40**(3), 495
Lafrance P., (1975), *Phys Fluids*, **18**, 428
McCormack P.D., Crane L., Birch S., (1964), *Brit. J. Appl. Phys.* **15**, 743
Plateau M., (1856), *Statistique Experimental et Theoretique des Liquides Soumis aux Seule Forces Moleculaires*, Paris
Rayleigh, Lord F., (1878), *Proc. London Math. Soc.*, **11**, 4
Rutland D.F., Jameson G.J., (1970), *Chem. Eng. Sci.*, **25**, 1689
Sakai T., Hoshino N., (1980), *J. Chem. Eng. Japan*, **13**(4), 263
Sakai T., Sadakata M., Saito M., Hoshino N., Senuma S., (1982), *Proc. Int. Conf. Liquid Atomisation and Spray Systems, ICLASS-82*, Japan, **2-1**, 37
Sakai T., (1985), *Proc. Int. Conf. Liquid Atomisation and Spray Systems, ICLASS-85*, England, **VII-13(b)2**, 1

Chapter 7

- Savart F., (1833), *Ann. Chim. (Paris)*, **53**, 337
Scarlett B., Parkin C.S., (1977), *Chem. Eng. J.*, **13**, 127
Yuen M.C., (1968), *J. Fluid Mech.*, **33**(1), 286
Weber C., (1931), *Z. für Angew. Math. Und Mech.*, **11**, 136

... there is no greater delusion than to suppose that the spirit will work miracles merely because a number of people, who fancy themselves spiritual, keep on saying it will work them.

*L.P. Jacks, The education of the Whole Man, Univ. London Press 1931
Cedric Chivers, 1966, p. 77*

8 Stability analysis of cylindrical jets

A liquid jet is sensitive to any forces or disturbances which leads to a lower energy situation. These disturbances can be either natural or imposed. Natural disturbances can arise from all sorts of background noise. Alternatively, forces may be imposed by mechanical vibration or electrical forces.

The disturbances can lead to different modes of oscillation, e.g. axisymmetrical oscillation or transverse mode.

For the axisymmetric oscillation to grow, and eventually leading to break-up, Plateau (1856) found that the wavelength, λ , must be larger than the circumference of the jet: $\lambda > 2\pi a$, a being the radius of the jet, or: $k \cdot a < 1$, k being the wavenumber: $2\pi/\lambda$. In this case a jet is unstable to axisymmetric modes of break-up, but stable to all non-axisymmetric modes.

Experimentally it is observed that on a cylindrical jet only axisymmetrical disturbances of the following form grow:

$$r = a + \alpha(t) \cos(kz) \quad (33)$$

where a = radius of unperturbed jet [m]

$\alpha(t)$ = small time dependent disturbance amplitude [m]

r_s = radius of the swell [m]

z = axial distance [m]

This particular form of perturbation is often referred to as the "sausage perturbation", see Figure 8.1.

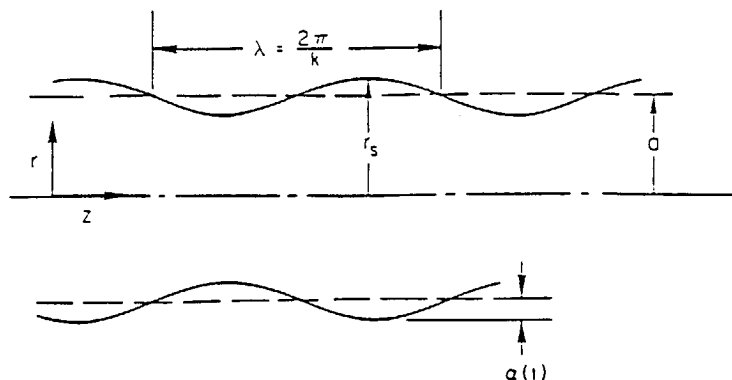


Figure 8.1 Geometry of a cylindrical jet with axial disturbance

Only this axisymmetric perturbation mode is investigated in this part of the thesis. A clear derivation of the Rayleigh and the Weber theory is given by Anno (1977). Here electric surface charge, surface shear, gravity and the Coriolis force effects are also included in the analysis.

8.1 Rayleigh Break-up: Inviscid cylindrical jet break-up

To investigate the growth rate of a disturbance on a jet consider the following. A control volume V being part of an incompressible inviscid cylindrical liquid jet obeys the equation of conservation of energy:

Rate of work done on the system = net outflow of kinetic energy + rate of increase of kinetic energy + rate of change of energy inside control volume due to mechanical forces

In tensor form:

$$\int_S \tau_{ij} n_j u_i dS - \int_S \rho u_j n_j \frac{1}{2} u_i u_i dS + \int_V \frac{\partial}{\partial t} \frac{1}{2} \rho u_i u_i dV + \int_V R dV \quad (34)$$

- with τ_{ij} = stress tensor = $p_h \delta_{ij}$
 p_h = hydrodynamic pressure [Pa]
 δ_{ij} = Kronecker delta [-]
 n_j = the projection of the outward unit normal vector to the surface in the j^{th} direction.
 u_i = the velocity component in the i^{th} direction [m/s]
 S = surface area of the control volume [m^2]
 ρ = liquid density [kg/m^3]
 R = viscous energy dissipation
 $= (\eta/2)(u_{i,j} + u_{j,i})^2$

Neglecting body forces, the only work done on the volume V is by the hydrodynamic pressure p_h . The kinetic energy outflow perpendicular to the surface is represented by $\frac{1}{2}\rho v^2$.

Neglecting the viscous energy term in equation (34) and substituting equation (33) leads to the following:

$$\dot{\alpha} - \alpha \frac{\sigma}{\rho a^3} \left[k a (1 - k^2 a^2) \frac{I_1(ka)}{I_0(ka)} \right] \quad (35)$$

σ = surface tension [N/m]

$I_1(ka)$ and $I_0(ka)$ are Bessel functions

Assume an exponential growth of the disturbance, given by:

$$\alpha(t) = \alpha_0 e^{\omega t} \quad (36)$$

with ω = the growth rate of the disturbance [s^{-1}]

α_0 = initial disturbance [m]

The solution is:

$$\omega^2 - \frac{\sigma}{\rho a^3} \left[k a (1 - k^2 a^2) \frac{I_1(ka)}{I_0(ka)} \right] \quad (37)$$

It is seen that the growth rate has a real, positive solution for values of the growth rate $0 < k \cdot a < 1$. This means that disturbances having a wavelength greater than the circumference of the jet will grow and lead to break-up. The maximum growth rate, for liquids of low viscosity occurs at $k \cdot a = 0.696$. This particular disturbance grows most rapidly. For the first time Rayleigh put forward the idea that the fastest growing disturbance would become the dominant one.

For simplicity the approximation $I_1(ka)/I_0(ka) = ka/2$ can be used when $k \cdot a < 1$, which reduces equation (37) to

$$\omega^2 = \frac{\sigma}{2\rho a^3} k^2 a^2 (1 - k^2 a^2) \quad (38)$$

8.2 Weber break-up: Viscous cylindrical jet break-up

Weber (1931) extended Rayleigh's instability analysis by including the effect of viscosity into the analysis. The factor R (Eq. 34) as the viscous energy dissipation is given by;

$$R = \frac{\mu}{2} (u_{i,j} + u_{j,i})^2 \quad (39)$$

where μ = fluid viscosity [Pa·s]

$$u_{ij} = \frac{\partial u_i}{\partial x_j}$$

u_i = velocity in the i^{th} direction

In this viscous case the integral energy equation, assuming an axi-symmetric perturbation, leads to the following equation:

$$\ddot{\alpha} + \left(\frac{\eta k^2}{\rho} \frac{(24 + k^2 a^2)}{(8 + k^2 a^2)} \right) \dot{\alpha} - \left(\frac{4 \sigma k^2 a^2}{\rho a^3} \frac{(1 - k^2 a^2)}{(8 + k^2 a^2)} \right) \alpha = 0 \quad (40)$$

By stating that $k^2 a^2 \ll 1$ equation 40 can be simplified, giving:

$$\ddot{\alpha} + \left(\frac{3 \eta k^2}{\rho} \right) \dot{\alpha} - \left(\frac{\sigma}{\rho a^3} (1 - k^2 a^2) k^2 a^2 \right) \alpha = 0 \quad (41)$$

Again, for $0 < ka < 1$, the jet is unstable. The exponential growth solution $\alpha(t) = \alpha_0 e^{\omega t}$, combined with equation (41) gives:

$$\omega^2 + \frac{3\eta k^2}{\rho} \omega - \frac{\sigma}{2\rho a^3} (1 - k^2 a^2) k^2 a^2 = 0 \quad (42)$$

From this equation it can be seen that viscosity decreases the growth rate of the instability dramatically, although the instability is only completely damped by an infinite viscosity. For $\eta = 0$, eq.42 results in Rayleigh's simplified formula (Eq.38).

For a very viscous jet, where

$$\left(\frac{3\eta k^2}{2\rho} \right)^2 \gg \frac{\sigma}{2\rho a^3} \quad (43)$$

the solution reduces to

$$\omega = \frac{\sigma}{6\eta a} (1 - k^2 a^2) \quad (44)$$

The effect of viscosity is to decrease the magnitude of the growth rate. The maximum growth rate shifts towards smaller values of $k \cdot a$ due to the fact that viscous damping is more effective at larger $k \cdot a$ where there is a larger velocity gradient. Viscosity has an inhibiting effect on the break-up of liquid jets and also on the formation of satellites. Goedde and Yuen (1970) report that at higher viscosities the diameter of the neck has to become even smaller in order to overcome the dissipative and inhibiting effects of viscosity and thus create a pressure difference large enough to result in detachment. In these conditions the ligaments become more slender and threadlike.

For visco-elastic liquids, Bousfield *et al.* (1986) concluded that disturbances on visco-elastic jets will initially grow more rapidly than on the Newtonian jets, which are predicted by the linear stability theory. However there is a retardation of the growth of the disturbance and stabilization of the visco-elastic jets at longer times as a consequence of the build up of large extensional stresses. This retardation also prevents satellite droplet formation and remains the thinnest point of the filament at the midpoint between droplets.

8.3 Non-linear capillary instability

From the experimental results of many investigators it can be concluded that the linearised analyses of Rayleigh and Weber hold only for small disturbances and wavenumbers close to $k \cdot a = 1$. At lower wavenumbers and at larger disturbances asymmetrical development occurs, causing a liquid jet to disintegrate into drops with ligaments between. These ligaments form one or more satellite droplets. Rayleigh suggested that this is caused by the superposition of higher harmonics. Another explanation, investigated by Yuen (1968), is the role of non-linear effects. The influences of the non-linear effects is discussed in the next part. With those non-linear effects taken into account, the satellite formation can be explained.

Yuen developed a third order solution of the non-linear theory to predict an asymmetrical development of an initially sinusoidal wave. He expressed the surface disturbance in the following form:

$$\alpha - \sum_{m=1}^{\infty} \alpha_0^m \alpha_m \quad (45)$$

The first three terms were evaluated. Yuen concluded that the third-order solution represents the asymmetrical development.

The growth of harmonics is partially due to the non-linear terms present in the fundamental growth. This means that, even when there is no initial harmonic on the input, the fundamental will feed energy to the induction of harmonics. The growth of harmonics is also caused by the instability of the harmonic itself when its wavenumber is smaller than one.

Yuen's result also predicts different growth rates of the neck and the swell. A decreasing wavenumber implies a narrowing of the swell and a broadening of the neck on the wave. Taub (1976) found that the exponential growth rate of surface deformation is not constant, thereby confirming Yuen's theory. At small values of $k \cdot a$ ($= 2\pi a / \lambda$) the non-linear effects are more pronounced. The neck portion of the jet, which, after detachment forms the ligament, is much longer and almost stops contracting while the swell portion of the jet narrows and grows rapidly. Thus the point of detachment of the jet occurs away downstream from the centre of the neck, simply because this portion has had more time to contract.

Yuen's theory was also tested by Taub (1976). He pointed out that Yuen describes a periodic disturbance on an infinite cylindrical column of fluid and does not describe the spatial instability of a finite jet. The difference between the two cases is that the temporal instability method describes the jet as a standing wave on an infinitely long cylinder with the nozzle at infinity. It assumes that the wavelength of the disturbance remains constant as the disturbance evolves and this analysis is, therefore, limited to the early stages of growth. The spatial instability method describes the disturbance of the jet as a travelling wave in the axial direction. This method has been used, amongst others,

by Busker (1989).

These two approaches yield different results at low jet velocities. However, in cases where the jet velocity is much greater than the characteristic velocity $u_c = \sqrt{(\sigma/\rho)R}$, both solutions coincide.

Taub measured the amplitude of the growth of the fundamental and the first and second harmonic disturbance for a fundamental $k \cdot a$ -value at which the first three modes of the disturbance were unstable. He separated the harmonic terms from Yuen's equation and compared them to his experimental observation. This takes the form:

$$R = 1 + A_1(t) \cos \pi z + A_2(t) \cos 2\pi z + A_3(t) \cos 3\pi z + \dots \quad (46)$$

The agreement with theory was excellent. It appeared that for small disturbances and at a short distance from the nozzle the harmonic components are negative, just as Yuen's theory predicts.

Rayleigh's theory, although linear, predicts the growth rates but is not able to predict the asymmetrical behaviour. The theory of Yuen must be used in these cases, but this theory does not hold for the large displacements which occur near the point of break-up.

The size of the ligament decreases with increasing wavenumber. The reason for this is the fact that the non-linear effects diminish at higher wavenumbers so that the sinusoidal wave shape is preserved at much larger wave amplitudes. This was shown by Yuen (1968).

This asymmetry of the surface disturbance occurs earlier for large initial disturbances than for those having a small amplitude.

The dimensionless cut-off wavenumber, $k_c \cdot a$, which separates the region of stability from instability, ($k \cdot a = 1$ for the linear case) turns out to be dependent on the initial disturbance:

$$k_c a = 1 + \frac{9}{16} \alpha_0^2 \quad (47)$$

and the maximum growth rate occurs at

$$k a_{\max} = 0.697 - \alpha_0^2 \frac{3.26}{4} \quad (48)$$

8.4 Detachment from the jet

These non-linear effects cause two droplets to be detached in each wavelength instead of one as in the linear, purely sinusoidal, case: a nearly spherical main droplet and a highly extended ligament.

Goedde and Yuen (1970) explained the detachment of ligaments qualitatively by estimating the pressure distribution in the jet from principal radii measured by using enlarged pictures.

It is obvious that, at least at low viscosity, the capillary pressure gradients commensurate with the varying radius at different places in the jet initiate fluid motion which try to eliminate the pressure differences. The higher the pressure at one spot the faster a fluid element will flow towards places of lower pressure. Since the fluid is incompressible, this causes a contraction of the surface at this spot followed by an increase in the pressure gradient, accelerated contraction and eventually break up.

The size of the ligament decreases with increasing wavenumber. The reason is the fact that the non-linear effects diminish at higher wavenumbers so that the sinusoidal wave shape is preserved for much larger wave amplitudes. This has been shown by Yuen (1968).

The main droplets observed by Goedde and Yuen do obey Lamb's equation (1932) and oscillate at the predicted resonance frequency. The water-glycerin droplets, having a radius of approximately 0.5 mm, were damped periodically as predicted by Chandrasekhar (1961).

8.5 Satellites

If the wavenumber becomes too low, satellites start to form as predicted by Yuen (1968). Ligaments between the main droplets become separated. It has been observed that they either contract to form single satellite droplets or break up into even smaller drops due to the oscillations of the ligament. Until now there is no theory predicting exactly whether further break-up (more than one satellite) will occur.

However, Goedde and Yuen (1970) give a good qualitative description of the process.

8.6 Ligament detachment

At the later stages of growth, the non-linear effects become very pronounced. For small values of $k \cdot a$, the neck portion of the jet actually stops contracting while the swell portion of the jet narrows and extends rapidly. The point of detachment of the jet occurs away from the centre of the neck at the point where the internal pressure has its

maximum.

According to Goedde and Yuen (1970) the internal pressure distribution dictates the place where the detachment takes place.

Flow data for water and viscous jets show that the size of the ligament decreases with increasing wavenumber of the disturbance. This occurs because the non-linear effects diminish as the wavenumber increases so that the sinusoidal wave shape is preserved for much larger wave amplitudes. This is predicted by Yuen's analysis. The ligament of a short wavelength disturbance will, therefore, grow to a relatively smaller diameter before the non-linear effects can create the strong pressure gradient necessary for detachment. Viscous jet data also reveal that the ligament diameter decreases with increasing fluid viscosity for jets perturbed by the same wave-number. It originates from the need for an increased pressure difference between the ligament and droplet. This difference is needed to overcome the dissipative and inhibiting effects of viscosity and to create detachment of the ligament from the drop.

An increase in viscosity enhances the inhibiting effects and in order to effect detachment the ligaments have to be more slender and threadlike.

8.7 Contraction of extended droplets

The ligaments formed due to the non-linear effects will relax to their most favourable energy situation, spherical, at which droplets have a minimum surface area. The main droplets are somewhat deformed and starts to oscillate in their resonance frequency. This oscillation is gradually damped (Chandrasekhar (1961) and Reid (1960)).

As soon as the ligament has been detached from the drop it will start to contract due to three mechanisms: swell formation, global contraction and capillary instability. Those three mechanisms are discussed in more detail in the next part.

8.7.1 Swell formation

The sharply pointed end of the ligament formed during detachment has an internal pressure which is much higher than in other parts of the almost cylindrical ligament due to the capillary pressure gradient. In order to alleviate this pressure difference, the end of the ligament tends to contract to form a swell. From surface tension considerations, for the pressure to be equal, the radius of the swell R_s , must be twice that of the cylinder R_c :

$$\sigma \left(\frac{1}{R_c} + \frac{1}{\infty} \right)_{\text{cylinder}} = \sigma \left(\frac{2}{R_s} \right)_{\text{sphere}} \quad (49)$$

However, when the swell has attained this radius, contraction continues due to global contraction.

8.7.2 Global contraction

Experiments performed by Goedde and Yuen show a constant contraction rate for both water and glycerin-water droplets. From this experimental results a rough estimate of the velocity of contraction, v_c , was proposed:

$$v_c = \sqrt{\frac{2\sigma}{\rho R_c}} \quad (50)$$

R_c equals the radius of the cylindrical portion of the ligament.

8.7.3 Capillary instability

The capillary instability refers to the instability of the ligament between the main droplets. Capillary instability occurs in cases of low viscosity when disturbances on the ligament surface tend to propagate as a surface wave. Short wavelength waves are caused by the initial contraction of the sharp detached end. As the end rolls up to form a larger and larger swell, the disturbance which propagates upstream becomes bigger and its wavelength longer. Nevertheless these wavelengths are smaller than the local circumference of the ligament and should, therefore, be stable.

However, because of the large amplitude of these waves and the contraction of the ligament, a condition can develop such that the pressure at the neck is higher, thus creating an unstable situation. Left to itself, fluid would flow away from the neck leading eventually to detachment. If the contraction rate is high enough the two swells coalesce before disengagement at the neck occurs. The result of the competition between the contraction and this local disengagement are not always one-sided. Sometimes a swell is actually detached from the main ligament. This normally occurs for the larger swell at the lower end, where local contraction is slower.

Surface waves on the thin ligaments can also be initiated by background noises causing unpredictable break-up.

8.7.4 Competition of the mechanisms

Whether break-up of the ligament occurs depends largely on the characteristic velocities of the different mechanisms involved. In the case of a highly viscous liquid, the speed at which swell formation occurs is much lower than the rate of contraction and the growth-rate of any disturbances is also very low. Hence, the ligament does not split into smaller satellites. In the case of liquids of low viscosity capillary instability is much less inhibited and break-up due to this mechanism can occur.

8.8 Coalescence of satellite with main droplet through harmonics

In some cases it is seen that the satellites formed are recaptured into the main droplet, causing the jet to break up into uniformly sized droplets. Chaudhary and Redekopp (1980) made a solution to the third order using the temporal instability method, similar to that of Yuen (1968).

From the solutions they observed, that with a fundamental input only, theoretically the satellites do not move relative to the main droplet and therefore will not merge. However, combining the fundamental with a harmonic results in a time dependent phase behaviour of these harmonics and of the satellites. By changing the phase of the input harmonic, the motion of the satellite relative to the main droplet can be controlled. Chaudhary and Maxworthy (1980) performed experiments and showed that by using the second and the third harmonic in the region between $0.34 < k \cdot a < 0.6$, merger of the satellite and main droplet could be achieved. This could be an important factor in broadening the range of wavenumbers giving uniformly sized droplets.

8.9 Calculations based on Yuen's theory

With the theory derived by Yuen (1968), the displacement of the jet can be predicted as a function of the applied $k \cdot a$ values. Scarlett and Parkin (1977) calculated the volume of the main droplets and the satellites formed, thus predicting the diameters of the main and satellite droplets. The jet profile was calculated as a function of the wavenumber, axial distance and time. Rutland and Jameson (1970) calculated that, at a certain wavenumber ($k \cdot a \approx 0.2$), the main and satellite were equal in volume. According to Scarlett and Parkin this is not possible. On the other hand, Lafrance (1975) also calculated that the volumes of the main and satellite can become equal. When one looks at the break-up at these low wavenumbers it is seen that there is usually more than one satellite. Those two or more satellites together may have the same volume as the main droplet, but no single satellite drop can be found of the same size as the main droplet. What was found by Lafrance (1975) and Scarlett and Parkin (1977) was that the volume

of the satellite decreases with increasing wavenumber, eventually becoming zero at wavenumbers larger than 0.7-0.8. Figure 8.2 shows the decrease in size of the satellite with increasing wavenumber, eventually leading to no satellites at a value of $k \cdot a = 0.7$. Here true uniformly sized droplets are produced.

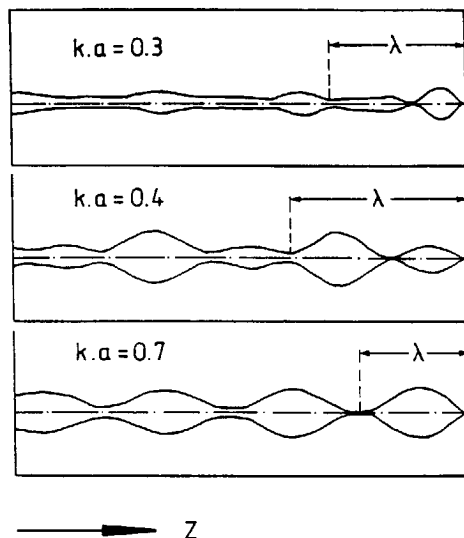


Figure 8.2 Wave profiles as calculated using Yuens Theory (from Busker et al. 1989) (dimension of z-axis is different for every wave)

8.10 References

- Anno J.N., (1977), *The Mechanics of Liquid Jets*, D.C. Heath and company, USA
 Bousfield D.W., (1986), *J. Non-Newtonian fluid Mech.*, 21, 79
 Busker D.P., Lamers A.P.G.G., Nieuwenhuizen J.K., (1989), *Chem. Eng. Sci.*, 44(2), 377
 Chandrasekhar S., (1961), *Hydrodynamic and Hydromagnetic Stability*, Clarendon Press USA, p.466
 Chaudhary K.C., Redekopp L.G., (1980), *J. Fluid. Mech.*, 96(2), 257
 Chaudhary K.C., Maxworthy T.M., (1980), *J. Fluid. Mech.*, 96(2), 287
 Goedde E.F., Yuen M., (1970), *J. Fluid Mech.*, 40(3), 495
 Lamb H., (1932), *Hydrodynamics*, 6th edt. Cambridge Univ. Press, reprinted by Dover, New York, p.473 and 639
 McCormack P.D., Crane L., Birch S., (1964), *Brit. J. Appl. Phys.* 15, 743
 Plateau M., (1856), *Statistique Experimental et Theoretique des Liquides Soumis aux Seule Forces Moleculaires*, Paris
 Rayleigh, Lord F., (1878), *Proc. London Math. Soc.*, 11, 4
 Reid, W.H., (1960), *Quart. Appl. Math.*, 18, 86
 Taub H.H., (1976), *Phys. Fluids*, 19(8), 1124
 Yuen M.C., (1968), *J. Fluid Mech.*, 33(1), 286
 Weber C., (1931), *Z. für Angew. Math. Und Mech.*, 11, 136

A pinch of probably is worth a pound of perhaps

James Thurber

9 Uniform droplets

Using Yuens theory, calculations by Rutland and Jameson (1970), Lafrance (1975) and Scarlett and Parkin (1977) showed that the volume of the main droplet becomes equal or almost equal to the volume of the satellites produced around wavenumbers $k \cdot a = 0.2$. This indicates the possibility of producing two equally sized droplets per wavelength. In practice this is not achievable. The main droplet becomes equal or almost equal to the total volume of the satellites, but this is further divided into at least two droplets.

Using the same third order solution of the non-linear instability theory, as described by Yuen (1968), Lafrance (1975) and Scarlett and Parkin (1977) the volume of the main and satellite droplets can be predicted. At wavenumbers $k \cdot a > 0.7-0.8$ the volume of the satellites becomes zero. Thus uniform droplets are produced but now only at a rate of one droplet per wavelength. It is this field of high wave number jet break-up which was experimentally investigated and is now reported.

Experiments were performed to verify that uniformly sized droplets are formed only at wavenumbers greater than about $k \cdot a = 0.6$. Also the existence of regions of uniform jet break-up were determined and general equations predicting the upper and lower limits of this region were determined. The growth rates of the disturbances and the initial disturbances of free and forced oscillating jets were determined and compared to the literature values. The uniformity of the droplets was also measured. Using this knowledge the apparatus was automated to produce tailor-made size distributions

9.1 Jet break-up, giving uniformly sized droplets

This method of producing uniformly sized droplets, without any satellite formation by using mechanical vibrations has been described by many investigators. It has special merits because of the simplicity of the apparatus used. It can easily produce uniform droplets of desired size and number. Both Newtonian and non-Newtonian liquids and slurries of low and high viscosity can be atomised. Although the production of uniformly sized droplets has been mentioned, it still remains difficult to predict what the size of the droplets produced will be. Not only the liquid properties but also the apparatus parameters, such as the imposed frequency, the amplitude of the disturbance, the liquid flow rate and the orifice diameter must also be considered. Schneider *et al.* (1964) reported the production of uniform droplets within the range $3.5d_j < \lambda < 7d_j$, where λ is the wavelength of the disturbance and d_j is the jet diameter, using a longitudinally vibrated capillary. Dabora (1967) produced uniform droplets using a capillary vibrating longitudinally with the frequency of the maximum instability given by Rayleigh's theory:

$$f = \frac{u}{4.508 d_j} \quad (51)$$

u = jet velocity [m/s]

d_j = unperturbed jet diameter [m]

Araki and Masuda (1978) also used a longitudinally vibrating capillary. When keeping the applied frequency, jet diameter and amplitude of vibration constant, they found at low liquid velocities that the break-up of the liquid occurs at the nozzle tip, producing droplets which are rather large and irregular in size. As the liquid velocity is increased a liquid column is formed and uniformly sized droplets are produced whose number is equal to the applied frequency. At still higher jet velocities the liquid jet is lengthened and becomes irregular, producing drops of irregular size. Clearly there exists an upper and lower limit of the liquid velocity between which uniform droplets are produced. In the same way there also exists an upper and a lower frequency limits. When the liquid flow rate is kept constant and the frequency of the vibration is varied, these last limits can be determined. At low frequencies the break-up length of the jet is rather large. The applied disturbance propagates and regular break-up occurs, but both satellite and main drops are observed, caused by the non-linear phenomena. At higher frequencies the satellite drops disappear and uniformly sized drops are produced. The break-up length is much shorter than at lower frequencies. At still higher frequencies the liquid jet is further lengthened and eventually the break-up becomes irregular and the applied disturbance will no longer propagate. Thus satellite break-up is a regular break-up, directed by the imposed frequency, while break-up at higher frequencies is not. Here the imposed frequency has no influence on the break-up.

The minimum break-up length occurs at the point of maximum instability predicted by

Rayleigh (1878), That is at a wavenumber $k \cdot a = 0.697$ for liquids of low viscosity. When plotting the minimum and maximum frequencies, on a log-log scale, as a function of the applied liquid velocity, a parallelogram is obtained. The area enclosed by the upper and lower liquid velocities and the upper and lower frequencies represents the region of uniform break-up. This is shown schematically in Figure 9.1. At liquid flow rates lower than the minimum liquid velocity line, only dripping is observed, no liquid jet exists. This transition from dripping to smooth jet is said by Lindbald and Schneider (1965) to occur when the Weber number has a value of:

$$We = 8 \quad (52)$$

with $We = \text{Weber number} = \rho u^2 d / \sigma [-]$

ρ = liquid density [kg/m^3]

u = liquid flow rate [m/s]

d = jet diameter [m]

σ = liquid surface tension [N/m]

Above the higher liquid velocity boundary the jet is no longer laminar, a transitional jet is formed. The jet will show some turbulence near to the orifice and the ambient air friction also cause turbulence and instability at the jet surface as well. Grant and Middleman (1966) found for the transition from smooth to transitional jet the following relationship:

$$\frac{du\rho}{\eta} = 325 Oh^{-0.28} \quad (53)$$

$Oh = \text{Ohnesorge number} = We^{1/2}/Re = \eta/(\sigma\rho d)^{1/2} [-]$

η = liquid viscosity [$\text{Pa}\cdot\text{s}$]

Sakai (1980) proposed the following relationship for the upper limit of velocity:

$$\frac{du\rho}{\eta} = 300 Oh^{-0.33} \quad (54)$$

These frequency limits as shown in Figure 9.1 are not well described. Only Sakai *et al.* (1982) published overall equations describing the frequency limits as a function of the liquid parameters and apparatus dimensions.

Figure 9.1^b clearly shown that the droplets produced have a maximum and a minimum size, mainly determined by the nozzle diameter. The frequency of producing these droplets can be altered by increasing the liquid velocity of the jet and by adjusting the frequency to this liquid velocity. Due to pressure limitations, the upper limit of liquid velocity was not determined.

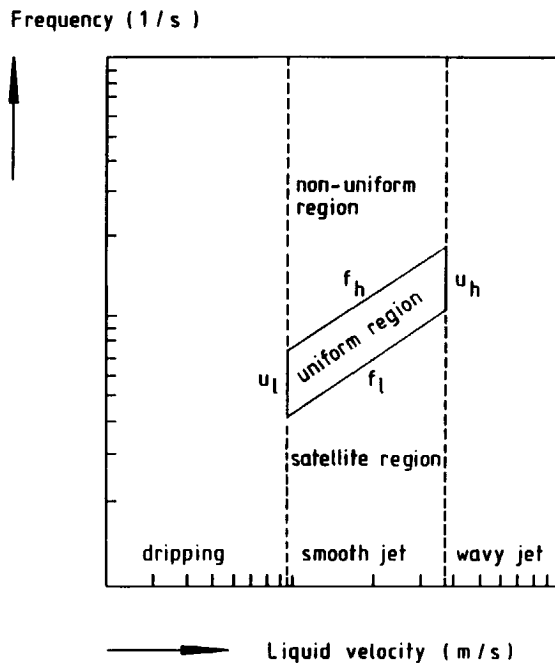


Figure 9.1^a Schematic drawing of the region of uniform jet break-up, with upper and lower limits of frequency and liquid velocity

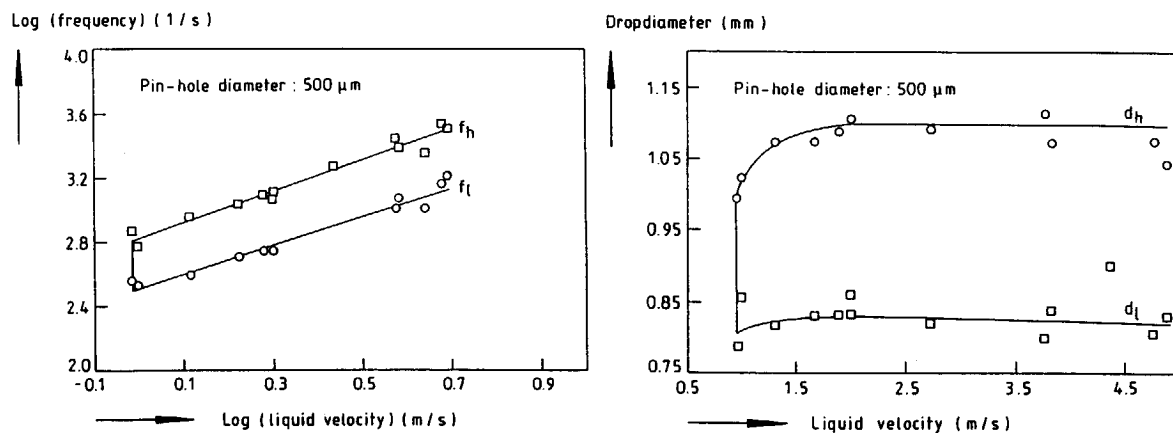


Figure 9.1^b An experimentally determined region of uniform jet break-up, and the corresponding droplet diameters obtained, using the apparatus as described in paragraph 9.2 (Meesters et al. 1989)

9.2 Experimental setup

The apparatus used in our experiment is shown in Figure 9.2.

A metal pin was mounted on the centre of the loudspeaker, which is connected to a frequency generator and an amplifier. This pin vibrated longitudinally. The metal pin was connected to bellows which protruded into the small vessel, thus transmitting the disturbance to the liquid. The liquid flows through a small, smooth, agate pin-hole from the small vessel. The pin-hole was fixed, thus not vibrated, in contrast to Sakai's vibrating needle. The pin-hole diameter could be varied from $70 \mu\text{m}$ to 1.5 mm by mounting different nozzles. The liquid was fed to the small vessel from a larger storage tank which was maintained at a constant but adjustable pressure, enabling the effect of liquid flow rate to be investigated. The break-up of the liquid jet was observed by means of a photo-camera and a stroboscope, which was triggered by the frequency generator. The stroboscope was used to determine the upper and lower frequency limits. A electronic counter measured the exact frequency of jet break-up.

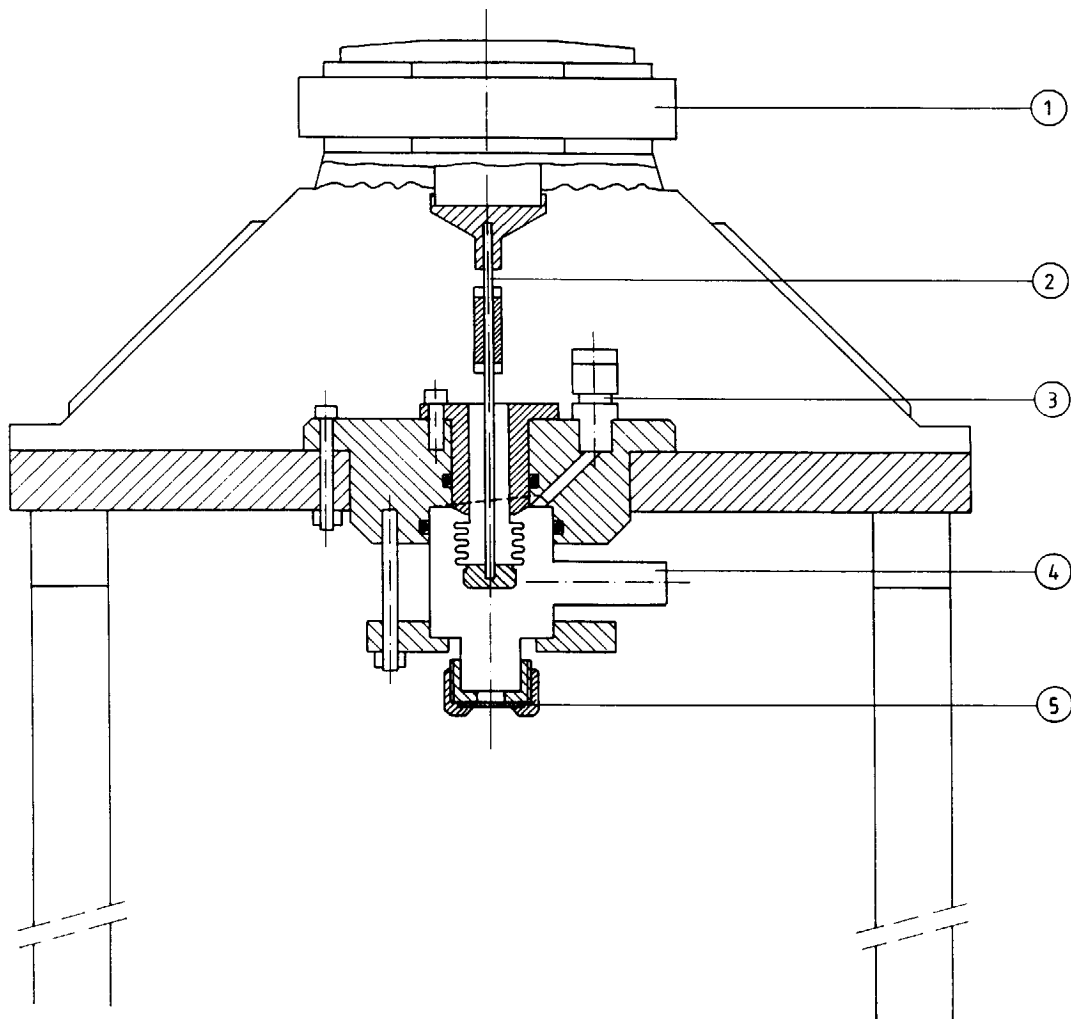


Figure 9.2 Schematic drawing of the apparatus, as used to vibrate the liquid jet coming from the orifice. 1)=loudspeaker, 2)=vibrating metal rod connected to bellows, 3)=air exhaust, 4)= liquid inlet, 5)=nozzle (removable pin-hole plate)

9.3 Initial displacements

Rayleigh and Weber assumed that the displacement, α , corresponding to all possible wavelengths is initiated at the nozzle exit on the liquid jet and they calculated that only disturbances with wavenumbers $0 < ka < 1$ can propagate. Weber assumed that break-up of the jet occurs when the amplitude α of the wave equals the radius of the jet. The liquid column length, L , can then be calculated by:

$$L = \frac{u}{\omega} \ln\left(\frac{a}{\alpha_0}\right) \quad (55)$$

with u = liquid velocity [m/s]

ω = growth rate [s^{-1}]

α_0 = initial displacement [m]

a = jet radius [m]

Concerning the factor $\ln(a/\alpha_0)$, experimental studies of free undisturbed jets have been reported by Weber (1931), Haenlein (1931) and Takahashi (1972). Weber reported that the value of $\ln(a/\alpha_0)$ obeys;

$$\ln\left(\frac{a}{\alpha_0}\right) = 12 \quad \text{for } Oh > 0.015 \quad (56)$$

$$\ln\left(\frac{a}{\alpha_0}\right) = 6.5 (Oh)^{-0.25} \quad \text{for } Oh < 0.015 \quad (57)$$

With forced oscillation of the jets other values are expected. To verify this, several experiments were carried out to establish the break-up length of the jets.

Three liquids were used; tap water, a 2:1 (V/V) mixture of ethylene glycol and water and a 1% (w/w) solution of sodium alginate in water. The properties of the liquid are given in Table 9.1.

These three liquids have different viscosities which influences the growth rate of the disturbance and influences the $k \cdot a$ value of the maximum growth rate. This is shown in Figure 9.3, where the dimensionless growth rate ($\omega/(2\rho a^3/\sigma)$) is plotted as a function of the dimensionless wavenumber $k \cdot a$, according to the theory of Weber.

Table 9.1 Liquid properties of the liquids used to determine the break-up length of the smooth jets.

	density ρ [kg/m ³]	viscosity η [mPa · s]	surface tension σ [mN/m]
water	1000	1.00	72.7
ethylene glycol/water 2:1 (V/V)	1081	6.86	55.9
1% (w/w) Na-alginate in water	994	74.0	72.1

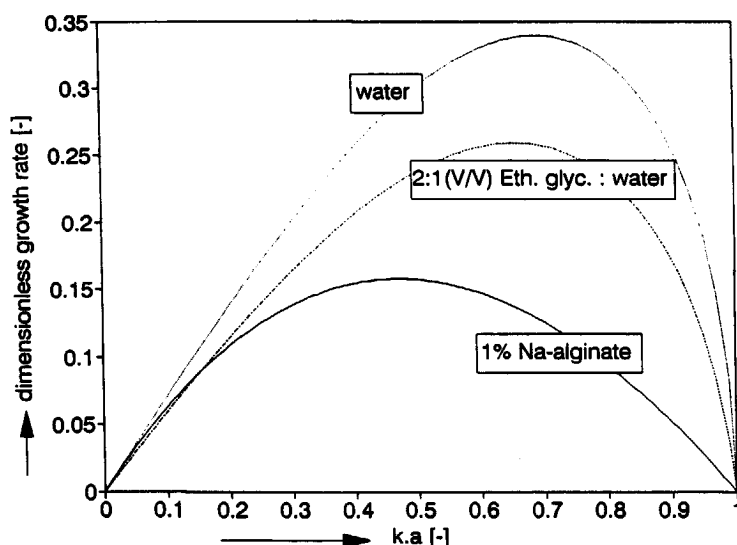


Figure 9.3. Calculated dimensionless growth rate as a function of the dimensionless wavenumber for three liquids having different viscosities.

The break-up length was measured by using a precision displacement measuring device with a resolution of 10 μm . For each liquid the break-up length was measured as a function of $k \cdot a$, at different liquid velocities. Figure 9.4 shows an example of the measured break-up length as a function of $k \cdot a$.

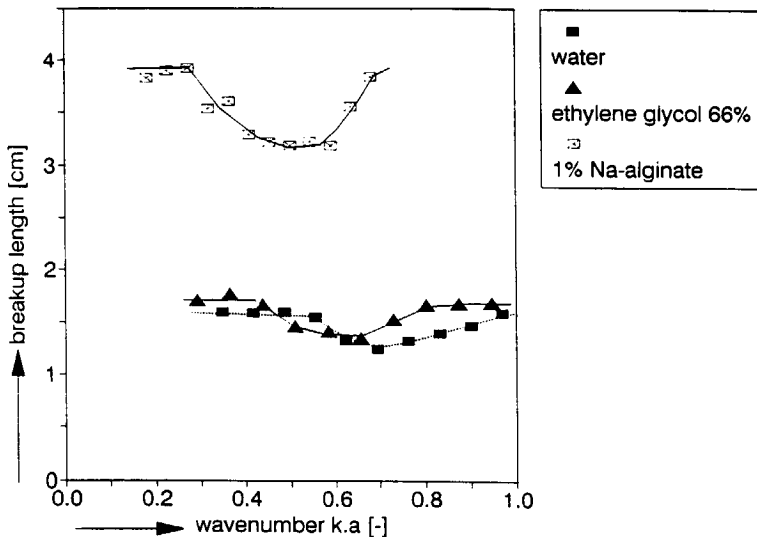


Figure 9.4 Break-up length as a function of $k \cdot a$, for three different liquids.

From all these measurements, the minimum break-up length, that is at maximum growth rate, was determined as a function of the liquid velocity. The results are shown in Figure 9.5.

From the slope of these lines the $\ln(a/a_0)$ value can be determined by applying Weber's equation. The disturbance will grow with the maximum growth rate ω^* to a value where $r=a$, the jet radius, in a time t^* , obtained from

$$a = a_0 e^{\omega^* t^*} \quad (58)$$

The length of the jet is then given by;

$$L - ut^* = \frac{u}{\omega^*} \ln\left(\frac{a}{a_0}\right) \quad (59)$$

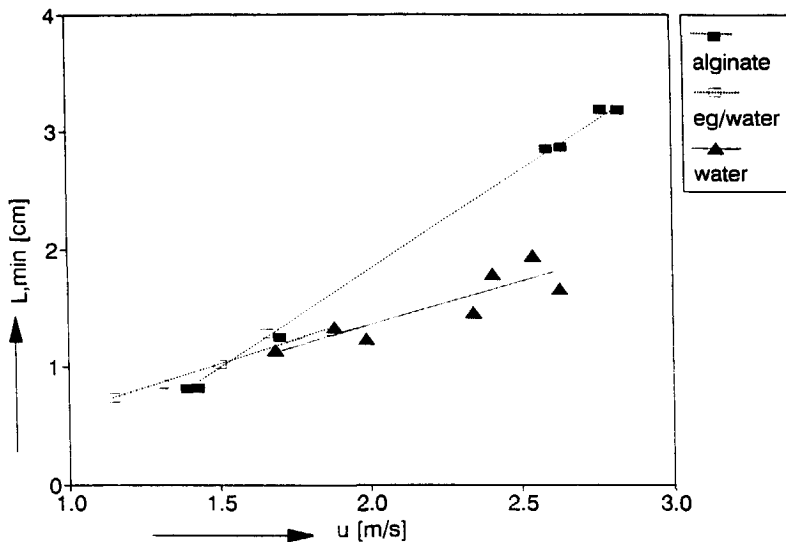


Figure 9.5. Minimum break-up length as a function of the liquid velocity, for a 1% (w/w) Na-alginate in water, a 2:1 (V/V) ethylene glycol water mixture and water

By straightforward differentiation of the Weber equation in dimensionless form

$$\beta^2 + \beta (6\Omega_h k^2 a^2) - k^2 a^2 (1 - k^2 a^2) = 0 \quad (60)$$

where β = dimensionless growth rate = $\omega \sqrt{(2\rho a^3/\sigma)}$ [-]

It is seen that β has a maximum value β^* , when

$$k \cdot a = \sqrt{0.5 (1 + 3\Omega_h)} \quad (61)$$

from which it follows that

$$\beta^* (\Omega_h) = 0.5 (1 + 3\Omega_h) \quad (62)$$

This equation combined with Eq. 59 leads to

$$\frac{L_{\min}}{d} = \sqrt{We} (1 + 3 Oh) \ln\left(\frac{a}{a_0}\right) \quad (63)$$

This equation predicts the jet length with increasing jet velocity but only at small liquid velocities where the influence of the ambient air friction can be neglected.

By rearranging eq. 63 one gets

$$L_{\min} = u A \ln\left(\frac{a}{a_0}\right) \quad (64)$$

$$\text{where } A = \text{constant} - d \sqrt{\frac{\rho d}{\sigma}} + \frac{3 d \eta}{\sigma} \quad (65)$$

Thus by plotting L_{\min} as a function of the liquid velocity the value of $\ln(a/a_0)$ can be obtained, as is shown in Table 9.2. Table 9.2 also shows the values obtained for the free undisturbed jet, as given by equations 56 and 57, and the values observed during our experiments.

Table 9.2 Experimental values of $\ln(a/a_0)$ for the forced oscillating jet, the free undisturbed jet and the calculated values according to eq. 56 and 57, jet radius $a=220 \mu\text{m}$.

	forced oscillation	free undisturbed jet	
	$\ln(a/a_0)_{\text{exp}}$	$\ln(a/a_0)_{\text{eq}}$	$\ln(a/a_0)_{\text{exp}}$
1%(w/w) Na-alginate in water	6.98	12	8.3
2:1(V/V) ethylene glycol water	6.20	12	8.4
water	6.66	23.8	11.2

What is clear is that the initial disturbance on the forced oscillation jet is much higher than that of the undisturbed free jet. However, the initial disturbance on this free jet is much higher than is predicted by equations 56 and 57. As the initial disturbance of a free jet is initiated by vibrations from the surroundings and by the nozzle roughness, this value changes from day to day and depends also on the apparatus itself.

This conclusion is only applicable for low liquid velocities. For higher velocities a non-linear relation between jet length and liquid velocity is seen. At higher velocities the aerodynamic forces also affect the break-up. Weber derived a correction for the aerodynamic interactions, but overestimated the effect. Sterling (1978) corrected this after extensive measurements and calculations by adding a factor of 0.175 to the aerodynamic term of Weber.

9.4 Growth rate of disturbance

Without the application of a forced oscillation a smooth jet will break up into irregularly shaped droplets. Disturbances from the surroundings are initiated on the liquid surface. When the wavenumber, $k \cdot a$, of these disturbances lies in the region $0 < k \cdot a < 1$, they can propagate and lead to the break-up of the jet. The disturbance which has the maximum growth rate among the surrounding disturbances will grow fastest and dominate the jet break-up. This means that for a free undisturbed low viscous jet, it will break up with a wavenumber of about 0.7, as calculated by Rayleigh (1878).

When looking at the upper limit of frequency, using forced oscillation of the jet, it is noticeable that the corresponding $k \cdot a$ -values are higher than the maximum Rayleigh value of 0.697, and often go to the limit of 1.0 at higher values of Re- and We-number. The same is seen for the lower limits of frequency. When the wavenumbers are calculated the values go lower than the Rayleigh limit of 0.697. There clearly exists a region of wavenumbers which give the desired uniformly sized droplets. The value of Rayleigh, $k \cdot a = 0.697$, is found in between these limits.

The values found for the wavenumbers giving uniformly sized droplets are given in Figure 9.6. The figures show the wavenumbers and the frequency with which they occurred during the experiments where the liquid velocities and applied frequencies are varied.

The values higher than 0.697 can be explained as follows. In Figure 9.7 the line indicated as the background corresponds with the break-up of a free jet at maximum growth rate, corresponding with $k \cdot a = 0.697$. At $t=0$ the initial disturbance is initiated and grows with the maximum growth rate. The amplitude of the wave grows with time until it reaches the value of half the jet diameter, then a droplet is formed and the jet breaks up. When a disturbance is forced on the jet this disturbance will propagate if $0 < ka < 1$. The initial disturbance is much larger in the case of forced oscillation, than the initial disturbances initiated from the surrounding. At maximum growth rate this leads to a shorter jet and thus a shorter break-up time than that of a free jet. When a disturbance is forced onto the jet with a value $k \cdot a > 0.697$, this causes the break-up time to increase. However, because the initial disturbance is much higher it has a strong advantage over the background noise. Thus the jet will break up according to the imposed $k \cdot a$ -value. In the limiting case of $k \cdot a = 1$ the jet will still break up according to the imposed disturbance because the break-up time is still shorter than that of a free, undisturbed jet. This applies

to both water and the ethylene glycol-water mixture (2:1 V/V) as shown in Figures 9.7 and 9.8.

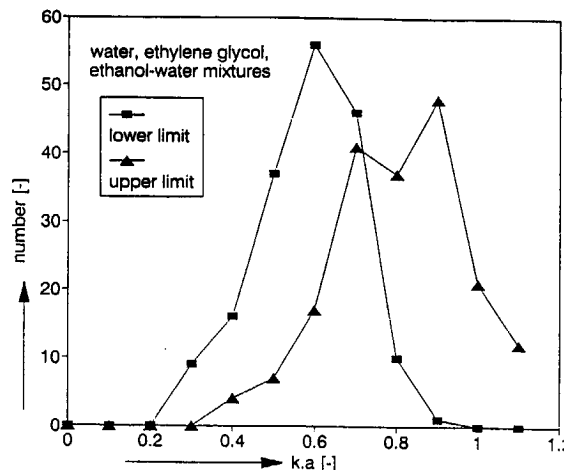
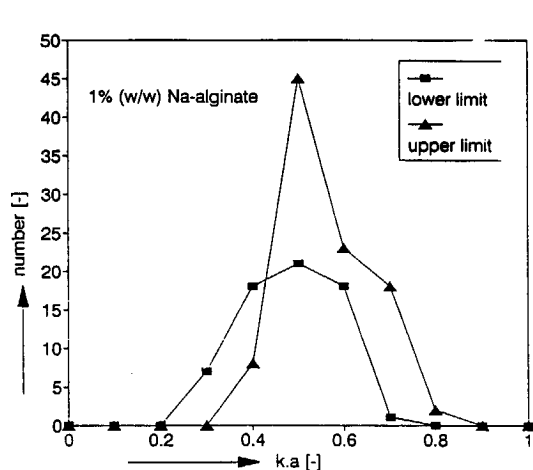


Figure 9.6 The frequency with which the wavenumbers occur which correspond with the upper and lower limits of frequency for the liquids given in Table 9.2

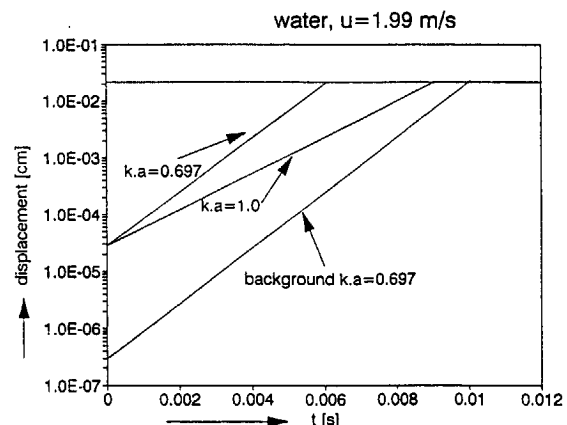
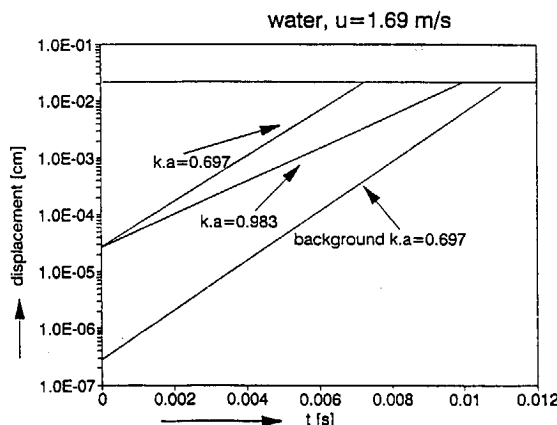


Figure 9.7 Comparison between the growth of the disturbance of free and forced oscillation water jets as a function of time, for different wavenumbers.

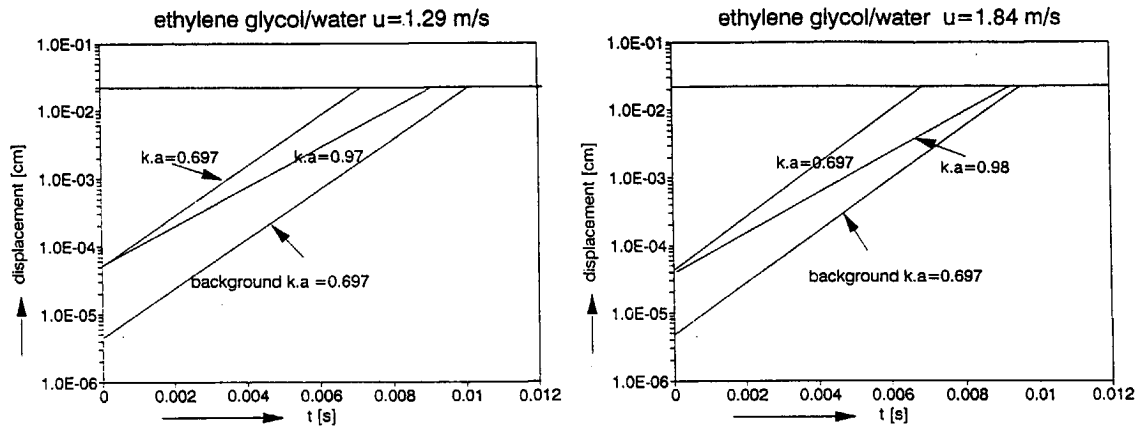


Figure 9.8 Comparison between the growth of the disturbance of free and forced oscillation ethylene glycol-water jets as a function of time, for different wavenumbers.

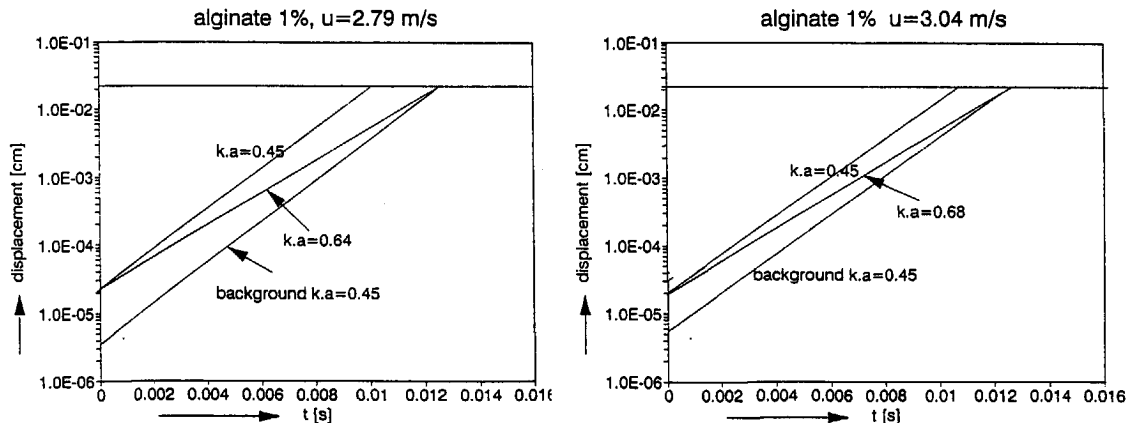


Figure 9.9 Comparison between the growth of the disturbance of free and forced oscillation jets of a viscous, 1% Na-alginate in water solution, as a function of time and for different wavenumbers.

In the case of a viscous liquid, in this case a 1% (w/w) solution of Na-alginate in water with a viscosity of $74 \cdot 10^{-3}$ Pa·s, something different is observed. For this liquid the maximum growth rate is calculated using Weber's equation at $k \cdot a = 0.470$. From our observations the upper limit of frequency is found at $k \cdot a$ -values of about 0.5 to 0.7. At higher $k \cdot a$ -values the imposed disturbance does not propagate. At this point the background noises dominate the break-up. Figure 9.9 shows the displacement of the disturbance of the jet as a function of time for the viscous alginate solution. Liquid jets which are subjected to forced disturbances with a higher initial disturbance and with $k \cdot a = 0.470$, grow the fastest. However, as with the liquids of low viscosity at higher $k \cdot a$ -values the growth rate decreases and the break-up time increases. Again, because of the higher initial disturbance they propagate in preference to the background noise and grow with maximum growth rate $k \cdot a = 0.470$. At $k \cdot a = 0.65$ the limit is reached and the jet break-up time of the background noise is shorter than that of the imposed disturbances. The background dominates imposed disturbance where $k \cdot a > 0.65$.

When the power input is increased, the initial disturbance increases, thus making it possible to break up a liquid jet at $k \cdot a$ -values higher than 0.65. Increasing the power input for liquids of low viscosity has little or no effect because the jet always breaks up at $k \cdot a = 1$, the limiting value.

With larger initial disturbances the theories of Rayleigh and Weber are no longer applicable and the maximum wavenumber and cutoff wavenumber change also (Yuen 1968).

9.5 Regions of uniform jet break-up

Thus, regions of uniform jet break-up can be determined. The influence of jet velocity, diameter of the nozzle and applied frequency were investigated by Araki and Masuda (1972, 1978). Sakai *et al.* (1980, 1982 and 1985) also included the liquid properties of viscosity η , surface tension σ , and liquid density ρ in their investigations. By using dimensional analysis general equations for the upper and lower frequency limits can be obtained, given by:

$$\frac{f_1 d}{u} = a Re^b We^c \quad (66)$$

$$\frac{f_n d}{u} = p Re^q We^r \quad (67)$$

Here, a, b, c, p, q, r are all constants, which depend on the liquid properties, applied liquid flow rate, applied frequency and the apparatus configuration.

Note that

$$\frac{fd}{u} = \frac{1}{\pi} ka \quad (68)$$

Sakai *et al.* (1980,1982) used a longitudinally vibrating needle from which the liquid issued. Thus the orifice was vibrated. In our case a stationary nozzle was used, and the vibration was applied to the liquid inside.

The regions of uniform jet break-up are established using various liquid (Table 9.3) and different pin-hole diameters. The pin-hole diameters used are 250, 330, 440, 480 and 500 μm .

Table 9.3 Properties of the liquid used. Percentages indicate the amount of the liquid when mixed with water.

	surface tension σ [mN/m]	density ρ [kg/m^3]	viscosity η [$\text{mPa} \cdot \text{s}$]
water	72.8	1000	1.00
ethylene glycol 66% V/V	44.6	1075	6.19
ethanol 96% (w/w)	24.9	804	1.24
ethanol 80% V/V	28.2	864	2.20
ethanol 20% V/V	44.3	972	1.76
Na-alginate 1% w/w	72.1	994	74.0

Figure 9.10 shows some of the measured uniform regions of jet break-up.

A total of 666 points were used to determine the constants of equations 66 and 67. They are determined using all the measured data points in a non-linear, data fitting program (Pastfit). Each point is weighted relative to the relative error of that point. The results of the fitting procedure are given in Table 9.4.

Table 9.4. Results of the non-linear fitting procedure to establish the value of the constants of eq. 66 and 67. The standard deviation of the constants calculated as well as the values obtained by Sakai *et al.* (1980,1982) are given.

constant	calculated value	standard deviation	results Sakai <i>et al.</i>
a	0.067	0.003	0.11
b	0.096	0.007	-0.066
c	0.096	0.014	0.17
p	0.101	0.006	0.18
q	0.123	0.008	0.031
r	0.060	0.013	0.12

From the fitting program it was shown that the constants were independent of each other. What is shown clearly is the strong dependence of the upper limit of frequency, (q), on the Reynolds number. This is in contradiction to the results of Sakai *et al.* who found a strong dependence on the Weber number.

For the lower limit of frequency there is not much difference between the exponent of the Reynolds and Weber numbers, while Sakai also found a stronger dependence on the Weber number.

Comparing the results of the numerical fit with the experimentally determined regions of uniform jet break-up, it is clear that equations 66 and 67 describe these regions well. The limits of frequency fitted, in most of the cases quite well our own uniform regions. They differed from Sakai's limits of frequency. However, Figure 9.10 shows a region of uniform break-up (ethylene glycol 66% V/V) where Sakai's equation for the upper limit of frequency fits better.

The slope of the lines does not differ much from those obtained by Sakai *et al.*. We found:

$$f_1 + d^{-0.808} u^{1.288} \quad f_h + d^{-0.817} u^{1.243} \quad (69)$$

while Sakai *et al.* found

$$f_1 + d^{-0.896} u^{1.274} \quad f_h + d^{-0.849} u^{1.271} \quad (70)$$

The bigger difference is found in the intercepts of the lines. This is due to differences in the equipment used. As expected for the liquids of low viscosity, the upper limits of frequency coincide good in most of the cases. This was expected because in most cases this indicates the limiting value of the wavenumber, $k \cdot a = 1$, for the jet break-up. During the fit procedure the equations of Sakai were also tested on there applicability to described the uniform regions. Again it showed that our equations fitted better to the our own uniform regions.

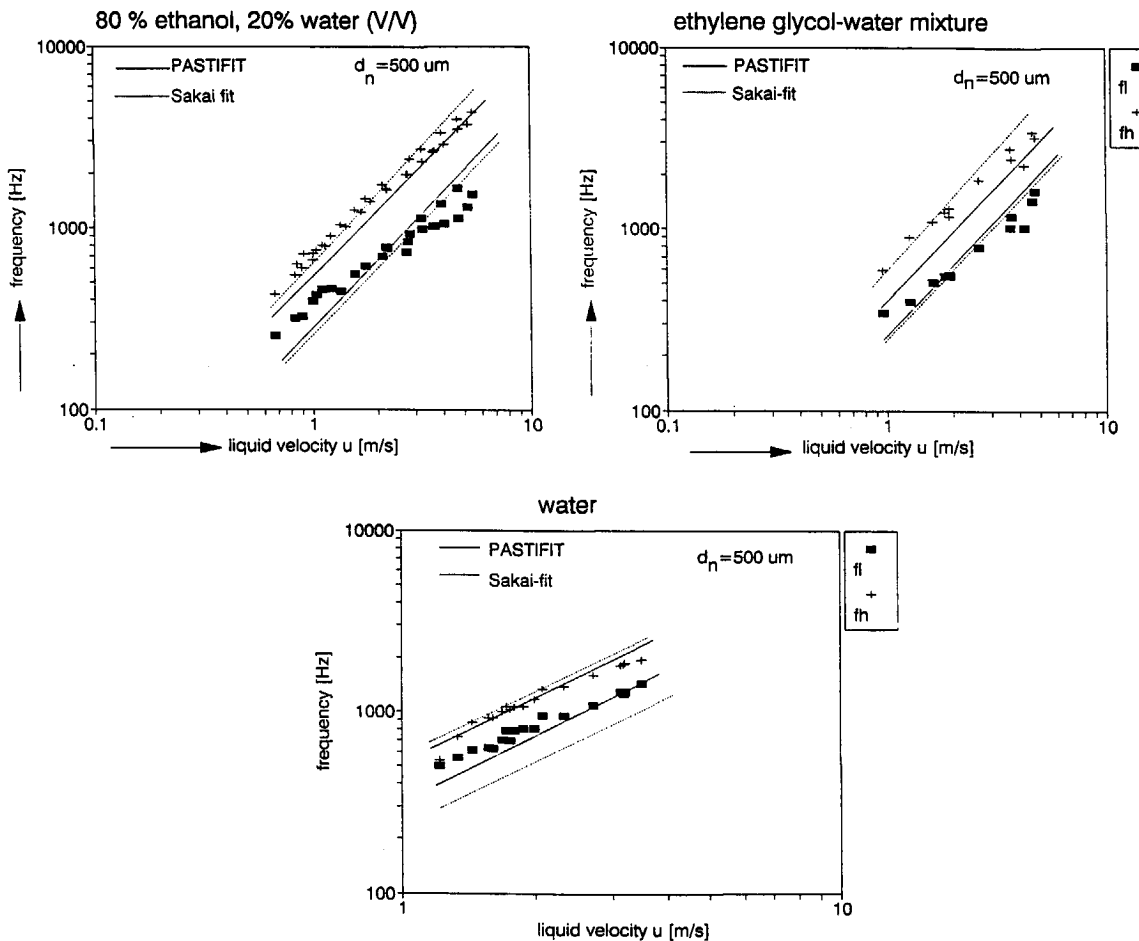


Figure 9.10 Regions of uniform jet break-up. Solid lines are determined using eq. 66 and 67, together with the calculated values of Table 9.4, dashed lines are determined using Sakai's equations

9.6 Size distributions of produced droplets

From photographs it is clear that the size of the droplets produced, while operating in the uniform region, are of very uniform size. In order to verify this, not only photographs were used but solid particles were also produced using solutions of sodium-alginate in demineralised water.

Sodium alginate is the sodium salt of alginic acid. Alginic acid is a co-polymer consisting of α -L-guluronic and β -D-mannuronic acid units (Painter 1983). The polymer molecule is constructed of three different blocks: G-blocks, consisting solely of guluronic acid, M-blocks consisting of mannuronic acid and blocks in which both units alternate. The G-blocks have a zigzag form, the other two form rather linear chains.

One important feature of alginate is that the Na^+ -salt is water soluble, but that the presence of polyvalent ions (except Mg^{2+}), such as a CaCl_2 solution, results in rapid solidification. The surface of an alginate droplet falling into the CaCl_2 -solution reacts immediately. The rest of the droplet hardens, depending on its size, in a few hours.

A diffusion limitation of the Ca^{2+} ions occurs, which have to cross the gel barrier to reach the liquid.

Due to this gelation it is possible to collect the droplets separately and measure them by digitalized image techniques.

The cause of this gelation is the presence of the zigzag formed G-blocks and the presence of polyvalent ions. These ions are cross-linking agents and connect the G-blocks of different polymer chains in a so-called 'eggbox' model. The polyvalent ions are the 'eggs' and the G-blocks is the 'box'. The other two blocks do not show this cross-linking since the position of the oxygen atoms is less attractive to the ions.

As a result, the degree of gelation increases with increasing ratio of G-blocks over the other blocks in the alginate. The alginate concentration in water and the polyvalent ion concentration also play an important role.

The degree of gelation not only depends on the known concentration of alginate and CaCl_2 , but also on the composition of the alginate.

An alginate droplet falling into a polyvalent solutions shrinks, because of the gelation. This is caused by the fact that the originally random orientated polymer chains become ordered. The degree of shrinkage depends on the degree of gelation. A droplet falling into a polyvalent ion solution reacts at the surface. Further gelation is hindered by the fact that the ions must diffuse through the gel-layer. It is not exactly known if, and how, the shrinkage is related to the droplet size.

The results of two measurements of samples of alginate are given in Table 9.5. The Table compares the measurements from photographs of the droplets taken just after they come from the nozzle with measurements of the solidified alginate droplets. Both size distributions were obtained using a digital image analyser.

Table 9.5 Particle size distributions obtained from the image analysis of photographs of Na-alginate and solid Ca-alginate particles. (d_n =nozzle diameter [μm], f =applied frequency [Hz], u =liquid velocity [m/s])

process conditions $d_n=500 \mu\text{m}$	photographed droplets		solidified droplets	
	average drop size [mm]	sample standard deviation [mm]	average drop size [mm]	sample standard deviation [mm]
$f=417 \text{ Hz}$ $u=1.94 \text{ m/s}$	1.203	0.0245	0.897	0.0138
$f=642 \text{ Hz}$ $u=3.90 \text{ m/s}$	1.329	0.0221	0.767	0.0132

From these values it is clear that the particle size distributions are very narrow. Due to shrinkage of the droplets after solidification the average particle size of the Ca-alginate particles is difficult to correlate to the photographed droplets. The relative standard deviation of the samples is almost equal.

Figure 9.11 shows the particle size distribution of a second sample of solidified droplets. Also a slurry of 1.5 % Na-alginate in water with a 20% w/w solids was made into uniformly sized droplets. The solids were a zeolite catalyst. After drying of these solidified droplets a solid catalyst is obtained.

The size distributions of the solidified but wet and of the dried samples are given in Figure 9.12

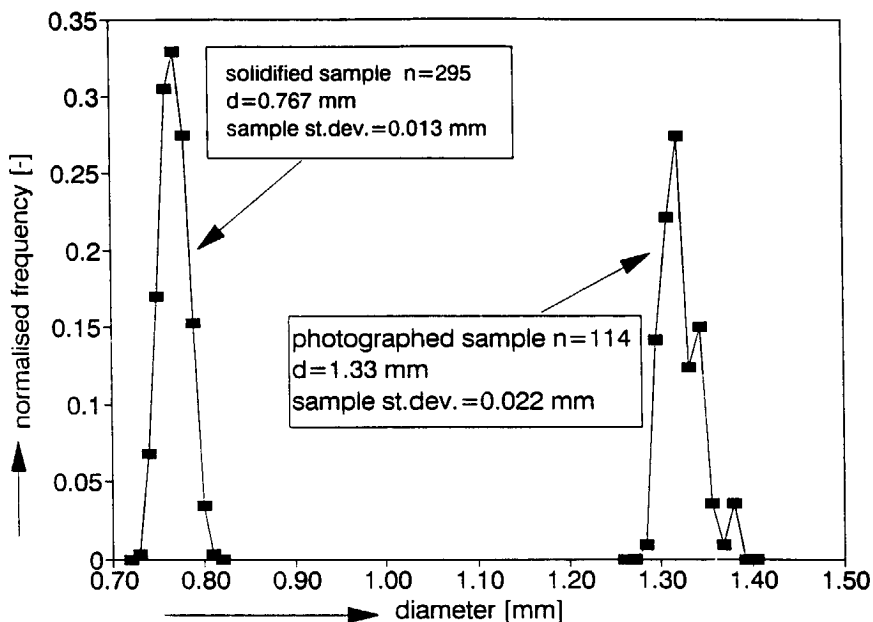


Figure 9.11 Particle size distribution of alginate particles produced at $f=642 \text{ Hz}$, $u=3.90 \text{ m/s}$, measured with the Magiscan Image Analyser. $n=\text{number of observation}$ (see Table 9.5)

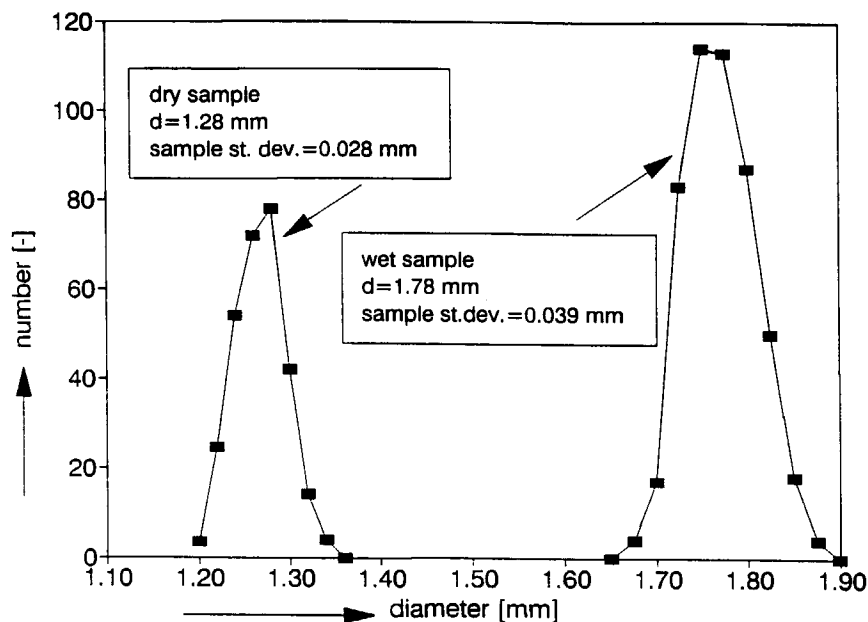


Figure 9.12 Particle size distribution of solidified, wet, Ca-alginate particles with 20% w/w solids and of the same sample after being dried

9.7 Tailor made particle size distributions

Well defined particle size distributions are useful in the production of numerous industrial products. Pharmaceuticals of a defined particle size distribution may have a controlled release to the body over a long period of time. In the production of catalyst particles and the immobilization of micro-organisms, both processes benefit from a better defined particle size distribution.

Currently the most common way to produce a defined particle size distribution is by grinding, classification, sieving and mixing of different sizes of particles. Particles which are too small are rejected, particles which are too big are recycled in the mill. Sometimes, however, the chemistry the recycle of particles and waste is produced.

In order to overcome these limitations, the atomisation apparatus was automated. The uniform regions of jet break-up were determined and included into a programme. In principle the programme adjusts the frequency at a certain liquid flow rate, so that the required droplet size is obtained. The process operates always in the uniform region. By

changing the frequency and maintaining a constant flow rate the droplet size can be altered. Thus a required size distribution can be produced over a cycle of operation. The software not only controls the applied frequency but at the same time monitors the liquid flow rate. The flow rate is established by controlled pressurisation of the vessel containing the liquid supply, and is monitored by a balance, which feeds data into the computer through a Labmaster.

The program worked as follows. The assignment procedure asks the liquid (density, surface tension and viscosity) and apparatus data (nozzle diameter, pressure/velocity relation), allows the user to determine the uniform region and asks for the desired particle size distribution. It will not accept droplet diameters which can not be produced within the limits of the uniform region.

Finally for each fraction the programme sets the pressure, using the given relation, measures the real pressure and sets the desired frequency for each fraction. Next it waits for a user command before it starts weighing, so that a container can be placed on the weighing scale underneath the nozzle.

Using the mechanical vibration process and knowing the uniform region, it is possible with only a few different nozzle sizes to define and manufacture a particle size distribution over a wide range of diameters.

9.7.1 Particle size distributions produced, using the software.

The main problem in practice was the reproducibility of the uniform region due to the fact that it is very small at higher values of viscosity. The particle size distribution which can be produced with a single nozzle is therefore limited.

Figure 9.13 shows the Image Analysis result from one production cycle. The shrinkage factor was fixed at 0.83. Assignment and result are presented in Table 9.6.

The shift of the peaks can be explained by the fact that the shrinkage factor was taken as a constant for all the particle sizes, which is clearly not the case.

Each fraction was produced for the same period of time. This accounts for the decrease in height of the peaks, although it is unclear why the 650 μm is so low. The width of the peaks is about 100 μm . There is substantial noise at higher diameters due to doublets and dumb-bells.

A block formed particle size distribution was obtained by programming four fractions, which lie 50 Hz apart, so that the normally distributed particle size distributions of the separate fractions overlap. Each of the fractions produced the same number of droplets. For each fraction an average deviation of $\pm 25 \mu\text{m}$ was assumed around the calculated value appertaining to the set frequency. The result, shown in Figure 9.14 and Table 9.7, summarizes the assignment and the achieved result.

Table 9.6 Production of separate peaks of desired size (Fig. 9.13).

d_w [μm]	d_{cor} [μm]	u [m/s]	P_{set} [bar]	P_{real} [bara]	f_{set} [hz]	d_{real} [μm]	dev. [μm]
650	783	3.7	1.49	1.48	912	610	-40
700	843	3.3	1.48	1.52	760	780	+80
800	964	3.7	1.49	1.50	471	920	+120
850	1024	3.7	1.49	1.52	425	1010	+160

 d_w : desired diameter [μm] d_{cor} : diameter corrected for shrinkage [μm]

u: liquid velocity wanted [m/s]

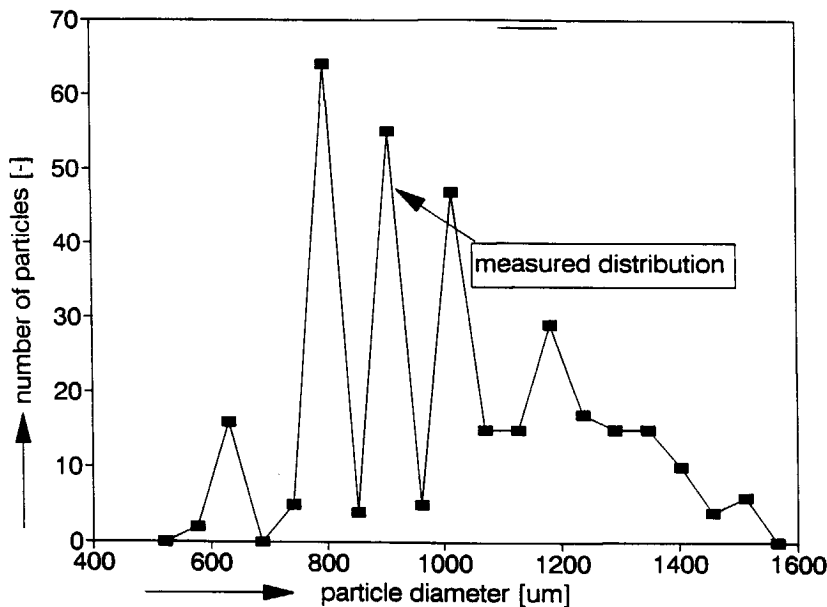
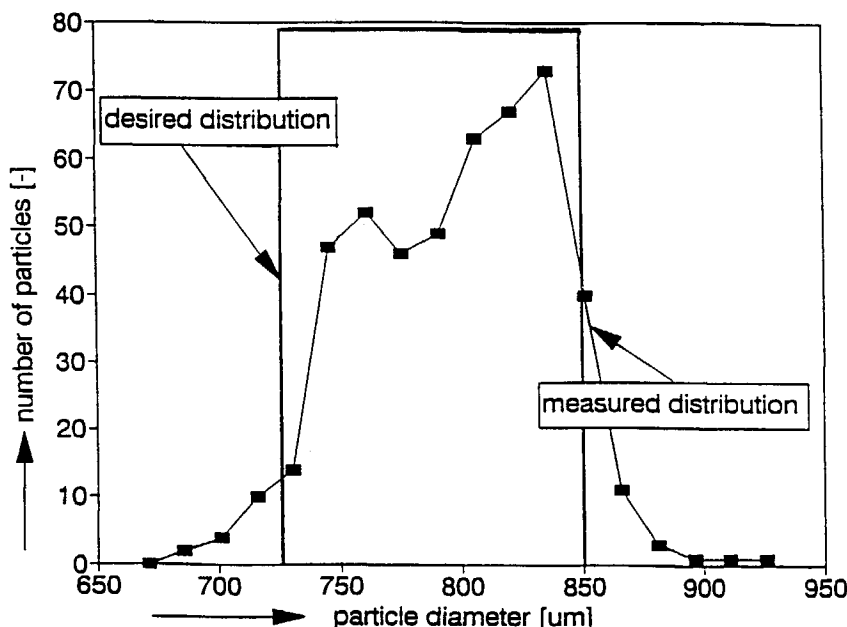
 P_{set} : pressure set [bara] P_{real} : pressure actually set [bara] f_{set} : frequency set [Hz] d_{real} : diameter obtained [μm]dev.: difference between d_w and d_{real} [μm]Figure 9.13 Results of a tailor made particle size distribution, producing four separate peaks at 783, 843, 964 and 1024 μm

Table 9.7 Produced block shaped distribution (Fig. 9.14). $d_{jet} = 480 \mu\text{m}$

p_{real} [bar]	u_{real} [m/s]	f_{set} [Hz]	d_{theor} [μm]	theoretical block range [μm]	obtained block range [μm]
1.64	4.5	539	825	725-850	700-875
		575	803		
		615	786		
		700	753		

 u_{real} : actual set liquid velocity [m/s] d_{theor} : theoretical expected droplet size [μm]Figure 9.14 Results of a tailor made particle size distribution consisting of a block shaped distribution ranging from 725 to 850 μm

The deviation from a true block form is due to control limitations and to the small number of droplets which were analysed. It is also caused by the fact that there is always a distribution of size, because not perfectly monosized particles are produced. These production trials demonstrate that, when the regions of uniform break-up are known, desired size distributions can be obtained through automation of the process. The limitation of the particle diameters is caused by the nozzle diameter, which only allows a certain range of droplets to be produced. When broader size distributions are desired, different nozzle diameters must be used in combination.

9.8 References

- Araki N., Masuda A., (1972), *Proc 1st Jap. Conf. Liquid Atomisation and Spray Systems*, p.13
Araki N., Masuda A., (1978), *Proc. Int. Conf. Liquid Atomisation and Spray Systems, ICLASS-78*, Japan, 8-1,173
Dabora E.K., (1967), *Rev. Sci. Instr.*, 38, 502
Goedde E.F., Yuen M., (1970), *J. Fluid Mech.*, 40(3), 495
Grant R.P., Middleman S., (1966), *AIChEJ.*, 12, 669
Haenlein A., (1931), *Forchung auf dem Gebiete des Ingenieurswesen*, 4, also Ref. Weber (1931)
Lafrance P., (1975), *Phys Fluids*, 18, 428
Lindbald N.R., Schneider J.M., (1966), *Rev. Sci. Instr.*, 42, 635
Painter T.J., (1983), *Alginates: Occurrence, Localisation and Native State, Molecular Biology II*, ed. G.O. Aspinall, Acad. Press Inc., Florida, p.263
Rayleigh, Lord F., (1878), *Proc. London Math. Soc.*, 11, 4
Rutland D.F., Jameson G.J., (1970), *Chem Eng. Sci.*, 25, 1689
Sakai T., Hoshino N., (1980), *J. Chem. Eng. Japan*, 13(4), 263
Sakai T., Sadakata M., Saito M., Hoshino N., Senuma S., (1982), *Proc. Int. Conf. Liquid Atomisation and Spray Systems, ICLASS-82*, Japan, 2-1, 37
Sakai T., (1985), *Proc. Int. Conf. Liquid Atomisation and Spray Systems, ICLASS-85*, England, VII-13(b)2, 1
Scarlett B., Parkin C.S., (1977), *Chem. Eng. J.*, 13, 127
Schneider J.M., Hendricks C.D., (1964), *Rev. Sci. Instr.* 35, 1349
Sterling A.M., Mahoney T.J., (1978), *Proc. Int. Conf. Liquid Atomisation and Spray Systems, ICLASS-78*, Japan, 1-2, 9
Takahashi T., Kitamura Y., (1972), *Kagaku Kogaku*, 36(5), 527
Yuen M.C., (1968), *J. Fluid Mech.*, 33(1), 286
Weber C., (1931), *Z. für Angew. Math. Und Mech.*, 11, 136

*A body of knowledge cannot be entirely translated into statistics,
But it may be of use to the outward sign of increased knowledge.*

Accident Prevention Manual for Ind. Appl. 1969, 6thed. Nat. Safety Council

10 General conclusions

It is clear that the theory of the laminar jet break-up is better understood by including the non-linear behaviour of the wave propagation. Much work has been done on predicting the occurrence of satellites, which accompanies the formation of the main droplets during the break-up of a jet. In these cases at least two droplets per wave length are formed. This kind of break-up occurs at low wave numbers. At increasing wave number the volume of the satellites decreases leading eventually to jet break-up producing uniformly sized droplets, that is without any satellites. The calculations performed by Lafrance (1975) and Scarlett and Parkin (1977) show that this kind of break-up is theoretically possible at higher wavenumbers ($ka > 0.7$).

The regions of uniform break-up, as reported by Sakai *et al.* are bounded by an upper and lower limit of frequency and liquid velocity. The location of these regions was found to depend on the liquid properties as well as on the configuration of the apparatus. These regions of uniform break-up were found to occur at the higher wavenumbers, as predicted.

By experimenting with several different liquids, general equations were obtained describing these regions of uniform jet break-up. The properties of the liquid are taken into account in these equations. The equations correlate the dimensionless wavenumber to the Reynolds and Weber numbers. Contrary to the conclusions of Sakai *et al.*, a strong dependence of the upper limit of frequency on the Reynolds number was found. The lower limit of frequency was found to be equally dependent on the Reynolds and Weber numbers. In both cases Sakai *et al.* found a strong dependence on the Weber number. This could well be caused by the different experimental arrangement used. Sakai *et al.* used a vibrating needle while we used a stationary pinhole. The slope of the

lines, indicating the frequency limits, were found to be almost equal to Sakai's values. The intercepts of the lines differed. In most cases the general equations determined describe the regions of uniform break-up well.

An explanation was found for the fact that a liquid jet follows the imposed frequency of a forced oscillation. The imposed disturbance has such an advantage over the background noise that the jet breaks up according to the imposed disturbance. For low liquids of low viscosity this was found to be true when the $k \cdot a$ value varied between values of 0.6 and 1.0. For a more viscous liquid, this was found to be different. Here the maximum value of the wavenumber imposed on the jet occurred at about $k \cdot a = 0.7$. At higher wavenumbers the disturbances from the surroundings dominated the jet break-up. Increasing the power input of the amplifier causes the bellows to have a larger amplitude and makes it possible to cause the liquid to break up at higher wave numbers. This because the imposed initial disturbance is larger.

The droplets produced were found to be very uniform in size. By using this fact and knowing the regions of uniform jet break-up, tailor made size distributions were obtained through automation of the apparatus.

Summary

This thesis describes two mechanisms of droplet formation. The first part describes the dispersion of liquids through exposure to high electric fields. The phenomenon investigated is known as the Taylor cone. The Taylor cone is a liquid droplet which takes a conical shape when it is exposed to an electric field close to the field breakdown value of $3 \cdot 10^6$ V/m. Sir Geoffrey Taylor described the theory of this phenomenon. In his description of the process he equates the pressure caused by the surface tension to the electric pressure. This is true for only one specific cone which has, according to Taylor, a half angle of 49.3° . In practice these cones emit charges and a hydrodynamic pressure is needed to supply the liquid. Liquid cones, like the Taylor cone, are only stable when semi-conducting liquids are used ($\rho = 10^{-10} - 10^{-4} \Omega^{-1} m^{-1}$). Because of this semi-conducting nature a resistance is induced when charges are emitted which have to be supplied again to the surface of the cone. This induces an additional component in to the field, tangential to the surface. This tangential component causes the liquid cone to be stripped of its surface, the fluid moving to the apex where it disperses into small droplets.

The liquid cones are shown to have many similarities to corona discharges from solid needles, caused by high electric fields. The first two characteristic corona regimes, the burst pulses and the pulseless glow regime, are found also to exist for the liquid cones. The burst pulses detected have a frequency of 20-150 Hz, about a hundred times lower than these from needle coronas. This is explained by the low mobility of the liquid droplets emitted from the cones which is about a hundred times than that of the ions formed around a solid needle corona discharge.

The second corona regime, the pulseless glow regime was also found. Here a gas discharge is seen around the tip of the cone. The current voltage characteristic in this region differs from the solid needle coronas. The difference is found in the fact that the electric current does not increase with increasing potential as it does for the solid needle corona discharge. An increase in potential applied to the liquid cones causes a temporary increase of the tangential shear, which strips the cone surface, causing the cone angle to increase. At the same time the tangential shear is reduced. Eventually the current is the same as in the previous state, only the cone angle is increased. Solid needle coronas increase the amount of space charge emitted and diverge the local electric field while the liquid cones change their shape, keeping the current almost constant.

At even higher potentials the liquid cones become skew, eventually leading to the formation of multiple cones on the rim of the nozzle. One single cone can no longer diverge the electric field enough and thus more cones are needed. The current now increases step wise, every time an extra cone is established on the rim, the amount of space charge increases. Other similarities to the solid needle coronas are the hysteresis at onset and the electric wind around the sharp points.

Simulation of the electric field around the cone shows that the potential drop over the surface remains constant with increasing liquid flow rate or with applied potential. The

Summary

normal force acting on the cone surface increases slightly with increasing potential while the tangential force does not. Calculations show that the field strength around the apex of the cone is high enough for the formation of a corona discharge. They also show that a space charge must be formed to diverge the local field.

Two practical applications of the liquid cones have been developed. An aerosol generator was built, and named the Delft Aerosol Generator (DAG). Highly charged droplets are partially or almost completely discharged, as required, through a corona discharge of opposite polarity. A strategically placed shielding ring causes the process to be very stable. Thus a collimated beam of droplets forms, making it possible to measure the size distribution.

When spraying ethylene glycol, droplets with modal sizes between 1.3 and 1.5 μm were produced with increasing potential. The relative standard deviation lies between 10 and 25 %. Droplets are produced at 10^8 to 10^{12} Hz. Using DOP (Di-Octyl-Phthalate), droplets as small as 0.08 μm were produced by using a mixture of DOP in ethanol.

The second application was developed by submerging the whole spraying system into an immiscible liquid. In this case the continuous phase was a paraffin oil, the droplets produced created an emulsion. These emulsions were found to be of narrow size distribution. When emulsifying ethylene glycol the droplets were around 4.5 μm in diameter. Using a mixture of ethylene glycol and water (40:60 w/w %), the droplets were about 1.6 μm , and when using water about 1.2 μm in diameter. The emulsions were stabilised by 2 w/w% of a 1:1 mixture of SPAN-80 and SPAN-85. Neither the applied potential nor the conductivity influenced the droplet size of the emulsions. The conductivity does influence the onset of emulsification of water. These droplets were also produced at very high frequencies, over 10^8 Hz.

How the droplets are formed at the tip of the cone remains difficult to predict. Photographs show a spiralling downwards path of the droplets produced. The high production rates make the simple formation of the droplets impossible. It seems most likely that the tip is disrupted because of the high local field, causing the tip to be dispersed by high shear rates or by a explosion similar to that seen for droplets charged above the Rayleigh limit. These two hypotheses are not yet proven.

The second part of the thesis describes the formation of droplets through the mechanical vibration of a liquid jet. In particular, jet breakup leading to uniformly sized droplets between 50 μm and 2 mm was investigated. Early works showed that at wave numbers above $k \cdot a = 0.7$, it is possible that one droplet is formed per wavelength induced on the jet surface, which results in droplets of the same size.

When a disturbance is forced onto a jet it will break up according to the imposed disturbance if the wavenumber is $0 < k \cdot a < 1$. The disturbance must be imposed such that an advantage is created over the random disturbances from the surroundings. Initial disturbances, imposed and natural, were measured and the imposed initial disturbances were found to be much larger. Because of this, jets will break up at even less energetically favourable wavenumbers.

Two low liquids of low viscosity (water and a mixture of water and ethylene glycol 2:1 V/V) and a viscous liquid (1% w/w Na-alginate in water) were used. For the low viscosity the $k \cdot a$ value for uniform breakup were found to lay between 0.6 and 1. For the viscous liquid it was found to be between 0.4 and 0.7. Above $k \cdot a = 0.7$ the disturbances from the surroundings again dominate the breakup.

General equations describing the uniform regions of jet break up were determined by a numerical fitting procedure using a total of 666 data points. The upper dimensionless limit of frequency was found to be strongly dependent on the Reynolds number. The lower dimensionless limit of frequency is equally dependent on the Reynolds and Weber numbers.

Size distributions were obtained by photographing the droplets produced and by solidifying Na-alginate solutions. The samples were very uniform in size. The relative standard deviations lay between 1.5 and 2 %.

The equipment used was automated, making it possible to create tailor-made particle size distributions when the uniform regions of breakup are known. Two examples are given. A tetra modal distribution was made, with peaks at 610, 780, 920 and 1010 μm . Secondly a block shaped distribution ranging from 725 to 850 μm was produced.

Samenvatting

In dit proefschrift worden twee manieren van druppels maken beschreven. Het eerste deel beschrijft het dispergeren van vloeistoffen, door gebruik te maken van sterke elektrische velden. Met name het fenomeen "Taylor cone" is nader onderzocht. Een Taylor cone is een vloeistofdruppel die, onder invloed van een sterk elektrisch veld, kegelvormig wordt. De opgelegde veldsterkte ligt in de buurt van de doorslag veldsterkte in lucht van $3 \cdot 10^6$ V/m. Sir Geoffrey Taylor heeft dit fenomeen voor het eerst wiskundig beschreven. Hij stelt in zijn beschrijving de druk veroorzaakt door de oppervlaktespanning gelijk aan de elektrische druk. Dit geldt alleen voor één specifieke kegel, met volgens Taylor een halve kegelhoek van $49,3^\circ$. Echter, in de praktijk zullen deze conische druppels lading wegschieten en zal er een hydrostatische druk nodig zijn om de vloeistof weer aan te voeren. Hierdoor kan Taylor's vergelijking in de praktijk niet meer worden toegepast. Conische druppel, zoals de Taylor cone, zijn alleen stabiel te krijgen als vloeistoffen met een elektrische geleidbaarheid, ρ , van 10^{-10} - 10^{-4} $\Omega^{-1}m^{-1}$ worden gebruikt. Door deze lage geleidbaarheid wordt er een elektrische weerstand geïnduceerd, wanneer er lading wordt afgestoten door de Taylor cone, als er weer nieuwe lading naar het oppervlak van de druppel moet worden aangevoerd. Hierdoor ontstaat er een extra komponent van het elektrische veld, tangentiaal langs het oppervlak van de vloeistofkegel. Deze tangentiale komponent zorgt ervoor dat het oppervlak van de vloeistofkegel wordt afgesneden, naar de punt toe, waar de afgesneden vloeistof in kleine druppeltjes dispergeert.

De vloeistofkegels vertonen een aantal overeenkomsten met coronas rond scherpe naalden. De eerste twee karakteristieke coronaregimes, het "burst pulse" en het "pulseless glow" regime bestaan ook voor de conische vloeistofdruppels. De pulsen van het burst pulse regime hebben een frequentie van 20-150 Hz, hetgeen honderd maal lager is dan de pulsen gemeten bij coronas rond scherpe naalden. Dit is verklaard door de lage elektrische mobiliteit van de vloeistofdruppeltjes, welke ook een honderd maal lager is dan de elektrische mobiliteit van de ionen rond de scherpe naalden.

Het tweede corona regime, het pulseless glow regime, is ook aangetoond. Zoals rond scherpe naalden, wordt ook rond de punt van de conische druppels een gasontlading waargenomen.

De stroom-spanningskarakteristiek van dit regime is anders in vergelijking tot die van vaste naalden. Het verschil is zichtbaar in het konstant blijven van de stroom met toenemende spanning, terwijl bij coronas rond naalden de stroom toeneemt met toenemende spanning. Een toenemende spanning bij de vloeistofkegels zorgt voor een tijdelijke toename van de tangentiale afschuifkracht. Deze stript het oppervlak van de conische druppel verder af zodat de kegelhoek toeneemt, tegelijkertijd neemt de tangentiale afschuiving weer af. Uiteindelijk is de hoeveelheid lading die per tijdseenheid wordt afgevoerd weer gelijk en is alleen de kegelhoek veranderd. Coronas rond scherpe naalden kunnen hun vorm niet veranderen en passen de hoeveelheid ruimtelading aan bij toenemende spanning, hetgeen de oorzaak is van de toenemende stroom.

Bij verder oplopende spanning worden de conische druppels scheef, en uiteindelijk vormen zich meerdere kleinere conische druppels op het randje van de nozzle. Eén enkele druppel kan het lokale elektrische veld niet ver genoeg meer divergeren, zodat nu meerdere kelgels gevormd moeten worden, zodat nu wel de hoeveelheid ruimtelading kan worden aangepast. Ieder keer als er een extra kegeltje bijgevormd wordt, neemt de stroom dan ook stapsgewijze toe.

Andere overeenkomsten met coronas rond vaste naalden zijn de hysterese bij de aanvang van de vorming van de conische druppel en de aanwezigheid van een elektrische wind rond de vloeistofkegel.

Simulatie van het elektrisch veld rond de conische druppels laat zien dat de potentiaalval over het conische vloeistofoppervlak constant blijft bij toenemende spanning en toenemende vloeistofsnelheid. De normaalkracht op het oppervlak neemt iets toe met toenemende spanning, terwijl de tangentiale kracht constant blijft. Uit de veldberekeningen blijkt dat de veldsterkte rond de punt van de conische druppel hoog genoeg is om een corona-ontlading te bewerkstelligen, terwijl duidelijk is dat er een ruimtelading aanwezig moet zijn om het lokale veld te divergeren.

Twee praktische toepassingen van de conische druppels zijn uitgewerkt. Allereerst is er een aërosolgenerator, genaamd de Delft Aerosol Generator (DAG), ontwikkeld. De hoog geladen druppeltjes die uitgestoten worden, worden geheel of gedeeltelijk, al naar gelang gewenst, ontladen. Het ontladen van de druppeltjes wordt door een tegengesteld geladen corona bewerkstelligd. Een strategisch geplaatste afschermmring zorgt voor een stabiel verlopend sproeiproces, zodat er een mist van druppeltjes verkregen wordt waarvan de druppelgrootteverdeling kan worden bepaald.

Bij gebruik van ethyleenglycol als de te versproeien vloeistof worden, met toenemende spanning, druppels met modale diameters van 1,3 tot 1,5 μm verkregen. De relatieve standaarddeviatie ligt tussen 10 en 25 %. De druppels worden met 10^8 tot 10^{12} per seconde geproduceerd. Bij gebruik van DOP (Di-Oktyl-Phtalaat) worden druppels van 0,08 μm geproduceerd, hierbij is DOP gemengd met ethanol.

Een tweede toepassing is gevonden in het maken van emulsies. Hierbij wordt het gehele systeem ondergedompeld in een niet mengbare vloeistof. In dit geval is de kontinue fase een paraffine olie. De druppeltjes worden in de kontinue fase geproduceerd. Hierdoor wordt een emulsie verkregen. De druppelgrootteverdeling van deze emulsies is smal. Bij emulgeren van ethyleenglycol in paraffine olie ligt de druppeldiameter rond 4,5 μm , terwijl bij het emulgeren van een mengsel van ethyleenglycol met water (40:60 gew.%) de druppelgrootte rond 1,6 μm ligt, en die van water rond 1,2 μm ligt. De emulsies worden gestabiliseerd met een 2 gew.% 1:1 mengsel van SPAN-80 en SPAN-85. De opgelegde spanning en de geleidbaarheid van de disperse fase hebben weinig of geen invloed op de druppelgrootteverdeling. De geleidbaarheid heeft wel een invloed of de aanvangsspanning van emulsifikatie van water. De druppelproductiefrequentie ligt ook hier weer hoog, boven 10^8 druppels per seconde.

Hoe de druppelvorming aan de punt van de vloeistofkegels precies verloopt is niet duidelijk en is moeilijk te voorspellen. Foto's laten een circulerend pad zien, waarlangs

Samenvatting

de druppels zich bewegen. De hoge produktiesnelheid van de druppels, sluit de formatie van één druppeltje per keer uit. Zeer waarschijnlijk lijkt het echter, dat de punt van de vloeistofkegel uit elkaar barst door een hoge elektrische afschuifsnelheid of door lokale hoge oplading. Dit laatste zien we ook wanneer druppels de Rayleigh ladingslimiet bereiken. Beide hypotheses zijn niet bewezen.

Het tweede deel van dit proefschrift beschrijft de produktie van druppels door middel van mechanisch trillen van een vloeistofstraal. Met name die manier van opbreken, die leidt tot druppels van uniforme grootte. Druppeldiameters tussen $50 \mu\text{m}$ en 2 mm zijn verkregen. Vroegere onderzoeken hebben aangetoond dat deze manier van vloeistofopbreken mogelijk is bij golfgetallen groter dan $k \cdot a = 0,7$, hierbij wordt per golflengte, geïnduceerd op de vloeistofstraal, één druppel gevormd.

Als er een verstoring op een vloeistofstraal wordt aangebracht, zal de vloeistofstraal opbreken onder invloed van deze opgelegde verstoring, als het golfgetal $0 < k \cdot a < 1$. Door het opleggen van een verstoring zal deze een zodanig voordeel hebben over de random verstoringen die uit de omgeving komen, dat deze geprefereerd zal worden, boven de de omgevingsverstoringen, en zich zal voortplanten. Initiële verstoringen, random, veroorzaakt door achtergrondstoringen en opgelegd via een mechanische verstoring, zijn gemeten. De opgelegde initiële verstoringen liggen veel hoger dan de initiële verstoringen veroorzaakt door de achtergrondstrillingen. Hierdoor zal een vloeistofstraal waarbij de trilling wordt opgelegd ook opbreken volgens energetisch minder gunstige golfgetallen.

Twee laag viskeuze vloeistoffen (water en een mengsel van water en ethyleenglycol 2:1 V/V) en een viskeuze vloeistof (1 gew.% Na-alginaat in water) zijn gebruikt. Voor de laag viskeuze vloeistoffen is gevonden dat de golfgetallen tussen 0,6 en 1 inderdaad uniforme druppels opleveren. Ook voor de viskeuze vloeistof geldt dit, echter dan voor golfgetallen van 0,4 tot 0,7. Bij golfgetallen boven 0,7 planten verstoringen uit de omgeving zich weer voor in de vloeistofstraal.

Algemene vergelijkingen die de gebieden van uniform opbreken van de vloeistofstraal beschrijven zijn bepaald door middel van een numerieke datafit-procedure van in totaal 666 metingen. De bovenste dimensioze frequentiegrens blijkt sterk afhankelijk van het Reynoldsgetal. De onderste dimensioze frequentiegrens blijkt even sterk af te hangen van het Reynolds- en het Webergetal.

Grootteverdelingen van de geproduceerde druppeltjes zijn bepaald, door deze te fotograferen gelijk nadat ze gevormd zijn en door een Na-alginaatoplossing te laten uitharden. De gemeten deeltjesgrootteverdelingen zijn zeer smal. De relatieve standaarddeviaties ligt tussen 1,5 en 2%.

Door automatisering van de gebruikte apparatuur, is het goed mogelijk om zelf deeltjesgrootteverdelingen samen te stellen. Hiervoor is het echter nodig om de ligging van de uniforme opbreekgebiedjes te weten. Twee voorbeelden zijn beschreven. Een tetramodale verdeling, met pieken bij 610 , 780 , 920 en $1010 \mu\text{m}$, en een verdeling in de vorm van een blok, van 725 tot $850 \mu\text{m}$, zijn gemaakt.

Dankwoord

Dit proefschrift is geschreven naar aanleiding van ruim vier jaren werk, maar was niet mogelijk geweest zonder de hulp van vele anderen.

Allereerst mijn afstudeerders. Na de voorbereidingen voor onze reis naar Japan zaten Aart en ik al zo diep in het onderwerp, dat we samen een soort vliegende start hebben gemaakt. Aart heeft door zijn nieuwsgierigheid en veel proberen de zogenaamde Taylor cone herontdekt. Voor ons was het een geheel nieuw verschijnsel, en naar later zou blijken het grootste deel van mijn onderzoek. Door Aart's enthousiasme voor het onderwerp kwam al gauw Anne Mieke op het onderwerp af, gevolgd door Alexander, die bij Aart en mij praktikum had gelopen. Paul heeft daarna als laatste de Taylor cone onder handen genomen, en heeft velen, met name van buiten de Universiteit, geïnteresseerd gekregen.

Maria en Marnix hebben het grootste deel van het werk aan het mechanisch opbreken van vloeistofstralen gedaan. Uiteindelijk heeft Edgar al de verworven kennis kunnen gebruiken om zijn afstudeeronderwerp voor Mijnbouw te kunnen uitvoeren.

Wij hebben al ons onderzoek kunnen verrichten dankzij de hulp van vele anderen. In het begin heeft dhr. van Heest ons enorm geholpen met het ontwerpen van de opstellingen, terwijl dhr. Oudijn en dhr. Stronk het elektrische deel voor ons hebben ontworpen. De latere ontwerpen zijn door dhr. Neervoort op dezelfde voortreffelijke wijze voortgezet. Aan goede ontwerpen heb je alleen iets als je een goede instrumentmakerij hebt. Gelukkig hebben we die en konden we over het vakmanschap van dhr. Willemse beschikken, om alles tot in de kleinste details uitgevoerd te kunnen krijgen.

Bij het ontwerp van de Delft Aerosol Generator is de inventiviteit van Rein Roos onontbeerlijk geweest. Peter Verheijen heeft ons enorm geholpen bij de numerieke data-fit-procedure, die we bij het bepalen van de uniforme gebiedjes nodig hadden. Loes Schouten stond ons op het analyselab meer dan alleen bij, met het doen van veel van onze, soms vergeefse pogingen, tot analyse van de monsters. Zonder de hulp van Jan-Willem Groenendaal had het ons veel meer tijd gekost om tot nette stabiele emulsies te komen. Peter Vervoorn, bedankt voor vooral hulp bij materiële en soms financiële obstakels die we tegen kwamen. Jan, je enthousiasme voor het aërosolonderzoek is voor mij een enorme stimulans geweest.

De resultaten van al ons werk zijn dus gebundeld in dit boek, maar pas na lange, soms vermoeiende diskussies met Jan Marijnissen en prof. Scarlett.

Op het lab was het altijd mogelijk om met lotgenoten over wetenschap te praten, maar vooral de "niet-wetenschap" tijdens de koffie- en theepauzes is enorm fijn en gezellig geweest. Bedankt Johan (leuke vakanties, gezelligheid en saunas), Arthur (lekkere zeiltochtjes en saunas), Ron (saunas en een leuke afstudeerster), Peter (ook een echte oude stijler), Einar (cultuur), Han (bedankt dat ik je mocht helpen verhuizen), Paul (vriendschap, gezelligheid, eigenwijsheid en lekker samen koken), Olaf, Lex, Michiel,

Dankwoord

Marcel en al de afstudeerders van de afgelopen jaren. Ik hoop dat ook in de toekomst de sfeer binnen de deeltjesgroep zo blijft, gezellig, fijn en wetenschappelijk.

Bij het echte schrijven van dit proefschrift, heb ik veel aan Jan te danken gehad, iedere zin is door ons samen onder de loep genomen. Saul en prof. Scarlett hebben iedere zin bekenen en er voor gezorgd, dat het geschrevene zoveel mogelijk op engels lijkt. Dit heeft jullie vele vrije uurtjes gekost. De meeste tekeningen en figuren zijn door Jan van Holst, na vele uren tekenen, tot een mooie eenheid gemaakt.

Natuurlijk was dit alles niet mogelijk geweest als ik niet de steun van mijn familie had gehad. Mijn zus en vooral mijn ouders zijn er altijd voor mij geweest. Tijdens mijn studie, maar ook tijdens mijn promotie, waren ze er altijd om mij te stimuleren, om naar me te luisteren, om met me mee te denken. Ze waren er! Prisca, Mam, Pap, bedankt!

Het schrijven van een proefschrift is een grote inspanning. Je gaat diep. Echter zonder jou Bernardine, was het allemaal veel moeilijker geweest. Tijdens de schaarse vrije uurtjes en de weekends, hielp je mij steeds weer zodanig dat ik alles weer even kon vergeten en ik me kon ontspannen. Ik was vaak duf, moe, misschien wel saai, maar je hebt het volgehouden met mij. Gelukkig geldt het nog steeds: Liefde maakt blind!

Bedankt allemaal,

A handwritten signature in black ink, appearing to read "Gabrie". It consists of a stylized "G" and "a" above a horizontal line, followed by a cursive "brie".

Curriculum Vitae

Gabriël Marinus Henricus Meesters werd geboren op 18 Januari 1962 te Den Haag.

- 1974-1979: Hoger Algemeen Voortgezet Onderwijs (HAVO). Het diploma werd verkregen aan het St. Maartenscollege te Voorburg op 30 Mei 1979.
- 1979-1981: Voorbereidend Wetenschappelijk Onderwijs (VWO). Het diploma werd verkregen aan het St. Maartenscollege te Voorburg op 3 Juni 1981.
- 1981-1987: Studie aan de Technische Universiteit Delft, bij de faculteit der Scheikundige Technologie en der Materiaalkunde.
Propedeutisch examen P1: 7 Maart 1983
Propedeutisch examen P2: 2 Maart 1984
Kandidaats examen: 27 Februari 1985
Doctoraal examen: 25 Augustus 1987
Het hoofdvak was bioprocestechnologie, het bijvak technische milieukunde. Afstudeerhoogleraar Prof. dr. J.G. Kuenen van de vakgroep microbiologie en Enzymologie.
- 1987-1991: Assistent in opleiding (promovendus) bij de vakgroep Chemische Processtechnologie, sectie Deeltjestechnologie. Onder leiding van de promotor Prof. B. Scarlett M.Sc. en de toegevoegd promotor Dr. ir. J.C.M. Marijnissen werd onderzoek verricht naar twee mechanismen van vloeistofopbreken.
- 1992- : Vanaf 17 Februari 1992 werkzaam bij Gist-brocades te Delft als medewerker van de afdeling research and development.

*When brought to meaning, all importance becomes small,
as in death, all life seems nothing
Knowing is destroyed by thinking
Not destroyed but sterilised; distilled into knowledge
Thinking, the processing of knowing to knowledge*